



ARCHITECTURE & ENGINEERING

Volume 10
Issue 2
June, 2025



By Architects. For Architects.
By Engineers. For Engineers.

Architecture
Civil and Structural Engineering
Mechanics of Materials
Building and Construction
Urban Planning and Development
Transportation Issues in Construction
Geotechnical Engineering and Engineering Geology
Designing, Operation and Service
of Construction Site Engines

Architecture and Engineering

Volume 10 Issue 2 (2025)

ISSN: 2500-0055

Editorial Board:

Prof. Askar Akaev (Kyrgyzstan)
Prof. Emeritus Demos Angelides (Greece)
Mohammad Arif Kamal (India)
Prof. Stefano Bertocci (Italy)
Prof. Tigran Dadayan (Armenia)
Prof. Milton Demosthenous (Cyprus)
Prof. Josef Eberhardsteiner (Austria)
Prof. Sergei Evtukov (Russia)
Prof. Georgiy Esaulov (Russia)
Prof. Andrew Gale (UK)
Prof. Theodoros Hatzigogos (Greece)
Prof. Santiago Huerta Fernandez (Spain)
Yoshinori Iwasaki (Japan)
Prof. Jilin Qi (China)
Prof. Nina Kazhar (Poland)
Prof. Gela Kipiani (Georgia)
Prof. Darja Kubečková (Czech Republic)
Prof. Hoe I. Ling (USA)
Prof. Evangelia Loukogeorgaki (Greece)
Prof. Jose Matos (Portugal)
Prof. Dietmar Mähner (Germany)
Prof. Saverio Mecca (Italy)
Prof. Menghong Wang (China)
Stergios Mitoulis (UK)
Prof. Valerii Morozov (Russia)
Prof. Aristotelis Naniopoulos (Greece)
Sandro Parrinello (Italy)
Prof. Paolo Puma (Italy)
Prof. Jaroslaw Rajczyk (Poland)
Prof. Marlena Rajczyk (Poland)
Prof. Sergey Sementsov (Russia)
Anastasios Sextos (Greece)
Eugene Shesterov (Russia)
Prof. Alexander Shkarovskiy (Poland)
Prof. Emeritus Tadatsugu Tanaka (Japan)
Prof. Sergo Tepnadze (Georgia)
Sargis Tovmasyan (Armenia)
Marios Theofanous (UK)
Georgia Thermou (UK)
Prof. Yeghiazar Vardanyan (Armenia)
Ikujiro Wakai (Japan)
Vardges Yedoyan (Armenia)
Prof. Askar Zhusupbekov (Kazakhstan)
Prof. Konstantin Sobolev (USA)
Michele Rocca (Italy)
Prof. Sergey Fedosov (Russia)
Francesco Di Paola (Italy)
Prof. Alexey Semenov (Russia)

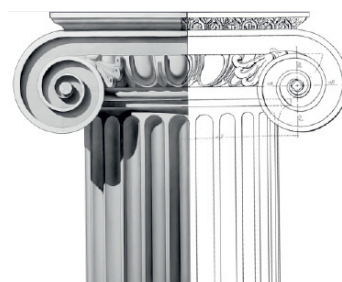


Editor in Chief:

Professor Evgeny Korolev (Russia)

Executive Editor:

Anastasia Sidorova (Russia)



CONTENTS

Architecture

- 3 **Sherif Mohamed Ali, Magdy Mohamed El Nahas, Mohamed Amin, Khadija Elsayed Shakra, Nourhan Alaa**
Structural analysis for environmental sustainability in traditional architecture
- 19 **Ayam Sh. Altameemi, Adil M. Jabbar**
Using digital software to design interactive smart canopies for the outdoor environment
- 33 **Ofita Purwani, Astri Resmi Enggarswi**
Asserting local identity in the public sphere: a top-down effort in the decentralized Surakarta

Geotechnical Engineering and Engineering Geology

- 43 **Hadj Bekki, Abdelhakim Guezzoul, Tefaha Cherrak, Rachid Boumeddiene, Hadj Benhebal**
Comparative study on enhancing the mechanical properties of clayey sand with waste plastic fibers and lime

Civil Engineering

- 53 **Sergey V. Fedosov, Vitaly G. Kotlov, Azariy A. Lapidus, Aleksandr M. Sokolov**
Physico-mathematical model of wood durability under cyclic environmental changes in temperature and humidity
- 63 **Amin Mohammadi, Shariyeh Hosseininassab, Seyed Mohammad Mousavi**
Optimizing energy consumption and structural performance of office buildings in Tehran city using cost-effective solutions: a modeling and simulation-based analysis
- 78 **Ilhem Sahnoun, Zhour Guemmadi, Belkacem Toumi**
Relationships between mechanical properties (compressive strength) and physical properties (porosity) at high temperatures
- 88 **Issaias Anday Sereke, Marina I. Rynkovskaya, Habte Yohannes Damir**
Plastic buckling analysis of conventional concrete and expanded polystyrene concrete spherical shells

Architecture and Engineering

peer-reviewed scientific journal
Start date: 2016/03
4 issues per year

Founder, Publisher:

Saint Petersburg State University
of Architecture and Civil Engineering

Indexing:

Scopus, Russian Science Citation Index, Directory of Open Access Journals (DOAJ), Google Scholar, Index Copernicus, Ulrich's Periodicals Directory, WorldCat, Bielefeld Academic Search Engine (BASE), Library of University of Cambridge and CyberLeninka

Corresponding address:

4 Vtoraya Krasnoarmejskaja Str.,
St. Petersburg, 190005, Russia

Website: <http://aej.spbgasu.ru/>

Phone: +7(812) 316 48 49

Email: aejeditorialoffice@gmail.com

Date of issue: June 30, 2025

The Journal was re-registered
by the Federal Service
for Supervision of Communications,
Information Technologies and Mass
Communications (Roskomnadzor)
on May 31, 2017;
registration certificate of media organization
EI No. FS77-70026

STRUCTURAL ANALYSIS FOR ENVIRONMENTAL SUSTAINABILITY IN TRADITIONAL ARCHITECTURE

Sherif Mohamed Ali¹, Magdy Mohamed El Nahas², Mohamed Amin^{1,3}, Khadija Elsayed Shakra⁴, Nourhan Alaa^{1*}

¹Suez University, Suez, Egypt

²Higher Institute of Engineering and Technology, Arish, Egypt

³Mansoura Higher Institute of Engineering and Technology, Mansoura, Egypt

⁴Beni Suef University, Beni Suef, Egypt

*Corresponding author's email: Han828889@gmail.com

Abstract

Introduction: This research is based on the premise that traditional architecture comprises buildings constructed using natural, locally sourced materials. These structures are designed to adapt to environmental changes and promote environmental compatibility — commonly referred to as environmental sustainability — by considering the design of the exterior form. The research problem centers on the negative impacts of modern industrial building materials. These materials are often costly, require significant energy for production, and rely on artificial means to ensure thermal comfort within spaces. Consequently, this research explores the inherent potential of natural materials in architectural design — examining their properties, climatic performance, structural strength, and the construction systems in which they are employed — to address the issue of high energy consumption. Additionally, **the research aims** to investigate the characteristics and performance of natural building materials, identifying their constants and variables, as well as their structural and architectural applications. **Results:** By harnessing the benefits of nature, the study seeks to advocate for the use of natural materials in sustainable building practices. This research adopts a combined descriptive and analytical methodology to support the economic and sustainable use of natural materials in architecture.

Keywords: environmental sustainability; vernacular architecture; traditional architecture; karshif; bamboo.

Introduction

In the past, people lived in natural shelters such as caves, the hollows of large trees, and underground pits, or in structures made from natural materials like reed and palm fronds. This was to protect them from the cold, lightning, thunder, and wild animals. In these shelters, people found refuge as well as psychological, physical, and climatic comfort. Many ancient civilizations inhabited these primitive shelters, including the people of ancient Iraqi cities and others who built underground dwellings or carved homes into mountains and ice. Over time, human intervention in material technology transformed these primitive forms into more geometric shapes, enhancing the performance of the materials and fulfilling functional needs. With each stage of scientific progress, people have sought to modify the natural forms of materials and load-bearing structural systems, especially when new methods of utilizing materials are discovered, which increase their natural capacities. Materials are often combined with others to alter their properties, improving their strength and adapting them to meet the demands of contemporary architectural

functions. While technological developments generally yield positive outcomes, they can also produce adverse side effects. For instance, in medicine, chemotherapy treats the affected organ but can harm other parts of the body. Similarly, in engineering, research has improved the structural strength of concrete, but at the cost of reducing thermal comfort, leading to greater reliance on air conditioning and increased energy consumption. Modern architectural materials often lead to problems such as the depletion of natural resources, excessive energy use, and diminished thermal and psychological comfort. These issues, in turn, affect the efficiency and livability of architectural spaces. This concern is echoed by Ramses Wissa Wassef, who stated: "Machines shall not be employed at the expense of humans; rather, the environment must be considered" (Steele, 1997). Vernacular architecture has attracted significant attention from architects because it offers optimal regional solutions. It provides ingenious responses to climatic, technical, social, and cultural challenges. Leading architects have described vernacular architecture in the following ways:

1.1 *Bernard Rudofsky*: Architecture without architects (Rudofsky, 1964).

1.2 *Christopher Alexander*: Distinctive primary architecture, with the foundational role in fostering social cohesion (Alexander, 1979).

1.3 *Hassan Fathy*: Environmentally sensitive architecture that preserves natural privacy (Fathy, 1973).

1.4 *Louis Kahn*: He believed that architecture should be inspired by local surroundings and grounded in inherited customs and culture. He considered vernacular architecture a true example of genuine architecture with a deep connection between people and place (Curtis, 2005).

1.5 *Kenzo Tange*: He drew inspiration from traditional architecture, creating contemporary designs that harmonize with local society and culture. He argued that architecture should integrate technology with local character to promote cultural identity and preserve the environment (Tange, 1984).

1.6 *Frank Lloyd Wright*: He adopted the concept of "organic architecture", an extension of traditional architectural philosophy. He also advocated that buildings should complement their natural surroundings and reflect the topography and features of the environment, rather than dominate or impose themselves upon it (De Long, 1996).

1.7 *Norman Foster*: Despite his focus on technology, he acknowledges the value of traditional architecture as a simple, environmentally friendly, and energy-efficient solution. These observations demonstrate that vernacular architecture is not merely a historical style, but a foundational element of global architectural discourse, deeply rooted in an understanding of the environment and society and offering sustainable solutions tailored to the specific conditions of each region (Sudjic, 2010).

1.8 *Alvaro Siza*: He believes that traditional architecture possesses an unparalleled ability to blend seamlessly with nature and local communities. He views it as a model of design that interacts harmoniously with the environment without relying on excessive industrial intervention (Frampton, 2000).

1.9 *Tadao Ando*: He emphasized that traditional architecture fosters a sense of tranquility and harmony with nature, strengthens the connection between humans and their surrounding environment, and creates spaces that positively impact mental health (Ando, 2011).

1.10 *Rudolf Schindler*: He emphasized the importance of employing sustainable construction methods inspired by vernacular architecture, explaining that a thorough understanding of the properties of local materials and their appropriate application can contribute to achieving environmentally sustainable architecture (Olsberg, 2001).

The aforementioned theories reflect a distinctive architectural style that relies on natural resources and manual craftsmanship, rather than the expertise of specialists, as seen in the visions of Bernard Rudofsky. This form of architecture is a cornerstone in the thought of Christopher Alexander, who emphasizes its role in strengthening social bonds. Similarly, Hassan Fathy highlights the importance of designs that respect the natural environment and preserve privacy within the framework of spontaneous and vernacular architecture.

Sustainable architecture offers a holistic approach to building design. On an individual level, buildings constructed with sustainable materials can enhance quality of life by providing healthier living environments and reducing energy consumption through improved insulation. At the community level, adopting sustainable technologies and materials reduces the carbon footprint, positively impacting environmental pollution and public health. Additionally, these practices create local job opportunities and contribute to the local economy by promoting the use of available resources. Traditional architecture stands out as a natural and effective solution to the challenges of climate change. In environments experiencing alarming climate fluctuations, traditional building methods offer innovative and sustainable solutions. For example, in hot and arid regions, the use of mud and timber provides natural cooling, reducing indoor temperatures without relying on energy-intensive air conditioning.

In areas prone to hurricanes and flooding, bamboo construction presents a sustainable and resilient alternative. Bamboo's inherent flexibility and strength make it ideal for withstanding high winds and water damage, offering crucial protection for coastal communities. Vernacular architecture is based on a philosophy of harmony between humans and the environment. The adoption of local and sustainable building methods and materials not only enhances environmental sustainability but also helps preserve cultural and architectural heritage. When architects rediscover and incorporate these methods, they contribute to developing contemporary designs that unite beauty, durability, and sustainability. Drawing inspiration from traditional architecture can lead to innovative solutions that address both current and future environmental challenges. Traditional architecture and sustainability together open new horizons in facing climate change. These methods invite us to return to our roots, where architectural heritage guides us toward a more sustainable future. Understanding the relationship between humanity and the environment within the framework of environmental architecture motivates us to protect the planet and ensure a better future. Traditional architecture symbolizes a positive interaction

between humans and the environment — it is an open-air museum offering ideas and solutions that strengthen our resilience to climate change and emphasize the importance of environmental sustainability in our lives.

This perspective is closely linked to the concept of local and traditional architecture, which reflects the cultural identity of communities. Earthen architecture, stone structures, oasis dwellings, and karshif architecture all embody a philosophy of skillfully harnessing environmental materials to create living spaces that connect with the human spirit and sustainably meet daily needs. The insight that buildings should not exist in isolation but rather as integral parts of the environmental and cultural fabric remains a cornerstone of our architectural heritage (Abd Elrahman and Saleh, 2015).

Methods

This research aims to identify, analyze, and document architectural elements found in traditional structures located in green environments. The goal is to develop a comprehensive checklist that incorporates diverse features from various global regions.

The study is divided into two parts:

2.1 A theoretical historical-inductive study.

2.2 An applied and analytical study focusing on thermal comfort, lighting, and ventilation in vernacular buildings, examining how building materials and construction methods affect spatial comfort.

Study Samples and Architects' Trends

A list of eight traditional buildings from different parts of the world was compiled. These structures are characterized by simplicity, durability, and a sense of tranquility. Selection was based on architectural, aesthetic, and historical significance. A detailed analysis of each building (Table 1) was conducted to examine their unique features and document trends. Tables 2-10 present an analysis of the selected buildings.

Table 1. **Selected buildings of aesthetic and historical value**

No.	Building	Location
01	Primitive Hut	North German Plain
02	Primitive Hut	Notre-Dame de Paris
03	Grass Lodge	Kansas City, USA
04	Dome of Shaykh Idris "Al-Mahjoub"	Northern Sudan
05	Manyatta Hut	Tanzania and Kenya
06	Stone House in Meyrals Commune	Southwest France
07	House in the Ancient City of Shali	Siwa Oasis
08	Bamboo Sports Hall	Panyaden International School, Thailand


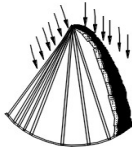




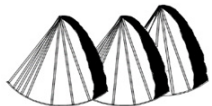
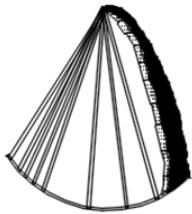
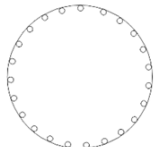
From the previous analyses, it is evident that traditional architecture offers a valuable global lesson in sustainable design. It is not merely a form of simple or vernacular construction but rather a reflection of a profound understanding of the balance between humanity and nature. The principles of traditional architecture can be leveraged to develop sustainable architectural solutions that are environmentally conscious and mitigate the negative impacts of modern technology. Striking a balance between technology and nature is essential for achieving sustainable development in the future. A prime example of this approach is the use of natural materials such as karshif and bamboo, both of which offer significant environmental and economic benefits:

- Karshif is a traditional, natural building material that has been used for thousands of years. Composed mainly of mud and straw, it is especially suited for desert and hot climates due to its exceptional thermal insulation properties and ability to regulate indoor temperatures. By combining simplicity with high efficiency, karshif promotes environmental sustainability and contributes to a stable indoor climate. As a thermal insulator, karshif helps maintain cool interiors in summer and retains warmth in winter, reducing the dependence on artificial cooling and heating systems. Due to its flexibility and moldability, karshif enables the creation of architectural designs that are well adapted to the surrounding environment. Its primary components — mud and straw — are both abundant and locally available, making it a practical and accessible building material.

From an environmental perspective, karshif is highly sustainable, relying on natural, renewable resources and leading to low production costs. While structures built with karshif may require periodic maintenance, especially in areas with significant rainfall, such maintenance is straightforward and can be performed using locally sourced materials. Shali, a city in the Siwa Oasis of Egypt, is a prime example of the use of karshif. It has stood as a complete urban settlement in a harsh desert environment since the 13th century. The thermal mass of its mud bricks provides exceptional insulation, ensuring a thermally comfortable interior environment throughout the year.










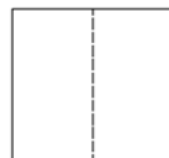
- Bamboo is one of the most prominent natural materials and has been widely celebrated in both traditional and contemporary architecture due to its unique properties — strength, flexibility, and rapid growth. As one of the most renewable and sustainable resources, bamboo can grow up to a meter per day in certain environments, making it an unparalleled natural alternative to timber, which requires significantly more time to mature. Extensively used in construction across Asia, Latin America, and Africa, bamboo is highly regarded

Table 2. Building analysis (primitive hut — North German Plain, prehistory)

1. Primitive hut — North German Plain, prehistory					
Materials	Disadvantages	These materials lack fame and recognition, and there is a prevailing trend toward using materials that negatively impact both the environment and human health.			
	Advantages	The structure is formed using bamboo sticks arranged in a tapered semicircular shape, pointing upward. Bamboo is a fast-growing plant, reaching full maturity within three years. According to Chinese belief, it brings good luck and absorbs negative energy.			
Construction system		Ribbed dome system.			
Loading			Skyline		
Ventilation openings	Windows	None	Load-bearing elements	The structure uses the same dome system, with beams at both edges of the dome to reduce lateral thrust.	
	Doors		Assembly	The cone shape is formed by assembling triangular components. 	
	Patios	None	Subtraction	A cone with a portion subtracted to create the door. 	
Building materials		Bamboo	Repetition	The same pattern is repeated in different areas. 	
Section			Roofs	The roof plan consisting of vertically oriented bamboo sticks, held together by a circular band at the base. 	




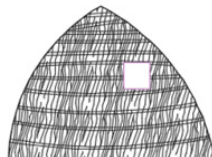
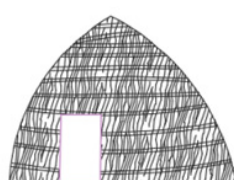
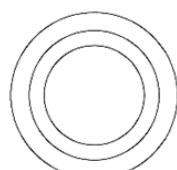
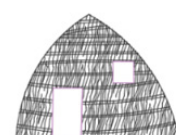
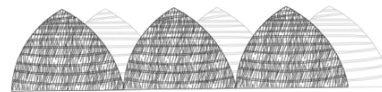

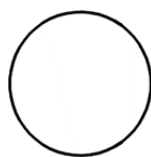
Reference: <http://ocw.nd.edu/architecture/nature-and-the-built-environment/lecture-6/primitive-huts/view>.

Table 3. Building analysis (primitive hut (shape) — “Notre Dame”, a city in Paris, prehistory)

2. Primitive hut — “Notre-Dame”, a city in Paris, prehistory					
Materials	Disadvantages	Natural materials are scarce. Preference for materials that have negative impacts on both the environment and human health.			
	Advantages	Natural materials harmonize with the surrounding climate, absorb negative energy, and provide thermal comfort.			
Construction system		A vertical system with a pyramidal roof.			
Loading			Skyline		
Ventilation openings	Windows		Load-bearing elements	Vertical elements consist of palm tree posts, while horizontal elements are made of brick beams and palm fronds.	
	Doors		Assembly	The building's cubic form is composed of squares combined with a triangle to shape the facade. 	
	Patios	The building does not contain a patio.	Subtraction	A cube from which parts are subtracted (the door and the window). 	
Building materials		Bricks, reeds, and straw.		Repetition	The same pattern is repeated within the same area. 
Section			Roofs	The plan of the pyramidal roof. 	









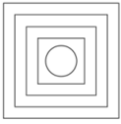
Reference: An article dated November 5, 2012 by Anna Longrigg, Marissa Morning, Logan Steele, Ilhan Gokay Ozdemir

Table 4. Building analysis (grass lodge — Wichita, Kansas City, USA, 1541)

3. Grass lodge — Wichita, Kansas City, USA, 1541					
Materials	Disadvantages	This type of building is rarely used.			
	Advantages	All materials used are natural and do not harm the environment or human health.			
Construction system		Dome system with concentric rings.			
Loading				Skyline	
Ventilation openings	Windows			Load-bearing elements	The same dome system, based on concentric rings — largest at the bottom, decreasing in size toward the top — with internal vertical tension elements connecting the rings.
	Doors			Assembly	Constructed using rings arranged from bottom to top, decreasing in diameter. 
	Patios	None		Subtraction	A vault from which parts are subtracted (the door and the window). 
Building materials		The structure is made of bamboo and covered with grass.		Repetition	The pattern is repeated with variations in height and spacing. 
Section				Roofs	The plan of the circular roof composed of rings. 




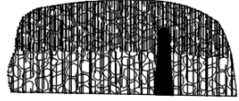
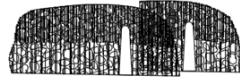
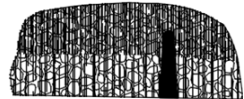


Reference: https://www.flickr.com/photos/smu_cul_digitalcollections/4876744423/

Table 5. Building analysis (dome of Shaykh Idris “Al-Mahjoub” — Kowikka village, Northern Sudan, 1836)

4. Dome of Shaykh Idris “Al-Mahjoub” — Kowikka village, Northern Sudan, 1836					
Materials	Disadvantages	Natural materials are scarce.			
	Advantages	The structure was built using natural materials, specifically mudbrick, which is inexpensive and environmentally balanced.			
Construction system		Stepped pyramidal system.			
Loading			Skyline		
Ventilation openings	Windows		Load-bearing elements	A brick dome composed of multiple tiers. The structure relies on vertical load-bearing elements.	
	Doors		Assembly	The building has a stepped cubic form made up of squares, topped with a hemispherical vault. 	
	Patios	The building includes a patio that appears on multiple levels and features ventilation openings.	Subtraction	A stepped pyramidal form from which parts are subtracted (the door and the window). 	
Building materials		Mudbrick and stones.	Repetition	The design is repeated vertically rather than horizontally to enhance ventilation.	
Section			Roofs	The plan of the roof consists of a stepped pyramidal structure topped with a dome. 	




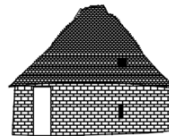
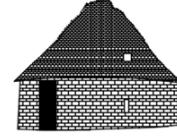



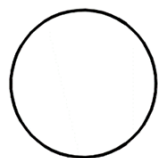
Reference: Article dated February 18, 2019, Al-Tahrir newspaper, “Here is Sudan” by Mohamed Mostafa Farah (Abu Mostafa)

Table 6. Building analysis (Manyatta hut — Tanzania and Kenya, 2007)

5. Manyatta hut — Tanzania and Kenya, 2007					
Materials	Disadvantages	It has a pungent smell initially, but this dissipates after drying.			
	Advantages	The plastering material, made from cow dung, is a mineral-rich, protein-based mass. When applied to walls, it repels insects and serves as a thermal insulator.			
Construction system		Vertical system with a horizontal flat roof.			
Loading			Skyline		
Ventilation openings	Windows	None	Load-bearing elements	The vertical elements are made from posts of palm fronds.	
	Doors		Assembly	The building has an irregular shape, resembling a rectangular parallelepiped, assembled from rectangles. 	
	Patios	None	Subtraction	A vertical form with a flat roof, from which a part is subtracted (the door and the window). 	
Building materials		Posts of palm fronds and plastering material made from cow dung.	Repetition	The design was not repeated within the same context.	
Section			Roofs	The plan of the roof follows a vertical system with a horizontal flat roof. 	


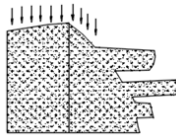

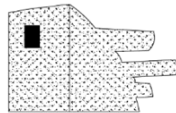
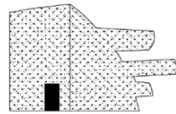
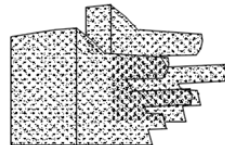
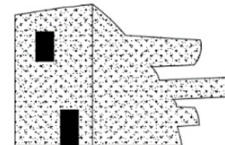


Reference: "From Vernacular to Modern" (2020), by Maureen Wangui Wanjiku and Samuel Mwituria Maina

Table 7. Building analysis (stone house in Meyrals commune — Southwest France, 2007)

6. Stone house in Meyrals commune — Southwest France, 2007					
Materials	Disadvantages	Natural materials are scarce.			
	Advantages	Constructed from natural materials that adapt well to human needs, providing thermal comfort and adequate lighting.			
Construction system		Cylindrical structure with a conical roof.			
Loading				Skyline	
Ventilation openings	Windows			Load-bearing elements	The house consists of walls topped with a complete roof structure. It relies on vertical load-bearing elements and is designed to resist some shear forces.
	Doors			Assembly	The building has a cylindrical form, composed of a cylinder topped with a pyramidal roof. 
	Patios	None		Subtraction	A conical structure with a pyramidal roof from which some parts are subtracted (the door and window). 
Building materials		Stones		Repetition	The same pattern is repeated throughout the available space at varying distances.
Section				Roofs	Circular roof plan. 


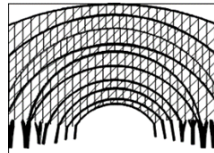


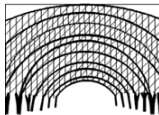

Reference: Boyer Site, Dordogne, France; author: Gilbert Bochenek

Table 8. **Building analysis (Siwa Center for Documentation of Cultural and Natural Heritage — ancient city of Shali in the Siwa Oasis, 2012)**

7. Siwa Center for Documentation of Cultural and Natural Heritage — ancient city of Shali in the Siwa Oasis, 2012					
Materials	Disadvantages	Natural materials are scarce.			
	Advantages	Constructed from environmentally friendly materials. The roof is made of palm trunks, and the walls are built using karshif, a mixture of salt and sand.			
Construction system		Vertical system with a horizontal flat roof. Load-bearing walls.			
Loading				Skyline	
Ventilation openings	Windows			Load-bearing elements	The loading is vertical, and the loads are distributed across the walls and roof.
	Doors			Assembly	The building has a cubic form composed of square elements. 
	Patios	A patio is essential in this building due to the intense desert heat.		Subtraction	A level structure from which parts are subtracted (the door and the window). 
Building materials		Karshif		Repetition	The design is repeated throughout the surrounding space, but in varied forms.
Section				Roofs	The plan of the roof. 









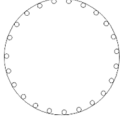

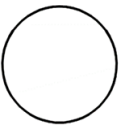
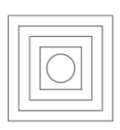
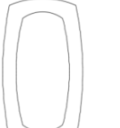
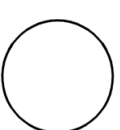
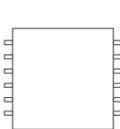
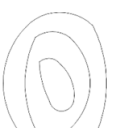
Reference: ©Hermann (FAO, 2016, www.fao.org/3/a-bp825e.pdf)

Table 9. Building analysis (Bamboo Sports Hall — Panyaden International School, Thailand, 2017)

8. Bamboo Sports Hall — Panyaden International School, Thailand, 2017					
Materials	Disadvantages	Natural materials are scarce.			
	Advantages	Bamboo was used, which is highly flexible and can be harvested without killing the plant. The building is designed to combat the hot climate.			
Construction system		Truss system with sections for transferring and evenly distributing loads.			
Loading			Skyline 		
Ventilation openings	Windows	None, as it is an open hall.		Load-bearing elements Curved horizontal elements such as domes, and vertical elements used to distribute loads in the truss.	
	Doors	Located at the beginning and end of the curved entrances.		Assembly The truss shape was formed by assembling bamboo sticks. 	
	Patios	None		Subtraction Entrances	
Building materials		Bamboo sticks (Moses stick).		Repetition The structural element was repeated over an area of 782 m ² to accommodate 300 people.	
Section			Roofs The plan of the roof. 		

Reference: Bamboo Sports Hall for Panyaden International School / Chiangmai Life Construction, ArchDaily, 2017 [Date accessed April 15, 2020].

Table 10. Comparative analysis of the eight buildings

	Case 1	Case 2	Case 3	Case 4	Case 5	Case 6	Case 7	Case 8
1. Disadvantages	None	None	None	None	It has a pungent smell at first	None	None	None
2. Advantages	Yes	Yes	Yes	Yes	Yes	Yes	Yes	Yes
3. Construction system	Ribbed vault	Vertical pyramidal roof	Ribbed vault	Stepped pyramidal structure	Vertical flat roof	Cylindrical conical roof	Vertical flat roof	Trusses
4. Skyline								
5. Windows	None	Yes	Yes	Yes	None	Yes	Yes	None
6. Doors	Yes	Yes	Yes	Yes	Yes	Yes	Yes	Yes
7. Roofs								
8. Building materials	Bamboo	Bricks + reeds + straw	Bamboo covered with grass	Mudbrick + stones	Palm fronds and cow dung plaster	Stones	Karshif	Bamboo

for its exceptional strength-to-weight ratio. This makes it ideal for structures that must withstand earthquakes and harsh weather, enhancing both safety and comfort. Bamboo's compatibility with traditional techniques — such as lashing and knotting — further increases its appeal for those prioritizing sustainable practices. Beyond its role as a construction material, bamboo serves as a holistic environmental solution. Its rapid growth and low energy requirements make it a highly eco-friendly alternative to synthetic materials. Bamboo contributes to ecological balance by absorbing large amounts of carbon dioxide and releasing oxygen, playing a significant role in mitigating climate change. Additionally, bamboo offers natural thermal insulation, improving the energy efficiency of buildings. Its versatility allows it to be shaped for a wide range of applications, blending tradition with modernity and offering architects virtually limitless creative potential.

The Arc, a gymnasium at the Green School in Bali, Indonesia, stands as a testament to bamboo's architectural potential. It seamlessly blends traditional Balinese design with contemporary principles, enhancing environmental integration and promoting sustainability. Thanks to bamboo's flexibility and strength, the gymnasium features curved walls, vaulted ceilings, and shaded outdoor areas. Bamboo can also be fashioned into a wide range of products — such as furniture, umbrellas, and even bridges — demonstrating its remarkable versatility. In bamboo-growing regions, local communities are developing new crafts and techniques that respect tradition while renewing local resources, thereby supporting both the economy and sustainable development. Ultimately, bamboo is more than just a plant: it symbolizes innovation, balance, and harmony with nature.

Laboratory experiment: breaking five brick samples

Objective of the experiment:

- To manufacture environmentally friendly building materials (bricks).
- To measure the compressive strength of the bricks.

Experimental design

- Sample preparation: Five brick samples were prepared and numbered from 1 to 5.
- Tools and equipment used:
 - Siwa sand;
 - Fire marble powder;
 - Lime marble powder;
 - Dry bamboo (1 cm diameter, semi-hollow);
 - Fire marble chips;
 - Karshif stone;
 - Addibond 65 (diluted in a 1:4 ratio);
 - 5 wooden molds for samples (dimensions 20 × 10 × 7 cm);
 - Measuring cup;

- Balance;
- Tamping tool.

Conducting the experiment:

- Sample casting date: 06.12.2024.
- The materials were mixed according to standard mixing procedures with compaction applied as shown in the Table 11.

- Sample 5 was subjected to drying at 140°C. Photographs and recording of the experiment are shown in Figs. 2-4.

Test results

- Sample crushing date: 21.12.2024.
- Sample 4 was not tested due to its fragility and perishability.

Comparison	Case 1	Case 2	Case 3	Case 4	Case 5	Case 6	Case 7	Case 8	Result	%
Disadvantages of building with natural materials	0	0	0	0	0	0	0	0	0/8	0 %
Advantages of building with natural materials	1	1	1	1	1	1	1	1	8/8	100 %
Circular roof	1	0	1	0	0	1	0	0	3/8	38 %
Square roof	0	1	0	1	1	0	1	0	4/8	50 %
Irregularly shaped ceilings	0	0	0	0	0	0	0	1	1/8	13 %
Ventilation openings	0.5	1	1	1	0.5	1	1	0.5	6.5/8	81 %
Climate resistance efficiency of natural materials	1	1	1	1	1	1	1	1	8/8	100 %

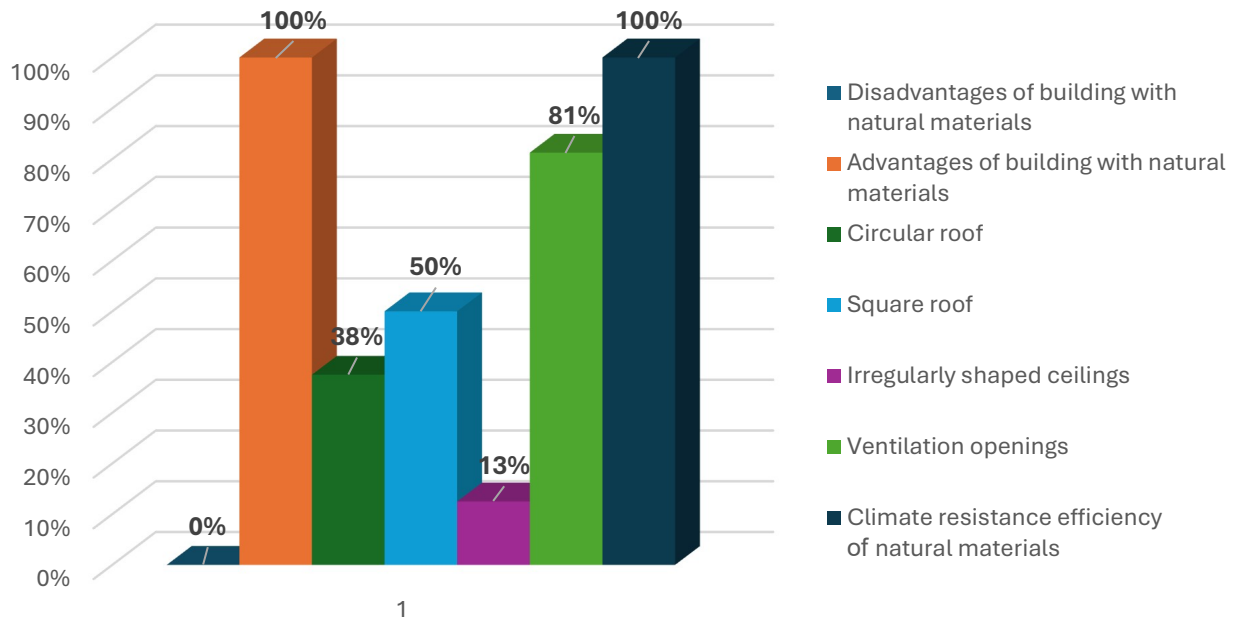


Fig. 1. Percentage of advantages, disadvantages, and effective ventilation in buildings constructed with natural materials

Table 11. Compositions of mixtures

Sample 1	Raw materials	Siwa sand	Water	—	—
	Standard number	12	3/4	—	—
Sample 2	Raw materials	Siwa sand	Fire marble powder	—	Addibond 65
	Standard number	6	2	—	2
Sample 3	Raw materials	Siwa sand	Bamboo	Lime marble powder	Addibond 65
	Standard number	6	Reinforcing	2	2
Sample 4	Raw materials	Siwa sand	Crushed karshif	Mousseline	Addibond 65
	Standard number	6	1	1	2
Sample 5	Raw materials	Siwa sand	Crushed karshif	Crushed fire marble	Addibond 65
	Standard number	3	3	1	1



Fig. 2. Broken karshif stone (researchers' work)



Fig 4. Five prepared brick samples (researchers' work)



Fig. 3. Bamboo reinforcement visible within the brick sample (researchers' work)

Results

1. The construction systems in vernacular architecture vary widely, including ribbed dome systems, conical systems with pyramidal roofs, stepped pyramidal systems, and vertical systems with both pyramidal and horizontally flat roofs.

2. Traditional heritage forms are utilized due to their ability to enhance the energy efficiency of buildings.

3. Primitive architecture demonstrated a richness in building forms that contributed to creating interior environments with thermal comfort, thereby reducing the need for artificial cooling and heating. This was achieved through methods such as integrated planning, narrow and winding streets, and the use of shrubs and trees.

4. Primitive architecture paid close attention to the treatment of building envelopes, aiming to reduce external environmental impacts and thus lower energy consumption and structural loads.

5. The internal environmental quality in primitive architecture was notable, relying on natural air renewal, interior humidification, thermal comfort, and effective use of natural lighting, while addressing limitations in lighting conditions through architectural design.

6. The results of the experiment, when compared with standard criteria for construction bricks, indicated that the four tested brick samples met the specified requirements.

Table 12. The results of compressive strength testing for the five brick samples

Sample No.	(1)	(2)	(3)	(4)	(5)
Weight, g	2132	1686	1335	0	1017
Dimensions, cm	19.8 × 10.0 × 5.6	19.8 × 9.6 × 5	19.9 × 9.8 × 4.0	0	19.5 × 10.3 × 3.3
Cross-sectional area, cm ²	198.0	190.1	195.0	0	200.8
Crushing load, kN	156.3	294.9	191.4	0	265.1
Compressive strength, kg/cm ²	80.5	158.1	100.0	0	201.8

References

- Abd Elrahman, H. O. and Saleh, M. A. M. A. (2015). Architectural techniques in traditional architecture and how to use them to reduce energy consumption in buildings. *Mansoura Engineering Journal*, Vol. 40, Issue 4, pp. 5–15.
- Alexander, C. (1979). *The Timeless Way of Building*. Oxford University Press, 552 p.
- Ando, T. (2011). Tadao Ando: The Colours of Light. Phaidon Inc Ltd, 263 p.
- De Long, D.G. (1996). *The Organic Architecture of Frank Lloyd Wright*. Harper & Row.
- Fathy, H. (1973). *Architecture for the Poor: An Experiment in Rural Egypt*. University of Chicago Press, 366 p.
- Olsberg, N. (2001). *Rudolf Schindler: The Search for Architecture*. Taschen.
- Rudofsky, B. (1964). *The Necessity of Architecture: A Vision for a New Building*. Harper & Row, 158 p.
- Frampton, K. (2000). *Alvaro Siza: Complete Works*. Phaidon Press, 620 p.
- Steele, J. (1997). *An architecture for people: the complete works of Hassan Fathy*. Cairo: The American University in Cairo, 208 p.
- Sudjic, D. (2010). *Norman Foster: A Life in Architecture*. Overlook Books, 320 p.
- Kuan, S. (2012). *Kenzo Tange: Architecture for the World*. Lars Müller Publishers, 192 p.
- Curtis, W.J.R. (2005). *Louis Kahn: The Power of Architecture*. Vitra Design Museum, 354 p.

СТРОИТЕЛЬНЫЙ АНАЛИЗ ЭКОЛОГИЧЕСКОЙ УСТОЙЧИВОСТИ В ТРАДИЦИОННОЙ АРХИТЕКТУРЕ

Шериф Мохамед Али¹, Магди Мохамед Эль Нахас², Мохамед Амин^{1,3}, Хадиджа Эль-Сайед Шакра⁴,
Нурхан Алаа^{1*}

¹Суэцкий университет, Суэц, Египет

²Высший институт инженерии и технологий, Эль-Ариш, Египет

³Высший инженерно-технологический институт в Мансуре, Мансура, Египет

⁴Университет Бени-Суэйфа, Бени-Суэйф, Египет

*E-mail: Han828889@gmail.com

Аннотация

Введение: данное исследование основано на предпосылке о том, что традиционная архитектура представляет собой здания, построенные из природных местных материалов. Эти сооружения спроектированы так, чтобы адаптироваться к изменениям окружающей среды, то есть обеспечивать экологическую устойчивость, за счет продуманного внешнего облика. Проблематика исследования заключается в негативных последствиях использования современных промышленных строительных материалов. Эти материалы зачастую дороги, требуют значительных энергетических затрат на производство и нуждаются в искусственных системах для обеспечения теплового комфорта внутри помещений. В связи с этим исследование направлено на раскрытие потенциала природных материалов в архитектурном проектировании — изучение их свойств, климатической эффективности, конструкционной прочности и строительных систем, в которых они используются — с целью снижения высокого энергопотребления. **Также исследование ставит своей задачей** анализ характеристик и эксплуатационных свойств природных строительных материалов, выявление их постоянных и переменных параметров, а также определение областей их архитектурного и конструкционного применения. **Результаты:** Используя преимущества окружающей среды, данная работа стремится обосновать целесообразность применения природных материалов в устойчивом строительстве. Методология исследования сочетает описательный и аналитический подходы в целях обоснования экономически выгодного и устойчивого использования природных материалов в архитектуре.

Ключевые слова: экологическая устойчивость; национальная архитектура; традиционная архитектура; каршиф; бамбук.

USING DIGITAL SOFTWARE TO DESIGN INTERACTIVE SMART CANOPIES FOR THE OUTDOOR ENVIRONMENT

Ayam Sh. Altameemi¹, Adil M. Jabbar^{2*}

¹Architectural Engineering Department, Engineering College, Wasit University, 52001, Al Kut, Iraq

²Civil Engineering Department, Engineering College, Wasit University, 52001, Al Kut, Iraq

*Corresponding author's email: adilmahdi@uowasit.edu.iq

Abstract

Introduction: Canopies can serve as valuable elements in the environment when designed to harmonize with their surroundings. Moreover, incorporating recyclable materials in their construction can enhance both their aesthetic appeal and environmental ecological integrity. **This study focuses** on the design and implementation of a responsive canopy that adapts to environmental conditions by employing advanced digital design software. It also aims to promote sustainability through the use of recycled materials, thereby contributing to environmental preservation and reducing negative impacts.

Methods: The canopy consists of a skin supported by a series of connected forms and features six circular mirrors that rotate about an axis to change their orientation. This innovative approach to intelligent and dynamic skin design is intended to optimize light management and control solar radiation. The portable modules are designed using Grasshopper and Rhinoceros software, in conjunction with Arduino and Firefly, ensuring a seamless integration between physical design and functional operation. These modules are programmed to close during the day and open at night, enabling effective responses to environmental changes. **Results:** The design encourages interactive engagement between the installation and its surroundings by utilizing reflective materials, enhancing both its aesthetic appeal and functional performance. However, it is important to note that the mechanisms controlling the mirror movements present certain functional challenges, requiring ongoing maintenance to ensure optimal performance.

Keywords: smart canopy; Grasshopper and Rhino software; Arduino; Firefly software; digital architecture; environmental response.

Introduction

Architecture merges technical skills with humanistic disciplines such as philosophy and engineering. A professional architect can propose practical solutions that result in attractive and functional designs, though the best option is not always the cheapest or most visually appealing (Mahmoodi, 2001). Debates surrounding appropriate structural forms have emerged in response to significant technological advances over the past two decades. This period, often referred to as the digital revolution, emphasizes the integration of human imagination with digital architectural technologies (Malkin, 2015; Spiridonidis and Voyatzaki, 2009).

The digital era has particularly influenced the contemporary architectural landscape, giving rise to digital architecture. This paradigm shift has introduced innovative concepts in both form and content, driven by advanced technological capabilities. The use of high technology in modern construction has opened new avenues for architectural form-making, structural design, and construction processes. It has also enabled the exploration of novel relationships between architectural form and structure through digital modeling (Petrova, 2017).

Integrating technology into traditional architectural forms is becoming increasingly important in today's rapidly evolving urban context. Smart canopies

with interactive digital features represent a fusion of architecture, environmental design, and digital innovation. These structures serve more than just functional purposes; they have the potential to transform outdoor spaces into dynamic environments that respond to user needs and environmental conditions.

The emergence of advanced digital design software has revolutionized the way architects and designers conceptualize and implement smart canopy systems. These tools enable the development of complex models, simulations, and visualizations, allowing for the exploration of interactive features such as lighting, sensors, and responsive materials. By leveraging these technologies, architects can design canopies that not only provide shade and shelter but also engage users through interactive displays, environmental monitoring, and adaptive features.

This approach supports sustainable design strategies, as smart canopies can be programmed to optimize energy consumption, enhance user comfort, and foster social interaction. As urban areas continue to expand and the demand for innovative public spaces increases, the role of digital software in the design of interactive smart canopies will be essential in shaping the future of outdoor environments. Through the integration of technology and creativity, such spaces can enhance quality of

life, promote community engagement, and adapt to the evolving needs of the environment.

Digital Architecture Importance Review

Globalization and the digital revolution have given rise to concepts referred to as digital forms, which have spread across many disciplines. The idea of contemporary formative theories — which respond to the demands of the modern era by incorporating current theories and trends — includes the philosophy and mindset behind digital forms (Bahlol, 2014).

Digital architecture involves the use of computer processes to design, control, and modify architectural forms. These processes can simulate motion and manipulate forms in a virtual environment that closely mirrors the physical world. This capability allows designers to define, create, and adapt forms in ways that were previously impossible. In digital architecture, a structure is no longer viewed merely as a static frame, as it was in traditional design. Instead, it is conceptualized as a dynamic system, often compared to a living organism imbued with a sense of spirit (Ahmad Fakhrey Farhat, 2021).

Digital architecture also has the potential to bridge Indigenous cultures with advanced technologies used in contemporary architecture and urban planning (Ganji Kheybari et al., 2015; Mahdavinejad, 2020). It is, therefore, regarded as a tool that facilitates and accelerates innovative artistic expression beyond the limitations of traditional methods. From this perspective, computer software can integrate elements and unify structural components, enabling a more fluid interaction between time and space (Ahmad Fakhrey Farhat, 2021; Lienhard and Gengnagel, 2018).

Reducing energy consumption and enhancing human comfort are two fundamental goals of smart building design. A critical topic in this domain is how a building responds to the needs of its users. Such responsiveness may be achieved through mechanical devices or adaptive systems, such as kinetic structural elements that can alter their form and perform intelligent interactions within the built environment — often at minimal cost (Bahlol, 2014). The potential of contemporary digital technologies goes far beyond creating imaginative architectural forms. Their influence extends to building techniques and materials. Digital technology has enabled the development of advanced, innovative materials and has facilitated the integration of traditional materials with microelectronic systems, thereby broadening the scope of architectural possibilities (Digrado et al., 2020).

Intellectual Source of Digital Architecture

Advancements in computer science at the end of the 20th century have significantly affected various aspects of human civilization. In parallel, architectural design has evolved alongside these developments, becoming a crucial medium through which climatic

and environmental elements are integrated across multiple disciplines during the digital revolution. This revolution represents the successful convergence of numerous technological innovations (Yang et al., 2023).

The global renewal of digital technologies has given rise to diverse structural systems, each with its own construction methods, materials, forms, functions, and techniques. This evolution reflects the profound impact of the digital revolution. According to recent guidelines for redefining architectural vocabulary (Al-Busaidi and Mohatram, 2020), the building and construction sector has become increasingly interconnected due to ongoing digital advancements. Moreover, digital tools have enabled the creation of geometric forms that cannot be produced using traditional manufacturing techniques (Prado et al., 2019). Digital architecture has transformed the very concept of a building. No longer perceived merely as a static structure, a building is now conceived as a dynamic entity (Şencan, 2023). A key approach within this new paradigm is parametric design technology, which relies on algorithmic thinking to manage and coordinate diverse sets of data. This information is translated into equations or graphs that are applied to the design process, resulting in shapes that are not only efficient and harmonious but also responsive to natural conditions. These forms are developed for specific functions, allowing for the creation of complex, dynamic, and organically structured designs in a systematic manner (Lee et al., 2021). The design process begins with the architect's view of life, which is then materialized using various digital tools and applications such as Autodesk 3ds Max, Grasshopper, and Rhinoceros (Rhino). These programs enable the precise generation of digital designs, including spatially fluid parametric forms whose geometries evolve through a set of mathematical algorithms. These algorithms often involve highly complex equations that cannot be solved through human cognitive capacity alone. Instead, they are executed by computer systems that generate the desired final form through advanced parametric logic (Lagios et al., 2010).

Analysis of Similar Existing Models

Canopies come in various shapes and types. However, it is desirable to be movable to adapt to its optimal functionality. Key factors in canopy design include appropriate size, suitable materials, responsiveness to environmental conditions, aesthetic appeal, lightweight construction, cost-effectiveness, and the ability to create comfortable environmental conditions (Dasari et al., 2023; Nagy and Katona, 2020). It is also essential to consider practical applications and environmental influences. Additionally, addressing psychological comfort is vital for user satisfaction and long-term usability. Therefore, selecting materials that effectively insulate against moisture and heat is crucial.

Elytra Filament Pavilion, Victoria and Albert Museum

The Elytra Filament Pavilion showcases how architectural design can be integrated with civil, environmental, and production engineering to create a unique spatial structure. Rather than presenting a static form, this pavilion exemplifies a dynamic and evolving design. It applies lightweight structural materials inspired by natural forms. The project is the result of four years of research that blends architectural principles with construction techniques and biomimicry. The concept of the canopy draws inspiration from the shape of elytra — the protective front wings of flying beetles. These were recreated using fiber-based structures. The pavilion's composite structure consists of two primary components: the canopy cells and the columns that connect the canopy to the ground, as shown in Fig. 1.

The load-bearing material used in both components is a transparent fiberglass reinforced with black carbon fibers. Each canopy cell is distinguished by the orientation and density of its fiber arrays, which are calculated to meet specific load-bearing requirements. One of the most notable features of these cells is their lightweight composition, which reduces the column weight by approximately 3 kg per square meter. The fiber-based shading not only lightens the structure but also enables measurement of internal forces within the system. The structural system of the canopy responds interactively — it can move, remain stationary, or close as needed. Additionally, air humidity and wind fluctuations, which depend on temperature and are determined by thermal imaging parameters, alter the necessary orientation of the canopy to adapt to the environment as needed (Mingallon, 2012; Shareef and Al-Darraj, 2022).

Advantages of this responsive canopy include environmental adaptability, inspiration from natural systems, transparency, flexibility, lightweight design, multifunctionality, and attention to user needs and environmental well-being. Furthermore, the pavilion

is scalable and can be expanded to accommodate future design visions (Egi and Eyceyurt, 2022).

Research Project Pavilion, Stuttgart

In the Bioplastic Facade research project, a team of academics and students from the Department of Building and Construction at the Faculty of Architecture, University of Stuttgart, developed a prototype for fully recyclable window coverings made of bioplastic material composed of more than 90% recyclable content (Fig. 2) (Shu et al., 2020).

The project aimed to fully leverage digital technologies to rethink conventional design and construction methods. This goal was achieved through the integration of advanced architectural design and computer engineering techniques, automated construction processes, and innovative human-machine collaboration. The project featured a bio-inspired polymer facade system, forming a thin, 145-square-meter shell shaped like a twisted horseshoe and held together with metal screws. Triangular bioplastic units were designed, precisely positioned, and assembled on a metal mesh frame to form the overall structure. Pyramidal openings and geometric patterns were fabricated using a CNC machine, as shown in Fig. 2. The resulting structure is a weather-resistant and self-supporting building envelope (Chairiyah et al., 2022; Köhler-Hammer and Knippers, 2014).

Canopy Concept: ICD/ITKE Research Pavilion

The University of Stuttgart's ICD (Institute for Computational Design and Construction) and ITKE (Institute of Building Structures and Structural Design) introduced an innovative research pavilion to demonstrate automated textile-based production techniques for constructing customized wooden shells. This project marked the first architectural application of industrial sewing techniques for wooden components, representing one of several successful research initiatives exploring computational design, modeling, and fabrication in architecture. The pavilion was a collaborative effort involving students and researchers from various fields, including architecture,



Fig. 1. Method of making the Elytra canopy (Prado et al., 2019)



Fig. 2. Interface model for durable and recyclable bioplastics, Stuttgart, 2013

engineering, biology, and paleontology (Sonntag et al., 2017). Industrial sewing was employed not only to minimize warping but also to connect multiple double-curved panels into a cohesive structural unit, as illustrated in Fig. 3. An industrial robot was used to assist in the assembly of the panels, bending each one to the required curvature and fixing it in place using sewing machines. This method enabled the industrial application of curved wooden components. However, one issue encountered during implementation

was ensuring the long-term stability of the project against wind and thermal change (Schwinn et al., 2016). The use of volumetric, curved sheet units enabled the construction of a larger architectural form using standardized sheet materials (Lienhard and Gengnagel, 2018).

Pavilion Canopy in Melbourne, Australia

This canopy is notable for its dynamic response to weather conditions and its attempt to replicate the audio-visual experience of an urban rainforest.



Fig. 3. New research pavilion with wooden shell structure (Schwinn et al., 2016)

Designed by Amanda Levete, a London-based architect, the pavilion features a stunning outdoor forest canopy designed for Melbourne. The architectural concept drew inspiration from modern marine technology. The canopy incorporates carbon fiber slats and is inspired by rose petals, designed to sway gently in the breeze. It supports a transparent roof, as illustrated in Fig. 4. Despite their delicate appearance, the “petals” were fabricated from composite materials with physical properties similar to those used in sailboats. Each petal is less than half an inch thick and measures between 10 and 16 feet in width. At the same time, the petals acted as speakers, allowing the canopy to pick up and process everyday noise. Carbon fiber speakers were integrated into the canopy structure, enabling it to respond to environmental stimuli. Rather than remaining static, the canopy moves with the wind. In motion, it resembles a semi-circular floral wall, rising with radial, petal-like shields. LED lights have been added to the speakers to enhance the visual experience. Together, the sound and light features created a vibrant viewing area, offering views of the Melbourne skyline to the north (Petrova, 2017).

Materials and Methods

Software Applied for Analysis and Design of the Experimental Canopy

Rhino 3D and Grasshopper

Rhino 3D has emerged as a preferred tool for addressing complex formal design challenges. Grasshopper, an open-source visual programming language and environment, operates within the Rhinoceros 3D application. It complements Rhino by simplifying the design process and enhancing connectivity between design components.

Grasshopper and Rhino are among the most widely used software programs in biomimetics and architecture in the globalization era (Mingallon,

2012). Grasshopper offers the unique advantage of efficiently generating a wide variety of forms and materials through mathematical and parametric calculations. It is particularly effective for translating natural inspiration into human-made technology, as it can accurately render the complexity of natural patterns in tangible forms (Dananjaya et al., 2024). The Grasshopper plugin helps develop algorithms, whereas Rhino can be used to construct models of more intuitive methods. As a result, Grasshopper and Rhino used a graphical engineering approach that can facilitate the production of models by architects without requiring them to study texts (Castro Pena et al., 2021). Grasshopper facilitates parametric and algorithmic modeling, offering countless design variations and creative possibilities. As a plugin for Rhino, it enhances Rhino’s already fast and user-friendly capabilities, making it a popular choice in many creative sectors. Together, these tools allow designers to quickly generate parametric shapes (Castro Pena et al., 2021; Shareef and Al-Darraj, 2022).

Arduino Software

Arduino is an open-source platform used to develop electronic projects. It consists of a physical programmable circuit board (microcontroller) and an Integrated Development Environment (IDE) that runs on a computer. The IDE is used to write and upload code to the Arduino board. Arduino is used extensively in interactive and robotic projects. It connects with various sensors to interact with the physical world and then processes sensor data through pre-coded logic. Based on this analysis, the Arduino board can control outputs like motors, lights, or sound devices (Manual, 2024).

Firefly Software

Firefly is a downloadable plugin for Grasshopper that bridges the digital and physical realms. It allows



Fig. 4. Pavilion in Melbourne, Australia (Petrova, 2017)

data to flow between the digital and physical worlds in real-time to enable the creation of virtual and physical prototypes with unprecedented smoothness (Mingallon, 2012). Fig. 5 shows the software components applied in this study to design the smart canopy.

Methodology for Building a Basic Prototype

Basic Steps to Create a Physical Model Simulating Engine Movement

This section outlines the tools, materials, and procedures used to build the physical models and apply electronic techniques. The process of creating the proposed model can be divided into five main stages, as described below:

Stage 1: The basic design of the dynamic units was created using the Grasshopper plugin. In this stage, the proposed movement pattern of the units was developed, with vertical motion selected as the primary movement. The rotation occurred around the vertical axis, and the proportion of opening and closing was also determined. Fig. 6 illustrates the process of designing the dynamic units, and Fig. 7 depicts the opening and closing stages.

Stage 2: This stage involved designing the sections of the physical model. Rhino software was used to create the 3D model, which helped

visualize how the dynamic units would move and how various parts would interact. Additionally, the model components were prepared for laser cutting by drawing them in 2D. The unit components and the external support structure were drawn using Rhino, as shown in Fig. 8.

Stage 3: The physical model was assembled. A 3 mm thick high-density fiberboard (HDF) was used to construct the main structure, assembled to simulate the model movement realistically. A plastic mirror — chosen for its lightweight, weather-resistant, and eco-friendly properties — was used for the dynamic elements. The parts were cut with a laser, as shown in Fig. 9. The outer plastic frame of the circular shapes served as the support structure for the moving units. Strong wire was used as the vertical axis to control the movement of the circular components. The plastic circular frame was mounted on the HDF structure for added strength and durability. The moving units were fixed in place using strong Maftol resin adhesive, and the frames were securely bonded together, as illustrated in Fig. 9.

Sensors were installed to capture light intensity readings relative to engine movement angles. The sensor unit records maximum values — typically around 1,000 — under soft daylight conditions, and

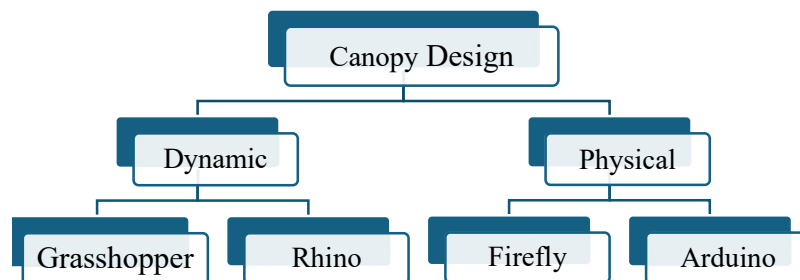


Fig. 5. Software components applied to design the canopy

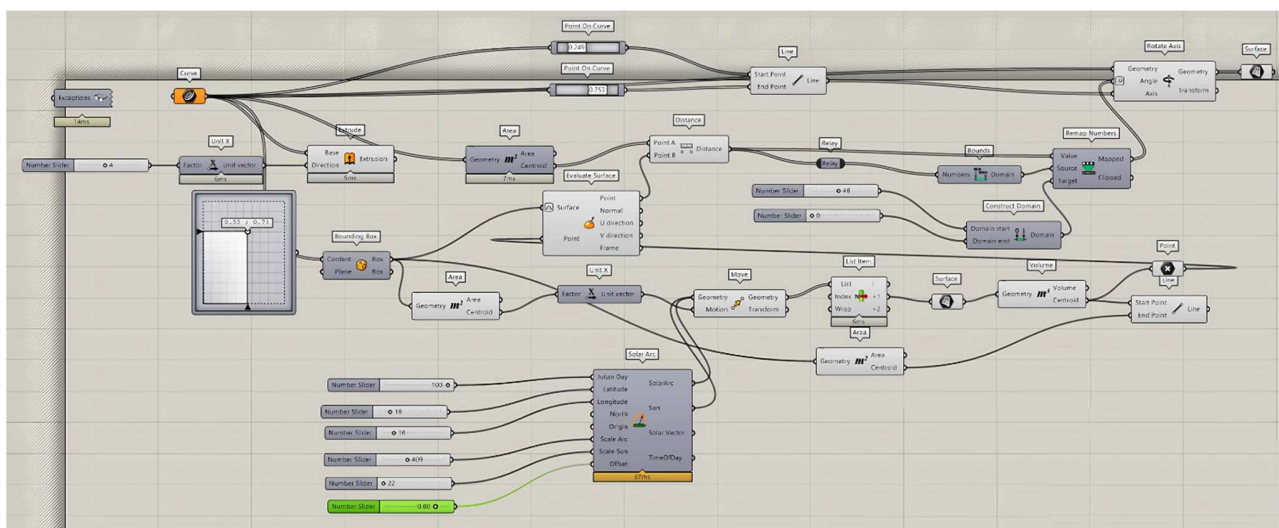


Fig. 6. Process of designing dynamic units

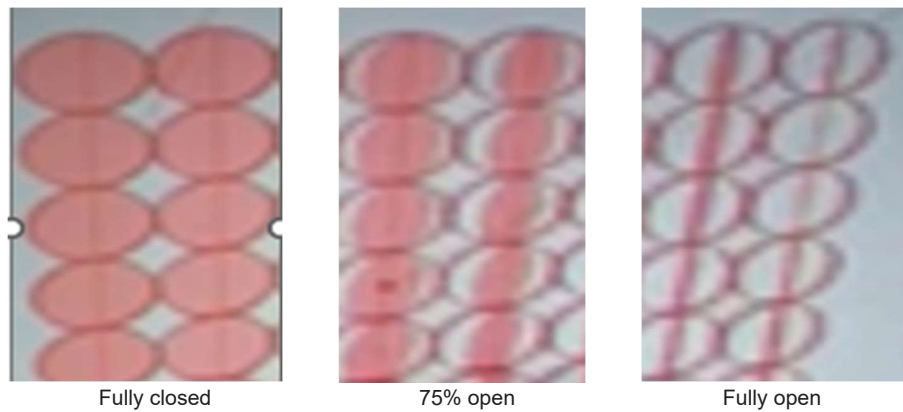


Fig. 7. Unit movement stages

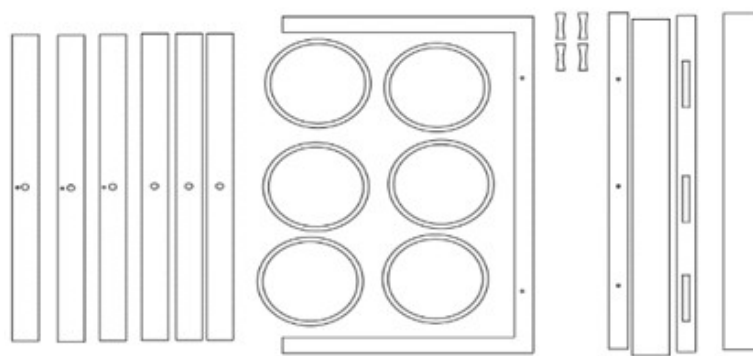


Fig. 8. Design of dynamic unit sections for laser cutting

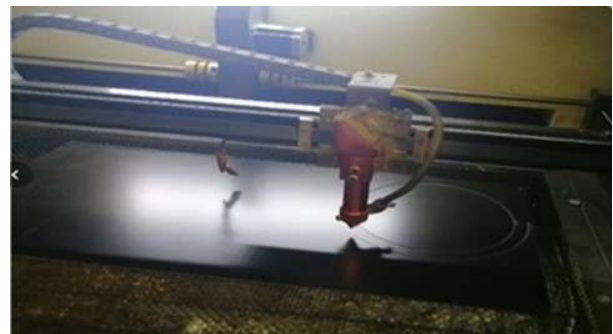


Fig. 9. Components of the physical model and dynamic units

minimum values during sunset, nighttime, or when sunlight reaches the sensor at oblique or indirect angles. An engine movement value of zero indicates that the unit is in a closed state during clear weather, while a maximum value of around 90 indicates a fully open dynamic unit during periods of darkness. These sensor units were positioned perpendicular to the external support structures.

The canopy was designed to dynamically and intelligently respond to light, adjusting its opening and closing behavior accordingly. In this study, an Arduino unit board was used to connect sensors to rotate the moving parts of the modules when the sensor senses sunlight and the major part of the

physical part that simulates the motor's movement, as illustrated in Figs. 10 and 11.

Fig. 12 shows the inputs and outputs of the Arduino board, which was connected to Grasshopper via the Firefly plugin. They were connected to the real world via this extension of the virtual world. The Arduino board continuously read sensor data and movement parameters, which were crucial for enabling dynamic responses of the engineered units to external environmental conditions. To construct the physical model, three motors were used. Each motor was connected to a vertical axis, with one side linked to the motor and the other to the Arduino board (Fig. 13). Using Firefly, the physical



Fig. 10. Steps in the physical model building process



Fig. 11. Configuration of moving units

model was linked to numerical readings, and motor movement was programmed to operate between 0 and 90 degrees. Based on the sensor readings, the motors adjusted the position of the units accordingly. To move three motors and provide power, an input voltage of 12 Volt was used for the motors because the output voltage of the Arduino board was 3.3 V and 5 V, whereas the motors with low power and voltage did not respond to the structure movement.

The dynamic units rotate along a vertical axis, starting from a 0-degree angle — which represents the fully closed position during daytime — up to a 90-degree angle, indicating the fully open position at night or under cloudy weather conditions. Fig. 14 illustrates the final form of the model.

Stage 4: Identifying the electronic components required to connect and operate the physical model. Various physical innovation tools were used to simulate the motor-driven movement of the proposed dynamic interface, as illustrated in Fig.15.

Stage 5: A method was developed to adapt the canopy system to variable weather conditions by using an Arduino control board. This enabled real-time interaction between environmental conditions and simulation software, allowing the geometric form of the canopy to adjust based on the sun's orientation. An LDR (Light Dependent Resistor) sensor was incorporated to monitor light intensity,

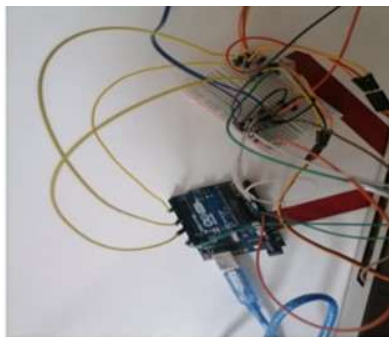


Fig. 12. Inputs and outputs of the Arduino control board connected to Grasshopper

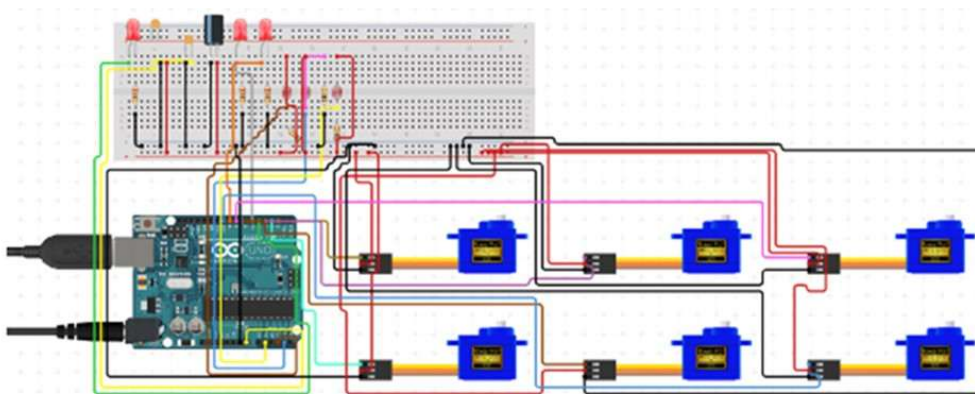


Fig. 13. Electrical circuit simulation of the physical model, showing motor and sensor connections to the Arduino board



Fig. 14. Final form of the composite material configuration

with its data linked to the motor's movement angle. This process utilized a Remap function to filter the maximum and minimum light readings from the sensors. The corresponding minimum and maximum angles of servo motor movement were then entered into the target section. Fig. 16 illustrates the reset parameters used for reading light intensity.

The highest sensor reading from the simulation under clear and sunny conditions is 850, while lower values corresponds to readings under cloudy skies or at night. For the servo motor, the lowest movement value indicates that the modules are closed — typically when sunlight is directly vertical on the dynamic units during clear weather. A value








Servomotors MG90S	Arduino Uno
	
Jumper Wire	Breadboard
	
Adapter 5 volts 3 amps	Resistance
	
LDR sensor	
	

Fig. 15. Physical tools used to build the physical model

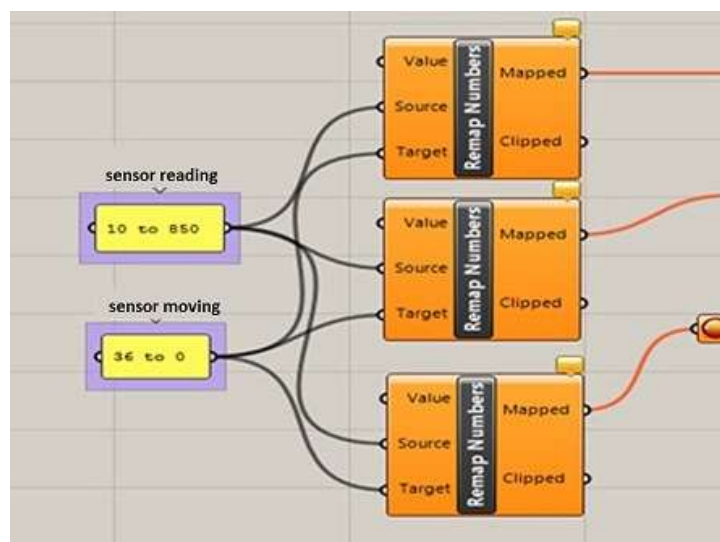


Fig. 16. Reset parameters for reading the light and motion sensor values

of 36 represents the maximum angle of servo motor movement. The study of the motor's motion and the behavior of the dynamic units in the physical model demonstrated that at an angle of 36 degrees, the units are fully open and oriented perpendicular to the supporting structure. When the modules are closed, the interior lighting decreases. To address this, the designer implemented a mechanism where reduced interior lighting causes the LED to glow more brightly. Conversely, when interior lighting is sufficient, the LED brightness decreases — eventually reaching zero — based on the external light readings. Fig. 17 illustrates the minimum and maximum LED reading values.

The controller board is connected to Grasshopper via the Firefly plugin. Fig. 18 depicts the inputs and outputs of the Arduino board: the sensor module readings act as primary inputs of the light intensity and the motor movement values are the main outputs as a response to the sensor's action. Each motor operates independently, and the same process is applied to control the corresponding LED.

Grasshopper was used to design the final virtual 3D canopy form. The Lumion program was then

utilized to render the final visual representation of the design (Fig. 19). Fig. 20 shows a 3D conceptual visualization of the canopy.

Results and Discussion

Rhino 3D and Grasshopper Plugin

When using Rhino 3D for designing smart canopies, its most significant feature is arguably its parametric modeling capabilities, especially when integrated with the Grasshopper plugin. Grasshopper enables architects to create algorithms that define relationships between various design components — an essential function for smart canopies, which must often adapt to environmental factors such as daylight, wind, and load conditions. Grasshopper's parametric tools provide real-time visual feedback, allowing designers to quickly and efficiently explore multiple design iterations. This capability is particularly valuable for optimizing the form and functionality of canopies based on specific performance criteria.

Additionally, Grasshopper can be linked to external data sources, allowing designers to incorporate real-time environmental data into their models. This feature is crucial for developing

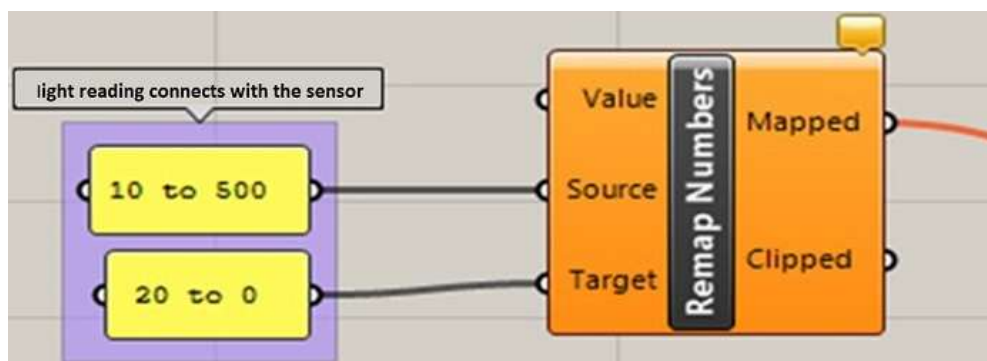


Fig. 17. Minimum and maximum LED reading values

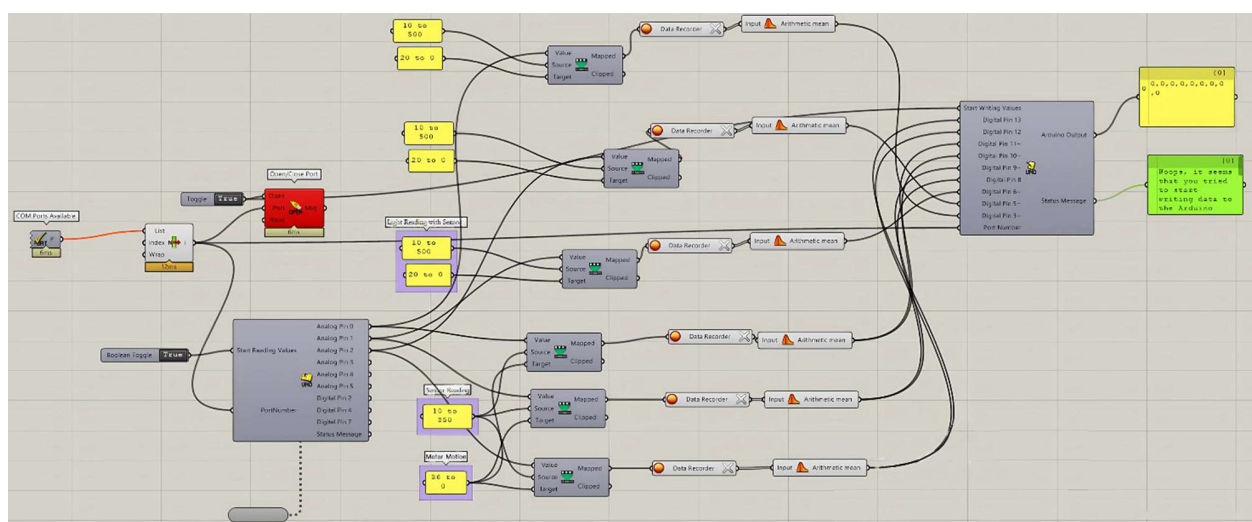


Fig. 18. Arduino board definition strategy in Grasshopper

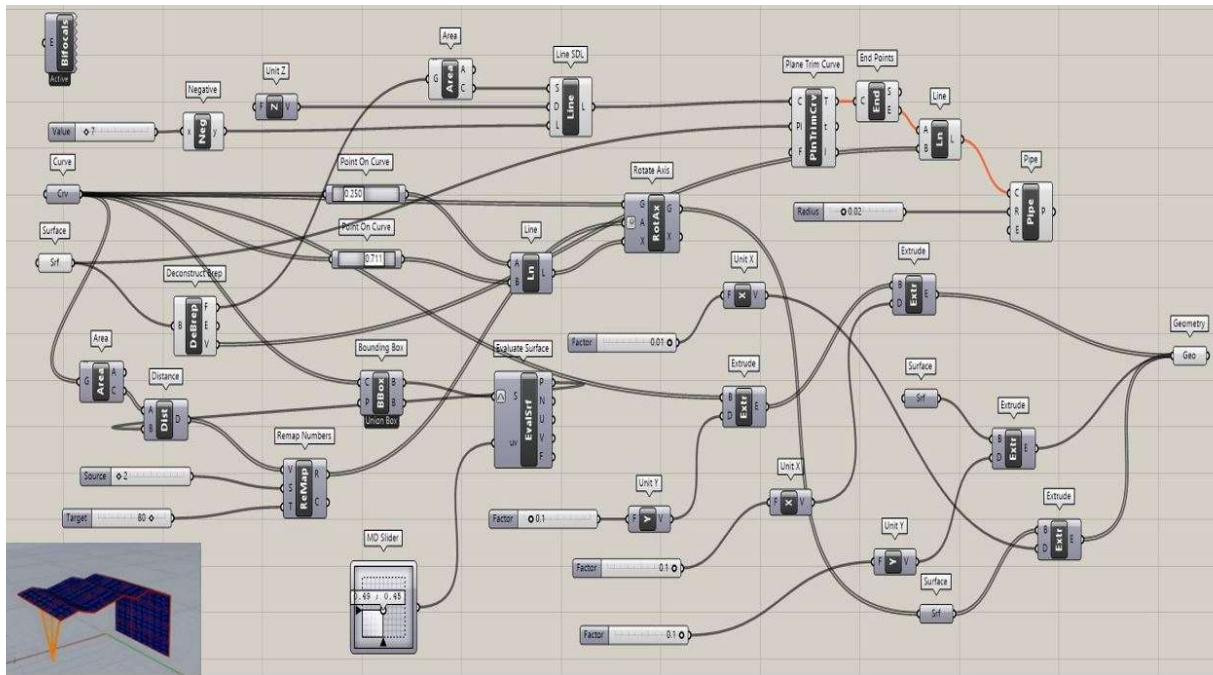


Fig. 19. Final design of the canopy using the Grasshopper plugin



Fig. 20. 3D conceptual visualization of the canopy

canopies that dynamically respond to changing weather conditions and user requirements. Its powerful handling of curves and surfaces also supports the design of complex, organic forms that are often desired in contemporary architecture.

Moreover, Grasshopper automates repetitive modeling tasks, allowing architects to focus more on creative aspects of design rather than manual adjustments.

Overall, Rhino's compatibility with a wide range of tools and plugins enhances its versatility, enabling seamless integration with structural analysis software and rendering tools that are essential for improving the performance of smart canopies.

Arduino Software

When using Arduino to manage a canopy system, the connection of sensors and motors can significantly affect the system's efficiency,

responsiveness, and reliability. Several key factors influence these performance aspects:

1. Connection Methods and Wiring Configuration: Sensors and motors can be connected using either digital or analog signals. Digital signals offer clear open/close states, making them easier to implement, while analog connections provide more detailed data — such as the precise canopy angle — but require more complex processing.

There are two primary wiring configurations: star and daisy chain. In a star connection, each sensor and motor links directly to the Arduino, whereas, in a daisy chain configuration, the tools are connected in series which can impact response time and troubleshooting.

2. Sensor Integration: The effectiveness of sensor integration depends on the sensor type and debouncing technique. Limit switches, used to detect fully open or closed positions, can provide

reliable feedback. Proximity sensors help detect obstructions and enhance safety. Debouncing — implemented in software — is essential to avoid false signals caused by mechanical switch noise during transitions.

3. *Motor Control*: This depends on the type of motor and its associated driver circuit. Common motor types used with Arduino include DC motors, stepper motors, and servo motors. The selection affects precision and power consumption. Servo motors provide accurate positioning, while DC motors require additional feedback mechanisms. Using appropriate motor driver circuits allows precise control over motor direction and speed, which directly affects the opening and closing speed of the canopy.

Proposed Site for the Canopy

The proposed location for this project is a temperate climate with an aesthetically pleasing environment, where the canopy's mirrored surfaces can reflect the surrounding beauty. The smart canopy is designed to enhance user experience by dynamically responding to lighting conditions, enabling effective control of sun exposure and shade. This design aims to improve environmental comfort while aligning with community expectations. Inspired by natural interaction systems, the canopy continuously adapts to changing conditions and the needs of outdoor users. Its functionality allows for shape modification through flexible materials, ensuring structural integrity throughout its operational life.

Conclusions

This study discussed the design and implementation of smart canopies using the computer programs Grasshopper, Arduino, and Lumion to blend aesthetic qualities with advanced technology, resulting in a practical design that is visually striking and in harmony with the surrounding environment. The following conclusions can be drawn:

1. Using lightweight natural materials such as carbon, cellulose, and glass fibers is an effective

approach for producing smart canopies that respond to environmental factors like light, wind, and humidity through sensors controlling canopy movement. Advantages of this responsive canopy include environmental adaptability, inspiration from natural systems, transparency, flexibility, lightweight design, multifunctionality, and attention to user needs and environmental well-being.

2. Recycled materials can be used to manufacture smart canopy membranes, providing environmentally friendly and lightweight solutions.

3. Employing digital software such as Grasshopper and Rhino for intelligent canopy design offers significant benefits. These tools enable complex parametric modeling, allowing architects to explore creative shapes and configurations that respond dynamically to environmental conditions. The integration of real-time data supports adaptive configurations, enhancing both functionality and sustainability.

4. The combined capabilities of these software programs streamline the design process and facilitate more effective interaction among users. Using Grasshopper and Rhino improves both the aesthetic and functional aspects of smart canopies, contributing to more sustainable and responsive architectural solutions.

5. Smart canopies can be designed to mimic the interactive behaviors observed in living organisms, enabling them to continuously adjust to changing environmental conditions and the needs of outdoor users.

6. The design concept can originate from the site itself, reflecting the exterior environment of the implemented design and emphasizing the connection between human heritage and nature.

Data Availability Statement

The data supporting the findings of this study are available from Ayam Sh. Altameemi upon reasonable request.

References

- Ahmad Fakhrey Farhat, M. (2021). Digital architecture and its impact on modeling of interior design of spaces. *International Journal of Architectural Engineering and Urban Research*, Vol. 4, Issue 1, pp. 226–260. DOI: 10.21608/ijaeur.2021.217858.
- Al-Busaidi, M. S. and Mohatram, M. (2020). Designing an automatic awning system powered by solar energy. *International Journal of Electrical and Electronics Research*, Vol. 8, Issue 2, pp. 29–37.
- Arduino Mauul. (2025). *The Lancet Arduino UNO R3 User Manual SKU: A000066 Description*. [online] Available at: <https://docs.arduino.cc/hardware/uno-rev3> [Access Date: March 26, 2025].
- Bahlol, W. S. E. (2014). The impact of digital revolution on the field of architectural function and form. *Journal of Urban Research*, Vol. 12, pp. 1–12.
- Castro Pena, M. L., Carballal, A., Rodríguez-Fernández, N., Santos, I., and Romero, J. (2021). Artificial intelligence applied to conceptual design. A review of its use in architecture. *Automation in Construction*, Vol. 124. DOI: 10.1016/j.autcon.2021.103550.
- Chairiyah, R., Yetti, A. E., and Pujiyanti, I. (2022). The Grasshopper+Rhino for 3D modelling in Indonesian's education of biomimetic architecture. In: Satwiko, P., Khaerunnisa, and Sekarlangit, N. (eds.). *Proceedings of the International Webinar on Digital Architecture 2021 (IWEDA 2021)*, pp. 223–229. DOI: 10.2991/assehr.k.220703.041.
- Dananjaya, S. A. V., Chevali, V. S., Dear, J. P., Potluri, P., and Abeykoon, C. (2024). 3D printing of biodegradable polymers and their composites – current state-of-the-art, properties, applications, and machine learning for potential future applications. *Progress in Materials Science*, Vol. 146, 101336. DOI: 10.1016/j.pmatsci.2024.101336.
- Dasari, S. K., Fantuzzi, N., Trovalusci, P., Panei, R., and Pingaro, M. (2023). Optimal design of a canopy using parametric structural design and a genetic algorithm. *Symmetry*, Vol. 15, issue 1, 142. DOI: 10.3390/sym15010142.
- Digrado, A., Mitchell, N. G., Montes, C. M., Dirvanskyte, P., and Ainsworth, E. A. (2020). Assessing diversity in canopy architecture, photosynthesis, and water-use efficiency in a cowpea magic population. *Food and Energy Security*, Vol. 9, Issue 4, e236. DOI: 10.1002/fes3.236.
- Egi, Y. and Eyceyurt, E. (2022). 3D point cloud-based tree canopy visualization for a smart deployment of mobile communication systems. In: Shirowzhan, S. (ed.). *Data Science, Data Visualization, and Digital Twins*, pp. 1–19. DOI: 10.5772/intechopen.96179.
- Ganji Kheybari, A., Diba, D., Mahdavinejad, M., and Shahcheraghi, A. (2015). Algorithmic design of “Palekane” in order to increase efficiency of daylight in buildings. *Armanshahr Architecture & Urban Development*, Vol. 8, pp. 35–52.
- Köhler-Hammer, C. and Knippers, J. (2014). Arbo Skin Fassaden-Mock up: Fassaden aus dauerhaften und rezyklierfähigen Biokunststoffen. *Fassade/Façade, Schweizerische Fachzeitschrift für Fenster- und Fassadenbau*, No. 1, pp. 9–12.
- Lagios, K., Niemasz, J., and Reinhart, C. F. (2010). Animated building performance simulation (ABPS) – linking Rhinoceros/Grasshopper with Radiance/Daysim. In: *Fourth National Conference of IBPSA-USA – SimBuild 2010*, New York City, New York, August 11–13, 2010, pp. 321–327.
- Lee, J. H., Ostwald, M. J., and Kim, M. J. (2021). Characterizing smart environments as interactive and collective platforms: a review of the key behaviors of responsive architecture. *Sensors*, Vol. 21, Issue 10, 3417. DOI: 10.3390/s21103417.
- Lienhard, J., and Gengnagel, C. (2018). Recent developments in bending-active structures. In: Mueller, C. and Adriaenssens, S. (eds.). *Proceedings of the IASS Annual Symposium 2018. Creativity in Structural Design*, July 16–20, 2018, MIT, Boston, USA, pp. 1–8.
- Mahdavinejad, M. (2020). Designerly approach to energy efficiency in high-performance architecture theory. *Basic Studies and New Technologies of Architecture and Planning*, Vol. 10, Issue 2, pp. 75–83.
- Mahmoodi, A. S. M. (2001). *The design process in architecture, a pedagogic approach using interactive thinking*. PhD Thesis (Philosophy), University of Leeds, School of Civil Engineering, pp. 353.
- Malkin, B. (2015). *Architecture and engineering in business and IT - tailored, through the use of analogy, to achieve success in large information technology projects*. Marder, SA: Enterprise Engineering Australia, 56 p. DOI: 10.13140/RG.2.1.4333.8727.
- Mingallon, M. (2012). *Introduction to Grasshopper for Rhinoceros*. Montreal: McGill School of Architecture. [online] Available at: https://www.academia.edu/41611450/Introduction_to_Grasshopper_for_Rhinoceros [Access Date: March 26, 2025].
- Nagy, M. and Katona, V. (2020). Soft folding: A morphogenetic approach to bio-based fibrous construction materials. *New Design Ideas*, Vol. 4, No. 2, pp. 85–97.
- Petrova, M. (2017). Design for ephemerality – idiosyncrasy and challenges. *New Trends and Issues Proceedings on Humanities and Social Sciences*, Vol. 4, Issue 11, pp. 259–272. DOI: 10.18844/prosoc.v4i11.2882.
- Prado, M., Dörstelmann, M., Menges, A., Solly, J., and Knippers, J. (2019). Elytra filament pavilion: robotic filament winding for structural composite building systems. *Fabricate 2017*, pp. 224–231. DOI: 10.2307/j.ctt1n7qkg7.35.

- Schwinn, T., Krieg, O., and Menges, A. (2016). Robotic sewing: a textile approach towards the computational design and fabrication of lightweight timber shells, In: Arbor, A. (ed.). *Posthuman Frontiers: Data, Designers, and Cognitive Machines, Proceedings of the 36th Conference of the Association for Computer Aided Design in Architecture (ACADIA)*, pp. 224–233.
- Shareef, A. and Al-Darraj, S. (2022). Grasshopper optimization algorithm based path planning for autonomous mobile robot. *Bulletin of Electrical Engineering and Informatics*, Vol. 11, No. 6, pp. 3551–3561. DOI: 10.11591/eei.v11i6.4098.
- Shu, Q., Middleton, W., Dörstelmann, M., Santucci, D., and Ludwig, F. (2020). Urban microclimate canopy: design, manufacture, installation, and growth simulation of a living architecture prototype. *Sustainability*, Vol. 12, Issue 15, 6004. DOI: 10.3390/su12156004.
- Sonntag, D., Bechert, S., and Knippers, J. (2017). Biomimetic timber shells made of bending-active segments. *International Journal of Space Structures*, Vol. 32, Issue 3–4, pp. 149–159. DOI: 10.1177/0266351117746266.
- Spiridonidis, C. and Voyatzaki, M. (eds.) (2009). *Architectural design and construction education - experimentation towards integration*. Thessaloniki: Art Of Text SA, 617 p.
- Şencan, İ. (2023). Progeny : a Grasshopper plug-in that augments cellular Automata algorithms for 3D form explorations. *Architecture and Planning Journal (APJ)*, Vol. 28, Issue 3, 12. DOI: 10.54729/2789-8547.1207.
- Yang, B., Yang, S., Zhu, X., Qi, M., Li, H., Lv, Z., Cheng, X., and Wang, F. (2023). Computer vision technology for monitoring of indoor and outdoor environments and HVAC equipment: a review. *Sensors*, Vol. 23, Issue 13, 6186. DOI: 10.3390/s23136186.

ИСПОЛЬЗОВАНИЕ ПРОГРАММНОГО ОБЕСПЕЧЕНИЯ ДЛЯ ПРОЕКТИРОВАНИЯ НАРУЖНЫХ ИНТЕРАКТИВНЫХ УМНЫХ НАВЕСОВ

Аям Ш. Альтамими¹, Адиль М. Джаббар^{2*}

¹Кафедра архитектурного проектирования, Инженерный факультет, Васитский университет, 52001, Эль-Кут, Ирак

²Кафедра гражданского строительства, Инженерный факультет, Васитский университет, 52001, Эль-Кут, Ирак

*E-mail: adilmahdi@uowasit.edu.iq

Аннотация

Введение. Навес может служить важным элементом окружающей среды, если он спроектирован в гармонии со своим окружением. Кроме того, использование перерабатываемых материалов в конструкции навеса может повысить как его эстетическую привлекательность, так и экологическую целостность среды. **В данном исследовании основное внимание уделяется** проектированию и реализации адаптивного навеса, который подстраивается под условия окружающей среды с помощью современного программного обеспечения. Кроме того, его цель заключается в содействии устойчивому развитию посредством использования переработанных материалов, что способствует сохранению окружающей среды и снижению негативного воздействия на нее. **Методы.** Навес состоит из оболочки, поддерживаемой рядом взаимосвязанных форм, и включает шесть круглых зеркал, которые вращаются вокруг своей оси, меняя свое положение. Данный инновационный подход к проектированию умной динамической оболочки направлен на оптимизацию регулирования освещения и инсоляции. Мобильные модули были спроектированы с использованием программ Grasshopper и Rhinoceros в сочетании с Arduino и Firefly, с обеспечением бесшовной интеграции между системой и ее функциональной работоспособностью. Модули запрограммированы так, чтобы закрываться днем и открываться ночью, что позволяет эффективно реагировать на изменения окружающей среды. **Результаты.** Дизайн обеспечивает интерактивное взаимодействие между установкой и ее окружением за счет использования отражающих материалов, улучшая как эстетическую привлекательность, так и функциональные характеристики конструкции. Однако стоит отметить, что механизмы, управляющие движением зеркал, имеют определенные сложности и требуют регулярного технического обслуживания для обеспечения оптимальной работы.

Ключевые слова: умный навес; программное обеспечение Grasshopper и Rhino; Arduino; программное обеспечение Firefly; цифровая архитектура; реакция на окружающие условия.

ASSERTING LOCAL IDENTITY IN THE PUBLIC SPHERE: A TOP-DOWN EFFORT IN THE DECENTRALIZED SURAKARTA

Ofita Purwani*, Astri Resmi Enggarswi

Universitas Sebelas Maret, Jl. Ir. Sutami 36 A, Surakarta, Indonesia, 57126

*Corresponding author's email: ofita92@yahoo.com

Abstract

Introduction: This paper focuses on the municipal government's efforts to cultivate local identity during decentralization, focusing on the case of public service buildings in the neighborhoods (*kelurahan*) of Surakarta. Surakarta has a long history of violence, which has always targeted minority groups. Therefore, identity politics are important in representation of all the city residents. **Purpose of the study:** In this paper, we examine public service buildings in Surakarta to understand how they manifest local identity. **Method:** We analyze the public buildings in Surakarta in terms of how they use identity. We took samples in each of the five Surakarta *kecamatan* and found out what kind of identity their public buildings manifest. We also interviewed stakeholders involved in the design of those buildings for clarification. The **results** reveal that the mayor played a prominent role in asserting the local identity, employing a top-down vision, which stands in contrast to the city's renowned bottom-up approach. However, the mayor's vision of identity is mainly dominated by Javanese values, even when it looks like it combines Javanese and colonial architecture. The Javanese values can be seen in the use of the *pendhapa* building for public gatherings, its location at the front part of the *kelurahan* complex, and the location of the colonial-styled building for the main office at the side or the rear. This resembles the layout of traditional Javanese architecture.

Keywords: identity; decentralization; public buildings; architecture; Surakarta.

Introduction

Identity formation has become a significant contemporary issue, as evidenced by the cases of Black Lives Matter and the removal of colonial statues, highlighting the consequences of underrepresentation within marginalized communities (Atuire, 2020). However, it is crucial to recognize that identity is not a fixed entity; rather, it is dynamic, ever-evolving, and socially constructed, making its definition complex. In multicultural communities, the pursuit of a cohesive identity can be particularly challenging, leading to questions like which identity should be represented and how to ensure acceptance among all citizens.

In the context of the city, the identity asserted by the government should accommodate all residents of the city. We argue that identity formation is inherently linked to the power structure. The shaping of identity is often influenced by those in positions of authority, and the resultant identity must align with the existing power dynamics to gain widespread acceptance. Nevertheless, this process requires utmost care and should encompass a multi-layered approach to ensure equitable representation of all citizens.

To illustrate our argument, we examine the case of *kelurahan* (neighborhood) buildings in Surakarta, Indonesia¹. These buildings were constructed between 2006 and 2012 during Mayor Jokowi's tenure, who later became the Indonesian

president. This period coincided with the onset of decentralization, prompting heightened awareness of identity, particularly at the city and district levels.

Defining identity carries inherent risks, as an accepted identity can unite society under its dominant narrative. However, such dominance is never without resistance, and the social structure, where one idea prevails over others, remains susceptible to change. These shifts in the social structure can profoundly impact society, as seen in the removal of statues linked to the Black Lives Matter movement. Once revered figures, who might have played a role in slavery centuries ago, they were previously embraced as part of the historical narrative closely entwined with identity. However, as time passes, the relevance of this narrative diminishes, leading to the statues' removal, either through consensus or by force. The marginalized communities took hold of the narrative, thereby altering the established identity.

A similar incident occurred in Surakarta when, in the 1990s, all public buildings in the city were painted yellow, signifying allegiance to the dominant political party in Indonesia, *Golongan Karya*. In response, a grassroots community led by Mudrick Sangidoe covertly repainted several buildings white to oppose the politicization of urban space (Mas' udi, 2017). This act exemplifies how defining identity must be meticulously managed to prevent such frictions and clashes.

In light of these examples, it becomes evident that the process of defining identity requires

¹ Kelurahan is the smallest governmental unit in Indonesia. For the governmental units in Indonesia, see Grillos (2017).

thoughtful navigation to strike a balance and mitigate potential conflicts that may arise from the dominance of a singular narrative. An inclusive approach that considers diverse perspectives and historical contexts can lead to a more cohesive and sustainable sense of identity within society.

Surakarta, a medium city in Central Java, Indonesia, traces its roots back to 1745 when the royal palace for the Javanese Mataram kingdom was constructed. The kingdom, considered one of Java's greatest, was compelled to relocate from Kartasura to Surakarta following a catastrophic event that befell the previous palace². Subsequently, the Giyanti treaty of 1755 divided the Mataram kingdom into two royal courts: those of Surakarta and Yogyakarta. Thus, Surakarta emerged as the capital of a new Sultanate claiming the former Mataram palace for its royal court. Despite its historical significance, the political influence of the Surakarta royal court waned during the anti-monarchy movement in 1945–1946. Nowadays, having lost its political role, the royal court serves as a cultural symbol.

However, in recent years, the royal court's status has faced challenges, particularly since the passing of King Paku Buwono XII in 2004 without appointing a clear heir. This led to internal conflicts over the throne, which remained unresolved for several years. The conflict took place not only inside the palace but also in public space. Consequently, the royal court whose role has been long reduced to symbolic, had to lose even more respect from the community. The situation was so dire that the nearby residents even resorted to reporting the court to the police, alleging that it obstructed their pass to the city. This happened after the royal court had decided to close one of its gates, which was now considered belonging to the public, to block their opponents' access to the palace.

Geographically, Surakarta lies along the banks of the Bengawan Solo River, Java's largest river. This strategic location bestowed numerous advantages upon the city, as the Bengawan Solo River served as the primary access route to the bustling port of Surabaya, a major trade hub in Java. The river's network comprised around 40 ports, facilitating the transportation of agricultural produce from the inland agrarian regions for trade with Asian and European merchants. Among these ports were those established by specific groups, such as the Chinese and Arab ports. However, the river lost its significance in the late 19th century when the Dutch developed a train network.

The existence of Chinese and Arab ports in Surakarta shows that from as early as the 18th century there were already a significant number of people of Chinese and Arab origin living in Surakarta.

² In Old Javanese, there was a belief that should a catastrophe occur, the royal palace had to be moved elsewhere.

During the Dutch colonial occupation, they typically acted as merchants and middlemen. However, the Chinese-descent community seems to have had a less fortunate position than the Arab one. The *Geger Pacinan* in the 18th century was a rebellion of Chinese-descent population against the Dutch VOC and the king of Mataram, which led to restrictions imposed on the Chinese community as a means of control. The attitude towards the Chinese community in Surakarta has been negative ever since. Surakarta witnessed more than 40 riots, which — regardless of the cause — targeted Chinese people. These includes *Geger Pacinan*, causing the Mataram capital to relocate from Kartasura to Surakarta in the 18th century. The most recent riot of 1999, although relating to the national political situation, specifically targeted the Chinese. In addition to racial tension, Surakarta is also the focal point of Islamic radicalism in Indonesia, particularly after 1998. Its root can be traced back to *Sarekat Islam*³, but it is also connected to the global populist movement. Thus, the potential for friction is both racial and religious.

This potential can be enhanced by the culture of resistance, which Mas'udi describes as rooted deeply in the collective memory of Surakarta society (Mas'udi, 2017). In the collective memory, resistance has proven to result in significant change throughout history. The anti-monarchy movement in 1945 changed the fate of Surakarta. The movement was caused by interrelated issues including the Dutch intervention in the succession, the royal court's exploitation of its people, and the attitude of the royal court and the king toward Independence. In addition, the relocation of the Indonesian capital from Batavia to Yogyakarta in 1945 was accompanied by the relocation of the radical opposition groups to Surakarta, which is only 60 km away from the new capital. Since then, the city of Surakarta has been the site for many radical movements such as the 'red' *Sarekat Islam*, the communist movement, and Islamic radicalism. This city has been popularly acknowledged as 'the short fuse city' (Mas'udi, 2017), referring to how easy it is to make a riot there.

As mentioned before, Surakarta is home to several main cultural and religious groups, including the Javanese, Chinese, Arab, Islamic, and non-Muslim communities. *Grebeg Sudiro*, an annual event, was created to foster cultural integration between the Javanese and Chinese communities, celebrating not only the anniversary of *Pasar Gedhe* but also the Chinese New Year (Purwani, 2014; Rahmatulloh et al., 2020). This event exemplifies the coexistence of the Chinese and Javanese communities. Additionally, as it involves prayers

³ This organization originated in the 20th century, when fierce competition with the Chinese unified Javanese merchants. It started as a trade organization and turned into a political entity (Shiraishi, 1990).

at the Chinese temple in Sudiroprajan (Purwani et al., 2022), it represents the non-Muslim community as well. *Parade Hadrah*, on the other hand, was established to accommodate various Islamic groups to perform *hadrah*, a form of Islamic art (Purwani, 2014, 2017), symbolizing the Islamic groups. Furthermore, the existing Islamic and Arab festival, *Haul* events (celebrations for the anniversaries of certain Islamic clerics, typically of Arab origin), have been recognized as city events representing Islamic and Arabic community by the municipal government.

The Javanese community, being the majority, is often represented by the royal courts in their rituals and cultural contributions. However, it is important to note that Javanese culture holds a dominant position throughout Indonesia, with all Indonesian presidents being Javanese. Javanese cultural products, such as batik and keris daggers, are widely regarded as representing Indonesia as a whole. Despite the diminished political power of the royal courts in Surakarta, the influence of Javanese culture remains strong, as evident in the city branding: “Solo, the Spirit of Java”, promoted by the municipal government, emphasizing Surakarta as the center of Javanese culture. Therefore, the Javanese community already enjoys ample representation.

Another group worth mentioning is the ‘low-economic class’. This group forms the basis for resistance to everyday life issues, as highlighted by Mas’udi (Mas’udi, 2017). To accommodate this group, the municipal government maintains open communication and provides essential services, including free healthcare and education. Mas’udi claims that those strategies are successful in building legitimacy for Mayor Jokowi.

The understanding of Javanese architecture is primarily rooted in the ‘traditional’ Javanese house. Within the Dutch East Indies, a debate arose between architects, notably between Wolf Schoemaker and Maclaine Pont, concerning whether the local houses could be classified as ‘architecture’. Advocates for labeling local houses as ‘architecture’, such as Maclaine Pont and Karsten, intriguingly cited buildings within the Javanese palace complex to bolster their argument⁴. They asserted that Javanese houses deserved to be recognized as ‘architecture’, and architects in the Dutch East Indies could utilize them,

Nonetheless, one challenge with local architecture is the scarcity of written literature available on the subject. Traditionally, knowledge was passed down

⁴ Maclaine Pont made a graphic analysis of several local houses including the one in the Javanese palace using Quatremère de Quincy’s theory of origin in order to make it acknowledged as ‘architecture’. Both Maclaine Pont and Karsten consistently designed buildings in the Dutch East Indies by using local architecture as the main reference. Some examples of them are Pohsarang Church, Institut Teknologi Bandung Hall, and the Sobokarti theater (de Vries and Segaar-Höweler, 2009; Jessup, 1985).

through oral tradition to succeeding generations. The first written account of Javanese architecture, known as *Kawruh Kalang*, was compiled by the royal court of Surakarta upon the request of the Dutch colonial government for the 1883 Colonial Exhibition in Amsterdam. The Javanese house, replicated to scale along with its inhabitants⁵, *Kawruh Kalang*, and the gamelan, a traditional Indonesian orchestra, was showcased at the exhibition (Bloembergen, 2006; Robertson, 2012). Although initially intended as a ‘catalog’ for the 1883 Amsterdam Colonial Exhibition, *Kawruh Kalang* became the main reference for subsequent literature on Javanese houses. Robertson (2012) observed that the 1980s literature on the national inventory project, such as Hamzuri’s, Wibowo and Dakung’s, and Ismunandar’s, heavily relied on *Kawruh Kalang*, even if it was not always cited appropriately⁶.

In this literature, Javanese architecture is defined as a complex of buildings, comprising *pendhapa*, *pringgitan*, *dalem*, and *gandhok*, arranged in a specific layout. The main buildings, *dalem* and *pendhapa*, are located in the middle of the site while *pringgitan* is the space in between them. *Dalem* or *omah jero* is the main house, while *pendhapa* is an open pavilion that mainly functions as a reception hall, or for wayang puppet performances. *Gandhok* are supporting buildings usually built around the main ones (Fig. 1). *Dalem* is usually considered to be sacred, with the most sacred part of the Javanese house, *senhong tengah*, located right in the middle of it. *Gandhok* is considered the most profane, but it is very important for day-to-day activities. Santosa (1997) identified how *gandhok* is used for everyday activities and stated that it is multifunctional. It can be used for sleeping, cooking, watching TV, receiving family guests and so on.

A study on the Javanese royal palace (kraton) shows that the flexibility of architecture can be found

⁵ Along with other local houses, as a foundation for their designs.

⁶ Robertson (2012) noted that the literature did not mention *Kawruh Kalang* as the source, but their contents are very similar to some point.

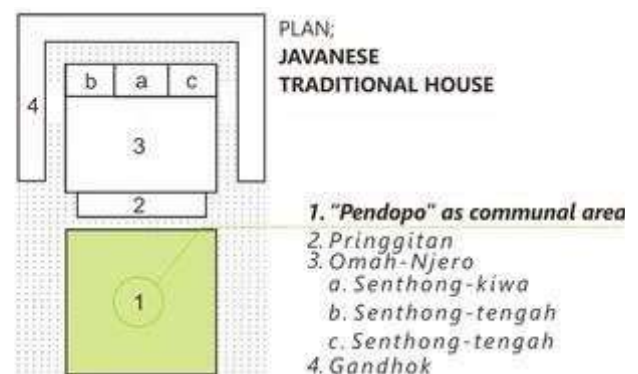


Fig. 1. The general plan of the Javanese house

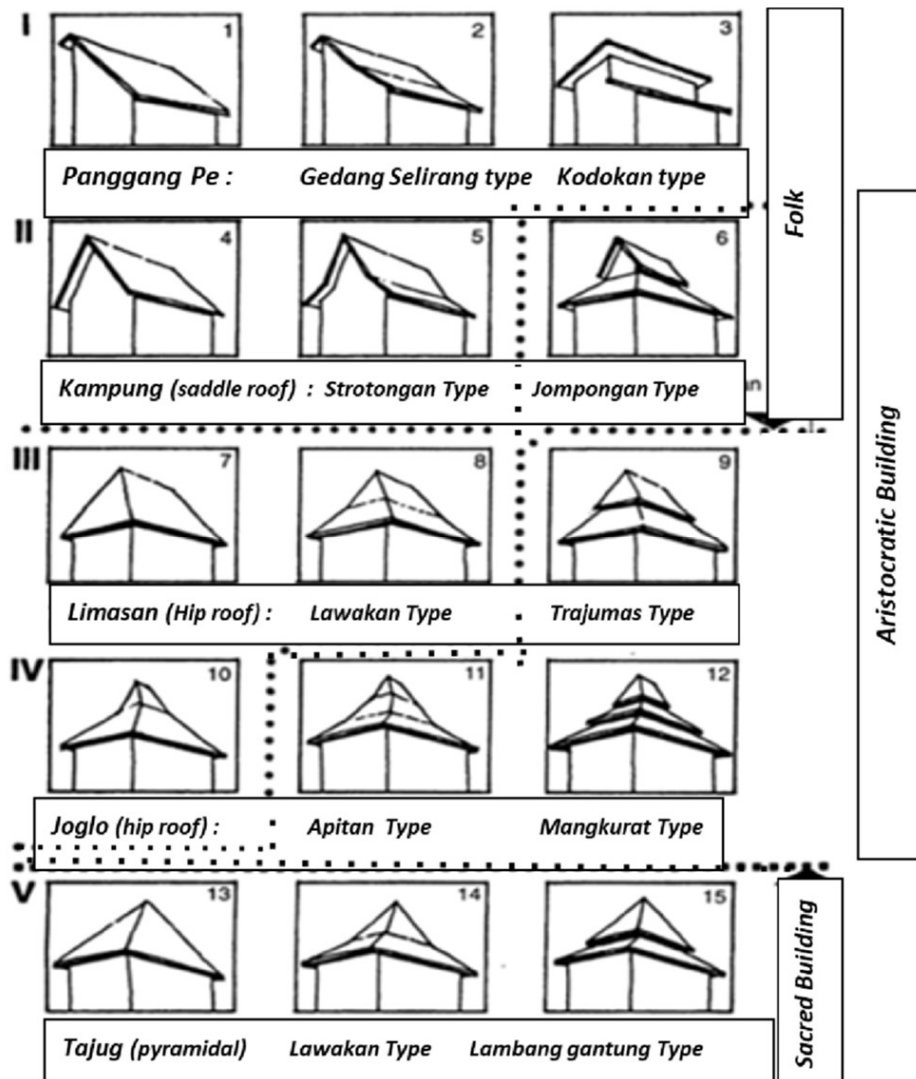


Fig. 2. The common roof types of Javanese architecture (Herwindo, 2023) signifying social status. Some types of roofs such as *joglo* can only be used by nobles or the royal family, while common people can only use *kampung* and *panggangpe* types

in the profane and peripheral areas such as the additional space of the main buildings, or supporting buildings such as *gandhok*. In case of *kraton*, the foreign architectural elements are placed at the supporting buildings, and at the extensions of the main buildings. The main buildings remain Javanese in style.

In a Javanese house, each building serves a distinct function and is characterized by a specific roof type. The main buildings, *pendhapa* and *dalem*, function as the reception hall and the main house, typically featuring a *joglo* roof⁷. Supporting buildings,

such as *pringgitan* and *gandhok*, may use *kampung* or *panggangpe* roof types (Fig. 2).

Joglo roof is considered the highest in status in Javanese houses. It has four columns at the center called *saka guru*, which support stacked beams called *tumpang sari* (Fig. 3). The roof above these *saka guru* has a steep angle, while the roof at the periphery has a more gentle slope.

The existing literature on Javanese houses holds significant importance as the primary source of Javanese architecture. These books have played a pivotal role in shaping the understanding of Javanese architecture as known today, akin to the influence that occurred in Bali. Additionally, the Indonesia Indah project, spearheaded by Tien Soeharto, the wife of president Soeharto, also played a crucial role in defining Javanese architecture. The project operated on the assumption that each province had a distinct culture, and these cultures were to

⁷ There are five main roof types in Javanese architecture: *tajug*, *joglo*, *limasan*, *kampung*, *panggangpe*. *Tajug* is usually used for a mosque, grave, or anything related to the divine. *Joglo* and *limasan* are used for important buildings; *kampung* and *panggangpe* are used for supporting buildings. However, this model is based on the noble houses that belong to the royal courts. Common people usually have a more modest model, which is described in detail by Santosa showing that it is possible for common people to use *kampung* and *panggangpe* type for their main house.

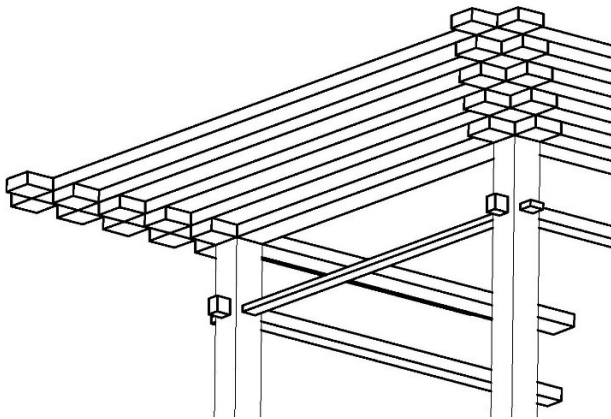


Fig. 3. The typical saka guru and *tumpeng sari* construction, where wooden beams are stacked to create an inverted pyramid. This *tumpeng sari* is usually ornamented either by carving or painting. Image source: Wibowo et al., 1998

be represented in Taman Mini Indonesia Indah, which included miniature representations of various architectural styles.

For the representation of Central Java, Taman Mini Indonesia Indah utilized the Mangkunegaran Palace as a model (*Anjungan Jawa Tengah: Taman Mini Indonesia Indah*, n.d.). This move further solidified the image of Javanese architecture, showcasing the rich cultural heritage and grandeur associated with the region's palaces and courts. From the model of the Javanese house in Taman Mini Indonesia Indah, we can see that the *pendhapa* features an additional element known as *kuncung*, serving as the front porch for horse carts and cars. This architectural element, along with other small additional structures, is a common characteristic of Javanese houses, although not always present.

Methods

This research centers around identity as expressed through the appearance of the *kelurahan* buildings. We collected data on 25 out of 54 *kelurahan* buildings in Surakarta and categorized them based on their architectural features. Additionally, we conducted interviews with four architects involved in the project to gain insight into the decision-making process concerning identity-related aspects. The reason why we took these four architects is that just these four are in charge of the design of 54 *kelurahan* buildings. To verify the data, we also utilized information from the official website of the municipal government.

The data analysis involved referring to existing discourse on Javanese architecture to establish connections between the works of literature and references that relate to the architecture of the *kelurahan* buildings. Subsequently, we examined how these connections align with the background information obtained from the interviews, providing valuable insights into the decision-making process.

Results and Discussion

The plan for the renovation of the *kelurahan* buildings in Surakarta was made by Mayor Jokowi during his first mayoral period. The construction took place between 2006 and 2012, or until the end of his term. The renovation aimed to improve public services, with a particular reference to the 'professional' bank services. In addition to that, the mayor wanted to establish a representative architectural style for the city, drawing inspiration from the existing buildings in Surakarta.

While the existing buildings in Surakarta were mostly typical modern structures, as most buildings in Surakarta are contemporary, the government decided to take precedents from buildings with traditional and colonial roots. This shows a preference for the Javanese and Western colonial styles. The other types of architecture such as Chinese, Arab, and other minority groups were ignored.

The reasons why the government preferred Javanese and colonial architecture is mainly due to the number of Javanese and colonial heritage buildings in the city. As this was a royal city, there were many inherited Javanese buildings scattered around the city, including royal palaces, public facilities, and noble houses. The city also used to be occupied by the Dutch, so there are many Dutch military buildings in the city center including the military fort, military residences, railway stations, and other public facilities. Heritage buildings of Chinese and Arab communities can only be found in a limited number, in a particular part of the city. Chinese heritage can be found around the *kelurahan* Sudiroprajan and Balong area, while Arab heritage in the form of residences can be found in *kelurahan* Pasar Kliwon.

Mayor Jokowi was directly involved in the design of each *kelurahan* building. The appointed architects had to follow some instructions on the building styles and consult the mayor directly for the design. A total of four architects were involved in designing the 54 *kelurahan* buildings during that period. All the construction was finished in 2012. Based on the interview, it was revealed that there was a 'design template' used for all of the *kelurahan* buildings. In that template, there was a public hall in the shape of Javanese *pendhapa*, and the office building in colonial style. Both of them were separated. However, the *pendhapa* was always located at the front of the whole *kelurahan* complex.

Based on our observation, out of 25 random samples of *kelurahan* buildings, most of them have two masses of buildings, one of which functions as a public hall, and another — as an office building. The office building is usually bigger than the public hall. The public hall is used for public events, while the office is used for public services and individual office rooms. When there are two main buildings for public

halls and offices, there are several basic layouts in the relation between the two buildings. If there is enough space at the site, the office building is placed at the rear of the public hall. However, when the site is too small and it is impossible to put the office building at the rear, then it is placed side by side with the public hall.

An exception to this arrangement can be found in *kelurahan* Kemlayan, Keprabon and Baluwarti. The small sites of Kemlayan and Keprabon *kelurahan* offices led to the design that consists of only one building. Meanwhile, at Baluwarti there is a compound of Javanese house buildings. The public hall takes place in the *pendhapa* building while the offices are located at *gandhok*, or the supporting buildings around the main building. The size of the office building in Baluwarti is smaller than the public hall, while in the other *kelurahan* buildings the office building is usually bigger.

In terms of architectural style, the building for a public hall is mainly Javanese. It follows the style of *pendhapa* of the Javanese house, with a *joglo* roof (with an additional *kuncung*) and 'wooden' construction. Some adjustments were made to fit the function of a public hall. The first is the addition of walls, mainly of wooden planks, and glass windows around the hall. In the original *pendhapa*, there are no walls and it is usually open on all sides. The additional wall is for blocking the dust and noise from the outside. The second is the construction materials. The original wooden buildings of the Javanese house are unattainable in the modern era, it is made of concrete, but covered in wooden panels to create an impression of wood. Some key elements of Javanese construction are still used such as the roof shape, *tumpang sari*, and wooden material. Some other

key elements such as the main columns of *saka guru* were sometimes absent (Fig. 4).

Meanwhile, the office building has a different style. It was claimed to be rooted in the colonial tradition. We can see the use of two rows of columns supporting the main porch with a pediment-like structure at the top (Fig. 5). These structures look like classical architecture but with a slight modern touch. Most of the office buildings found in the 25 samples had two floors, except for the one in Baluwarti.

The office building is for public service, the main function of the *kelurahan* building complex. The public hall has a supporting role in this compound. People go to the office building for day-to-day services such as civil registry, identification cards, and other related governmental documents. Meanwhile, people only go to the public hall only on occasional events. In this case, the office building holds more significance in function.

The *kelurahan* buildings follow the Javanese traditional house layout. The shape of *pendhapa* is used for *kelurahan*'s public halls, which function as the original Javanese house's *pendhapa*, while the second building, which is usually at the rear or the side, relating to the position of *gandhok* in the Javanese house, is intended for the *kelurahan* offices. In a traditional Javanese house, *gandhok* is the part that accommodates most day-to-day activities. Thus, putting the *kelurahan* offices in *gandhok* position fits the layout of the traditional Javanese house.

However, in terms of architectural style, the style of both buildings in the *kelurahan* building complex is different. The public hall uses the Javanese traditional style with some adjustments. The first adjustment is the addition of an enclosure to protect the *pendhapa* from dust and noise from the street.

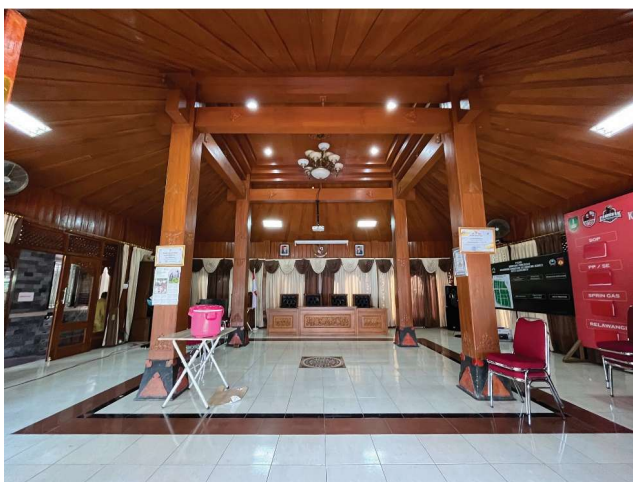


Fig. 4. The interior of public halls showing the use of 'wooden' materials. Some use *saka guru* and *tumpang sari* (left), while others only use *tumpang sari* without *saka guru* (right) revealing that those features are just ornaments. The materials used are usually concrete, with wooden tiles to make an impression of wooden posts/beams. Photos by author



Fig. 5. *Kelurahan* office building. Most of them have a similar style, with two rows of columns at the front supporting the front porch, and a pediment-like structure with a round ornament in the middle. Photos by author

The second adjustment is that in materials, as wood in certain dimensions commonly used for Javanese traditional buildings, for example, the ones for *saka guru*, is simply unaffordable. The office building is mainly modern with a classical touch, being claimed as rooted in the colonial style. Modern-style buildings are more functional and more acceptable to be used for offices. In relation to the Javanese traditional layout mentioned in the previous paragraph, it is also common for the buildings in *gandhok* position, which is at the periphery, to have the most physical and functional changes. The use of a modern classical style then, can be seen as acceptable in Javanese culture.

The use of a modern classical style for the office buildings, however, raises some questions as people of Western origin are not a minority group in Surakarta. Why modern classical? Why not the ones of minority cultures, such as Arab and Chinese, who are residents of the city? The fact that the minority groups are not represented in the *kelurahan* buildings brings a possibility of resistance, considering the city's history of violence. However, there was no resistance recorded in 11 years. This can only mean

that the use of Javanese and modern classical styles is commonly accepted by society.

The acceptance of the Javanese and modern classical architectural styles of *kelurahan* buildings as the governmental service buildings in the smallest unit in the city also means that those architectural styles are acceptable to represent the city, just like the city branding: 'The Spirit of Java'. The Javanese are the dominant cultural group. The use of the dominant group to represent the whole in the case of *kelurahan* buildings turns out to be acceptable. This brings us to the question of inclusivity. In the case of *kelurahan* buildings in Surakarta, it does not matter that they do not include minority groups in the design, but those minority groups have to be represented elsewhere, such as with essential services, as argued by Mas'udi or through cultural festivals like Grebeg Sudiro and Parade Hadrah.

Funding

This research is funded by RKAT PTNBH Universitas Sebelas Maret Fiscal Year 2023 through Research Grant Scheme (PENELITIAN HIBAH GRUP RISET-UNS) B with Research Assignment Letter Number: 30 228/UN27.22/PT.01.03/2023.

References

- Achmadi, A. (2008). The architecture of balinization. In: Herrle, P. and Wegerhoff, E. (eds.) *Architecture and Identity*. Münster: Lit Verlag, pp. 73–90.
- Anjungan Jawa Tengah: Taman Mini Indonesia Indah. (n.d.). [online] Available at: <https://tamanmini.com/anjungan/anjungan-jawa-tengah?lang=en> [Access Date: August 26, 2024].
- Atuire, C. A. (2020). Black Lives Matter and the removal of racist statues — perspectives of an African. *21: Inquiries into Art, History, and the Visual. Beiträge zur Kunstgeschichte und visuellen Kultur*, Vol. 1, No. 2, pp. 449–467. DOI: 10.11588/xxi.2020.2.76234.
- Bloembergen, M. (2006). *Colonial spectacles: the Netherlands and the Dutch East Indies at the world exhibitions, 1880–1931*. Singapore: NUS Press, 480 p.
- Cairns, S. (1997). Resurfacing wayang. In: Nalbantoglu, G. B. and Wong, C. T. (eds.) *Postcolonial Space(s)*. New York: Princeton Architectural Press, pp. 73–88.
- Carey, P. (1986). Yogyakarta: from sultanate to revolutionary capital of Indonesia. The politics of cultural survival. *Indonesia Circle. School of Oriental & African Studies. Newsletter*, Vol. 14, Issue 39, pp. 19–29. DOI: 10.1080/03062848608729628.
- Castells, M. (1999). Grassrooting the space of flows. *Urban Geography*, Vol. 20, Issue 4, pp. 294–302. DOI: 10.2747/0272-3638.20.4.294.
- de Vries, G. and Segaar-Höweler, D. (2009). *Henri Maclaine Pont. Architect, constructeur, archeoloog*. Rotterdam: Stichting BONAS, 128 p.
- Frick, H. (1997). *Pola struktural dan teknik bangunan di Indonesia*. Yogyakarta: Kanisius, 260 p.
- Grillos, T. (2017). Participatory Budgeting and the Poor: Tracing Bias in a Multi-Staged Process in Solo, Indonesia. *World Development*, Vol. 96, pp. 343–358. DOI: 10.1016/j.worlddev.2017.03.019.
- Hadiz, V. R. (2010). *Political Islam in post-authoritarian Indonesia*. Working Paper No. 74, Oxford: Centre for Research on Inequality, Human Security and Ethnicity, 38 p.
- Hamzuri (1985). *Rumah tradisional Jawa*. Jakarta: Proyek Pengembangan Museum Nasional, 180 p.
- Herwinda, R. P. (2023). A Study on the Relationship between Majapahit Temple and Joglo -nDalem Architecture as Preservation of Ancestral and Cultural Values. *Civil Engineering and Architecture*, Vol. 11, Issue 3, pp. 1355–1371. DOI: 10.13189/cea.2023.110320.
- Ismunandar, R. M. (1986). *Joglo, arsitektur rumah tradisional Jawa*. Semarang: Dahara Prize, 164 p.
- Jessup, H. (1985). Dutch architectural visions of the Indonesian tradition. *Muqarnas*, No. 3, pp. 138–161. DOI: 10.2307/1523090.
- Kusno, A. (2000). *Behind the postcolonial: architecture, urban space, and political cultures in Indonesia*. London and New York: Routledge, 250 p.
- Larson, G. D. (1987). *Prelude to revolution: Palaces and politics in Surakarta, 1912-1942* (Vol. 124). Foris Publications.
- Lavin, S. (1992). *Quatremère de Quincy and the invention of a modern language of architecture*. Cambridge: MIT Press, 350 p.
- Lombard, D. (1996). *Nusa Jawa: silang budaya kajian sejarah terpadu: Jaringan Asia* (Vol. 2). Jakarta: Gramedia Pustaka Utama, 498 p.
- Lukito, Y. N. (2022). Historical and cultural negotiations in Taman Mini Indonesia Indah: beyond the utopia of 'unity in diversity'. *Journal of Southeast Asian Studies*, Vol. 53, Issue 4, pp. 762–785. DOI: 10.1017/S0022463422000844.
- Mas'udi, W. (2017). *Creating legitimacy in decentralized Indonesia: Joko 'Jokowi' Widodo's path to legitimacy in Solo, 2005–2012*. PhD Thesis in the Faculty of Arts, Asia Institute, University of Melbourne.
- Miksic, J. (2004). *Karaton Surakarta*. Jakarta: Yayasan Pawiyatan Kabudayan Karaton Surakarta, 156 p.
- Pemberton, J. (1994). *On the subject of "Java"*. Ithaca, NY: Cornell University Press, 320 p.
- Purdey, J. (2006). *Anti-Chinese violence in Indonesia, 1996–1999*. Honolulu: University of Hawaii Press, 316 p.
- Purwani, O. (2001). *Identifikasi elemen arsitektur Eropa pada kraton Yogyakarta*. MA Thesis in Architecture.
- Purwani, O. (2014). *Javanese power: silent ideology and built environment of Yogyakarta and Surakarta*. PhD Thesis in Architecture.
- Purwani, O. (2017). Javanese cosmological layout as a political space. *Cities*, Vol. 61, pp. 74–82.

- Purwani, O., Rahmatulloh, O. R., and Rahayu, P. (2022). Invented traditions in Surakarta after decentralisation. *Cities*, Vol. 131, 103985. DOI: 10.1016/j.cities.2022.103985.
- Qomarun and Ikaputra (2007). *Urban space morphology and typology of the city of Solo in the early period (1500–1750)*. *Jurnal Teknik Gelagar*, Vol. 18, No. 02, pp. 110–118.
- Qomarun and Prayitno, B. (2000). Morfologi kota SOLO (tahun 1500-2000). *Dimensi Teknik Arsitektur*, Vol. 35, No. 1, pp. 80–87.
- Rahmatulloh, O., Purwani, O., and Rahayu, P. (2020). *The Consumption of Tradition and Heritage Areas in the Grebeg Sudiro Event in Surakarta*. [online] Available at: <https://ijbes.utm.my/index.php/ijbes/article/view/548>. [Access Date: August 26, 2024].
- Ravesteijn, W. and Kop, J. (2008). *For profit and prosperity: the contribution made by Dutch engineers to public works in Indonesia, 1800–2000*. Zaltbommel: Aprilis, 563 p.
- Ricklefs, M. C. (1993). *A history of modern Indonesia since c. 1300*. Stanford: Stanford University Press, 378 p.
- Robertson, S. B. (2012). *Significant pavilions. The traditional Javanese house as a symbolic terrain*. PhD Thesis in Architecture.
- Santosa, R. B. (1997). *Omah: the production of meanings in Javanese domestic settings*. MA Thesis in Architecture.
- Sejarah Konflik Keraton Solo Diawali Perebutan Tahta Keturunan Pakubuwono XII - Tribunjateng.com*. (2022). [online] Available at: <https://jateng.tribunnews.com/2022/12/25/sejarah-konflik-keraton-solo-diawali-perebutan-tahta-keturunanpakubuwono-xii> [Access Date: August 26, 2024].
- Shiraishi, T. (1990). *An age in motion: popular radicalism in Java, 1912–1926*. Ithaca, NY: Cornell University Press, 365 p.
- Sukirni, S. (2017). Permukiman Tionghoa Di Surakarta Pada Tahun 1900–1940. *Ilmu Sejarah-S1*, 2(3), pp. 414–429.
- Thufail, F. I. (2013). Becoming aristocrats: keraton in the politics of adat. In: Hauser-Schäublin, B. (ed.) *Adat and Indigeneity in Indonesia - Culture and Entitlements between Heteronomy and Self-Ascription*. Göttingen Studies in Cultural Property, Vol. 7. Göttingen: Universitätsverlag Göttingen, pp. 167–184.
- van Naerssen, F. H. (1968). Ancient Javanese recording of the past. *Arts: The Journal of the Sydney University Arts Association*, Vol. 5, pp. 30–46.
- Wibowo, H. J., Murniatmo, G., Dharmamulja, S., and Dakung, S. (1998). *Arsitektur tradisional. Daerah Istimewa Yogyakarta*. Jakarta: Departemen Pendidikan dan Kebudayaan RI, 284 p.
- Wild, C. (1991). The radio midwife: some thoughts on the role of broadcasting during the Indonesian struggle for independence. *Indonesia Circle. School of Oriental & African Studies. Newsletter*, Vol. 19, Issue 55, pp. 34–42. DOI: 10.1080/03062849108729763.
- Wildan, M. (2013). The nature of radical Islamic groups in Solo. *Journal of Indonesian Islam*, Vol. 7, No. 1, pp. 49–70. DOI: 10.15642/JIIS.2013.7.1.49-70.

УТВЕРЖДЕНИЕ МЕСТНОЙ ИДЕНТИЧНОСТИ В ОБЩЕСТВЕННОЙ СФЕРЕ: ПРОЕКТИРОВАНИЕ «СВЕРХУ-ВНИЗ» В ДЕЦЕНТРАЛИЗОВАННОЙ СУРАКАРТЕ

Офита Пурвани*, Астри Ресми Энгарсиви

Университет Себелас Марет (Университет 11 марта), ул. Сутами 36А, Суракарта, Индонезия, 57126

*E-mail: ofita92@yahoo.com

Аннотация

Введение: в данной статье рассматриваются усилия органов муниципального управления по формированию местной идентичности в период децентрализации, в частности, на примере зданий общественных служб в районах (*келураханах*) Суракарты. Суракарта имеет долгую историю насилия, объектом которого всегда становились меньшинства. Таким образом, политика идентичности важна для представления интересов всех жителей города.

Цель исследования: в данной статье мы изучили общественные здания в Суракарте, чтобы понять, как они отражают местную идентичность. **Метод:** мы проанализировали общественные здания в Суракарте с точки зрения использованной при их строительстве идентичности. Мы взяли образцы в каждом из пяти *кечаматанов* Суракарты и выяснили, какую идентичность демонстрируют их общественные здания. Мы также опросили заинтересованные стороны, участвовавшие в проектировании этих зданий, для разъяснения ряда вопросов.

Результаты показывают, что мэр сыграл важную роль в утверждении местной идентичности, используя видение «сверху-вниз», что контрастирует с известным в городе подходом «снизу-вверх». Однако видение идентичности мэра в основном определяется яванскими ценностями, даже если кажется, что оно сочетает в себе яванский и колониальный архитектурные стили. Яванские ценности можно заметить в использовании здания *пендхапа* для общественных собраний, его расположении в передней части комплекса *келурахана* и расположении главного офиса в колониальном стиле сбоку или сзади. Это напоминает планировку традиционной яванской архитектуры.

Ключевые слова: идентичность; децентрализация; общественные здания; архитектура; Суракарта.

COMPARATIVE STUDY ON ENHANCING THE MECHANICAL PROPERTIES OF CLAYEY SAND WITH WASTE PLASTIC FIBERS AND LIME

Hadj Bekki^{1,3*}, Abdelhakim Guezzoul¹, Tefaha Cherrak¹, Rachid Boumeddiene², Hadj Benhebal¹

¹Ibn Khaldoun University of Tiaret, Algeria

²Laboratoire des Travaux Publics de l'Ouest, Unité de Tiaret, Algeria

³Laboratoire LGéo2D, Ibn Khaldoun University of Tiaret, Algeria

*Corresponding author's email: h_bekki@univ-tiaret.dz

Abstract

Introduction. The stabilization of clayey soils remains a dynamic and evolving field, with ongoing research exploring new materials, techniques, and sustainable practices to address the challenges posed by problematic soils in construction and infrastructure development. **The aim of the study** is to investigate the improvement of compaction and mechanical properties of clayey sand by reinforcing its structure with polyvinyl chloride (PVC) plastic fibers of varying sizes and proportions, and/or by applying lime treatment at a minimal dosage. **Methods.** The different mixtures were evaluated through a series of tests, including Proctor compaction tests, California Bearing Ratio (CBR) tests, and direct shear tests conducted under unconsolidated undrained conditions, to assess their mechanical behavior and strength enhancements. **Results** indicated that larger PVC fibers yielded the highest CBR values, even surpassing those achieved through lime treatment alone. Furthermore, the CBR index of the soil increased proportionally with the amount of PVC fibers added. It was also observed that the short-term behavior of clayey sand is significantly improved when reinforced with plastic fibers, whether used independently or in combination with lime treatment. This improvement can be attributed to the combined effects of lime, which strengthens the soil by reducing plasticity and increasing cohesion, and the structural contribution of larger plastic fibers, which promote better interlocking and reinforcement. These findings suggest that stabilizing clayey soils using PVC waste fibers and/or minimal lime treatment offers a technically effective and economically viable solution, while also supporting sustainable development goals.

Keywords: clayey sand; stabilization; PVC plastic waste; lime; mechanical properties.

Introduction

Soil stabilization is a method widely used in geotechnical engineering to enhance the physical and mechanical properties of soil, thereby making it more stable and suitable for various construction applications. This process involves altering soil properties to improve its bearing capacity, shear strength, and resistance to moisture and other environmental factors (Behnood, 2018). Several stabilization methods are employed, including mechanical stabilization, chemical stabilization, and the use of waste materials (Afrin, 2017). Mechanical stabilization involves the physical modification of soil properties through compaction or by blending with such materials as gravel or sand to enhance bearing capacity and reduce settlement potential. Chemical stabilization uses additives like lime, cement, or fly ash, which react with soil particles to form cementitious compounds, thereby increasing strength, reducing plasticity, and improving durability. Recent studies have explored alternative binders such as geopolymers and nanomaterials offering

sustainable and effective stabilization solutions (Arora et al., 2019; Ayub and Khan, 2023). Reinforcement techniques involve synthetic or natural fibers (e.g., geotextiles, geogrids, and biochar) to improve the tensile strength and flexibility of the soil matrix (Liu et al., 2020). Recent research indicates that recycled fibers from waste materials — such as plastic bottles and tires — not only enhance soil stability but also contribute to environmental sustainability by diverting waste from landfills (Suthar et al., 2024). The use of waste materials like plastic fibers, tire shreds, and industrial by-products (e.g., slag, construction waste) is gaining traction due to its environmental and economic advantages. For example, recent findings show that incorporating waste plastic fibers into soil improves both compaction characteristics and bearing properties (Amena, 2022). While stabilization techniques are essential for ensuring the stability and longevity of structures built on weak soils, they often raise environmental concerns and may increase construction costs (Amakye and Abbey, 2021). However, by exploring alternative and sustainable

solutions (Fondjo and Theron, 2021), it is possible to achieve effective soil stabilization without excessive expense (Bekkouche et al., 2022; Gupta et al., 2024; Mishra et al., 2022). Combining multiple stabilizers is a practical approach when a single additive does not yield the desired strength improvement. This strategy leverages synergistic effects between materials such as lime, cement, fly ash, and plastic fibers to enhance both mechanical and physical soil properties (Meddah et al., 2022; Nujid et al., 2022; Thandabani and Letcham, 2023). Incorporating recycled plastic into construction materials and infrastructure provides a multifaceted solution that reduces environmental impact by diverting plastic waste from landfills and oceans. This practice enhances the durability and performance of construction materials, improving their resistance to weathering, cracking, and other forms of degradation. Moreover, the use of recycled plastic promotes sustainable development by reducing reliance on virgin raw materials, conserving natural resources, and lowering greenhouse gas emissions associated with traditional construction practices (Maitlo et al., 2022). Additionally, it offers significant economic benefits by reducing material costs and fostering innovation in green construction technologies, thereby contributing to a more sustainable and circular economy (Zulkernain et al., 2021). The stabilization of clayey soils continues to evolve, driven by ongoing research into innovative materials, advanced techniques, and sustainable practices. Researchers are increasingly exploring unconventional additives such as recycled plastics, industrial by-products, and bio-based stabilizers to improve soil performance while minimizing environmental impacts. This study investigates the enhancement of compaction and bearing capacity of clayey sand through the incorporation of polyvinyl chloride (PVC) plastic fibers of varying sizes and proportions, or through minimal lime treatment. The evaluation was conducted using Proctor compaction and California Bearing Ratio (CBR) tests to assess the effects of these stabilization techniques on the mechanical behavior of the soil and to determine the most effective combinations for improving soil stability.

Materials and Methods

Materials

In this experimental study, three primary materials — clayey sand, quicklime, and PVC plastic waste — were used to investigate the improvement of geotechnical properties through a combination of chemical and mechanical stabilization techniques.

The clayey sand was sourced from Lardjem located in the Tissemsilt Province of Algeria. Its main characteristics are summarized in Table 1. Particle size analysis of the material enabled the development of its granulometric curve illustrated in Fig. 1. According to the Technical Guide for Road

Table 1. Main Characteristics of the Soil

Symbol	Parameter	Value
Gs (g/cm ³)	Specific Gravity	2.7
% Fines	Sieve Percentage at 80 μ m	29
< 2 μ m	Sieve Percentage at 2 μ m	8
WL (%)	Liquid Limit	40.3
WP (%)	Plastic Limit	23.5
VB	Methylene Blue Value	3.27
% CaCO ₃	Carbonate Content	22
Wn (%)	Natural Water Content	23.8

Earthworks (LCPC & SETRA, 2000) and the NF P11-300 standard (AFNOR Editions, 1992), the soil is classified as clayey sand, ranging from plastic to very plastic. Based on the Casagrande plasticity chart, the soil is further classified as low-plastic clay. The granulometric curve (Fig. 1) shows that the material contains both fine and coarse particles reaching up to 4 mm in size. The curve also indicates that the material is poorly graded, meaning that the distribution of particle sizes is neither continuous nor uniform. This non-uniformity can negatively impact the compaction and stability of the material. X-ray diffraction (XRD) analysis was conducted at the Synthesis and Catalysis Laboratory of Ibn Khaldoun University, Tiaret, Algeria. The diffractograms were obtained at room temperature using a Rigaku MiniFlex 600 diffractometer. The XRD results (Fig. 2) revealed the presence of clay minerals such as kaolinite, illite, and chlorite, with traces of montmorillonite. Associated non-clay minerals identified in the soil included quartz and calcite.

The quicklime was sourced from the Lime-Saida Factory in the Saida Province of Algeria.

The PVC plastic waste used in the study was collected from carpentry workshops and subsequently sieved into three distinct size classes: PVC1 (1.0–1.6 mm), PVC2 (1.6–2 mm), and PVC3 (2.0–2.5 mm). This classification enabled a more

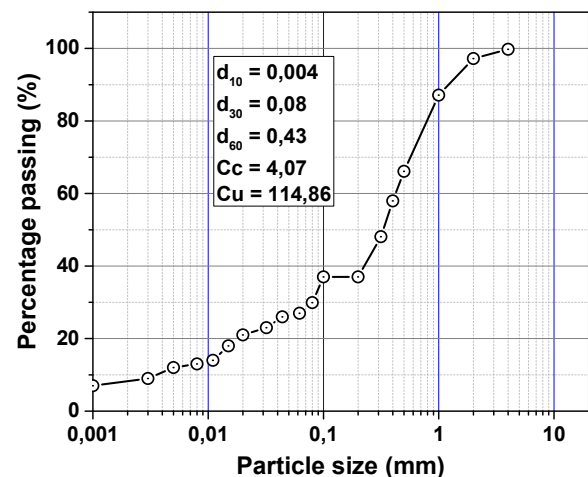


Fig. 1. Particle size distribution of the clayey sand

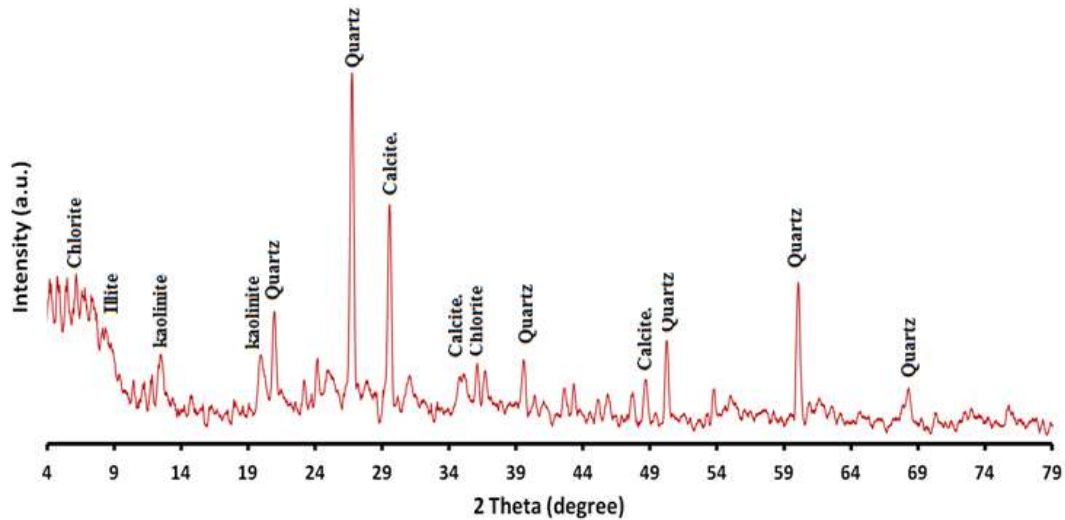


Fig. 2. X-ray diffraction (XRD) diffractogram of the clayey sand

detailed assessment of how varying PVC fiber sizes influence the geotechnical behavior of the stabilized clayey sand.

Methods

In this experimental study, the stabilization of clayey sand involved treating the material with lime and reinforcing it with PVC fibers. A series of tests were conducted to evaluate the effects of these treatments on the geotechnical properties of the material. The testing program included soil identification tests, Proctor compaction tests, California Bearing Ratio (CBR) tests, and direct shear tests. These tests were performed to assess how lime treatment and PVC fiber reinforcement influence the geotechnical properties of the clayey sand. The bearing capacity tests followed the ASTM D-698 standard (ASTM International, 2012) for Proctor compaction and ASTM D1883-21 standard (ASTM International, 2021) for the CBR test. The direct shear test was conducted in accordance with the NF P94-071-1 standard (AFNOR Editions, 1994), using a high shear rate of 1 mm/min to analyze the short-term behavior of the mixtures.

The Eades and Grim method (ASTM D6276-19 (ASTM International, 2019)) was employed to determine the optimal lime dosage required for treating the clayey sand. Lime content was varied from 1 % to 5 % (by total sample mass), and the pH of each mixture was measured. The optimum dosage corresponds to the “fixation point”, indicated by a pH of 12.4. Selecting an appropriate lime content aims to reduce the swelling potential of the clayey sand while maintaining cost efficiency. Optimizing the lime dosage ensures effective soil stabilization, enhances geotechnical properties, and minimizes treatment costs.

Four types of mixtures were prepared for the study:

1. *Soil*: Untreated clayey sand.
2. *Lime-Treated Soil*: Clayey sand stabilized with quicklime to reduce swelling behavior.
3. *Soil-PVC Fiber Mixtures*: Clayey sand reinforced with PVC fibers without lime treatment.
4. *Soil-Lime-PVC Fiber Mixtures*: Clayey sand treated with lime and reinforced with PVC fibers.

The PVC fiber-reinforced mixtures were prepared by adding different percentages (3 %, 4 %, and 5 % by total mass) of distinct PVC waste classes. These mixtures were tested to evaluate the effects of each treatment and reinforcement combination on the compaction and bearing capacity of the material.

Results and Discussion

The histograms in Fig. 3, which display the Methylene Blue Value (MBV) for the soil-lime mixtures, indicate that the clay content (or argillosity)

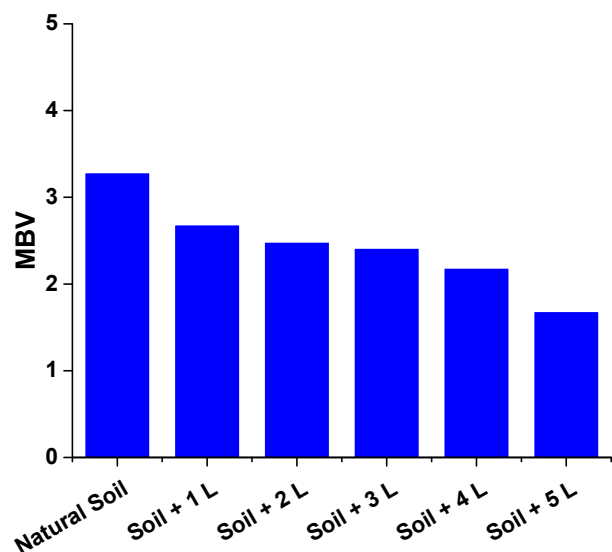


Fig. 3. Methylene Blue values for soil treated with varying lime content

decreases as the percentage of lime added increases. This trend suggests that lime treatment reduces the amount of active clay minerals in the soil.

Fig. 4 presents the Atterberg limit values for the different soil–lime mixtures. These limits — namely the liquid limit (LL), plastic limit (PL), and plasticity index (PI) — offer insights into the changes in plasticity and workability of the clay when treated with varying lime dosages. It is observed that the addition of lime significantly increases the liquid limit, while its effect on the plastic limit is less pronounced. This slight increase in the plastic limit may be attributed to the chemical reactions between lime and the soil, which modify the internal structure of the soil matrix. As a result, the plasticity index (PI), defined as the difference between the LL and PL, also increases. The substantial rise in the liquid limit, combined with a minor increase in the plastic limit, leads to a higher plasticity index. This implies that the treated soil becomes more malleable, thereby improving its workability, which is beneficial in various geotechnical applications.

To reduce lime-related costs, pH measurements were conducted for soil–lime mixtures with lime contents ranging from 1 % to 5 %. The goal was to determine the fixation point, which corresponds to a pH of 12.4. As shown in Fig. 5, the optimal lime dosage for treating the clayey sand is approximately 1 %.

Fig. 6 illustrates the Atterberg limit values for different mixtures of clayey sand and PVC fibers. Minor variations in these limits are observed, likely due to differences in sample preparation and handling. However, these variations are minimal, indicating that the addition of PVC fibers does not significantly alter the internal structure of the soil. While the fibers may slightly influence the workability of the mixture,

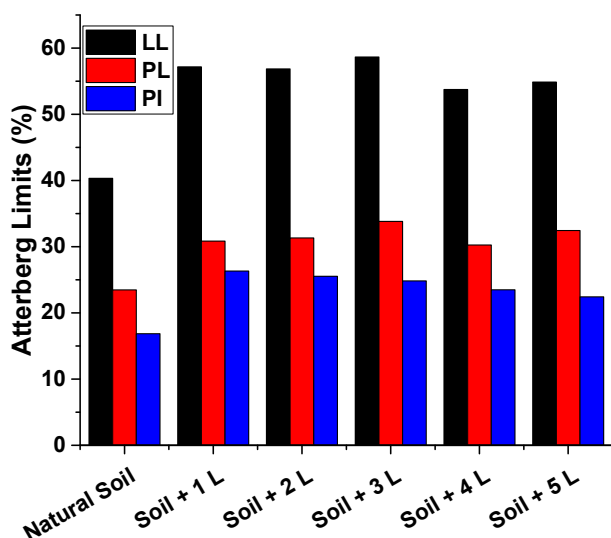


Fig. 4. Atterberg limits vs. lime content for treated soil

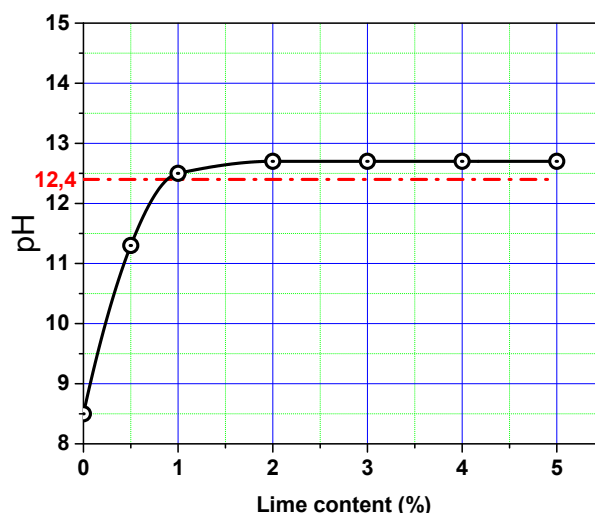


Fig. 5. pH measurements for different soil–lime mixtures

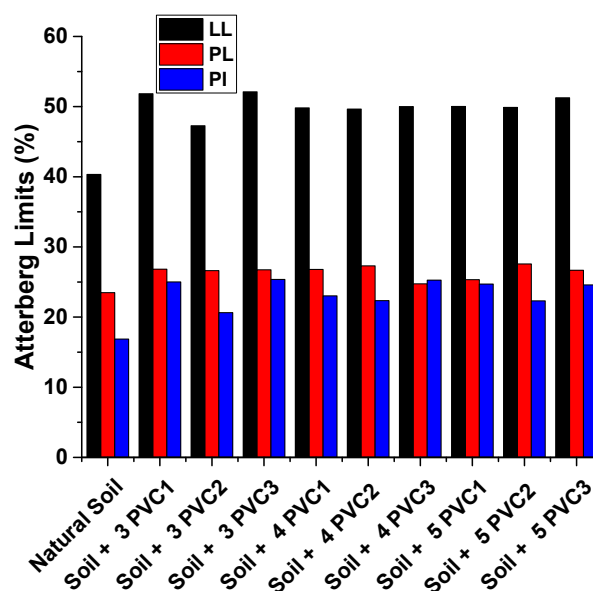


Fig. 6. Atterberg limits for mixtures of soil and PVC fibers

the fundamental properties of the soil — reflected in the Atterberg limits — remain largely unchanged. This suggests that the primary structure of the soil is preserved despite the incorporation of PVC fibers.

Regarding the 4th category of mixtures (clayey sand–lime–PVC) prepared with 1 % lime, it is observed that the plastic fibers influence the behavior between lime and soil (Fig. 7). The presence of plastic fibers introduces an additional variable that affects the overall behavior of the mixture. Specifically, these fibers can influence the plasticity index by modifying the consistency and plasticity of the mixture. While lime typically increases the plasticity index by enhancing the workability of the soil, the inclusion of PVC fibers alters this effect. The fibers may disrupt the uniform interaction between lime and soil particles, changing the consistency

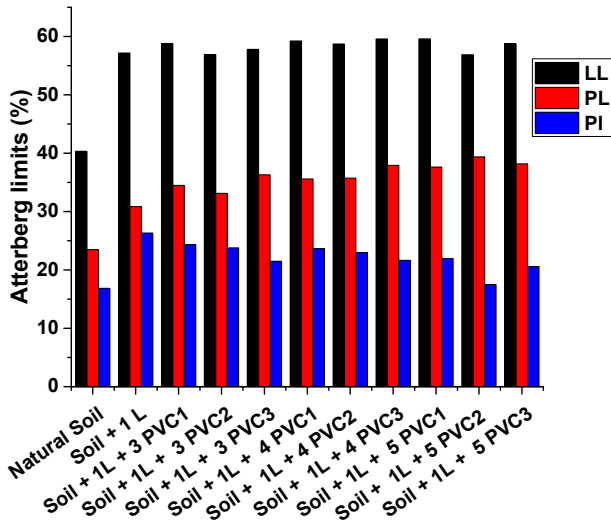


Fig. 7. Atterberg limits for mixtures of soil, lime, and PVC fibers

of the mixture. This suggests that the combination of lime and PVC fibers produces a more complex interaction, where the effectiveness of stabilization may be enhanced or limited depending on the fiber content and distribution within the mixture.

From Fig. 8, it is observed that plastic fibers alter the mechanical properties of the soil during compaction, which impacts the shape of the Proctor curve. This modification affects both the maximum dry density and the optimum water content. The reduction in maximum dry density can be attributed to the lower density of plastic fibers compared to soil particles. Variations in water content are influenced by the dimensions and proportions of the plastic fibers, which play a crucial role in determining the optimum water content for each mixture. Additional water is necessary for better handling, especially when plastic fibers are incorporated. It can be noted that the bell-shaped curve is maintained even after adding plastic fibers to the soil, indicating that

the mixtures retain their sensitivity to water. This suggests that while the inclusion of PVC fibers may improve certain mechanical properties, it does not significantly alter the fundamental water sensitivity of the soil. This retained sensitivity could be due to the fact that the plastic fibers, although affecting compaction and density, do not fully mitigate the behavior of the clay particles.

For soil mixtures containing 1 % lime and PVC fibers of various percentages and dimensions, Fig. 9 shows a notable decrease in dry densities. This decrease can be attributed to two main factors: (1) the addition of lime initiates a chemical reaction with clay minerals, causing flocculation and agglomeration, which increases the overall volume of the mixture; and (2) the incorporation of low-density PVC fibers further reduces the dry density by replacing denser soil particles. Notably, the Proctor curves for soil stabilized with lime and plastic fibers tend to flatten, indicating reduced sensitivity to water.

For the California Bearing Ratio (CBR) tests, samples were prepared using different compaction energies: 10, 25, and 56 blows per layer (B/L). After preparation, the samples were immediately subjected to penetration testing to determine the immediate CBR value. Fig. 10 presents the immediate CBR values for various mixtures composed of soil, PVC fibers and/or lime, compacted using a low compaction energy of 10 B/L. It was observed that the CBR values increase with the size of the PVC fibers at each dosage level. For example, at a 5 % dosage, the CBR values increased with increasing fiber dimensions, with the maximum values obtained for the 3rd class fibers (2–2.5 mm). This trend suggests that larger fiber sizes more effectively enhance the bearing capacity of the soil under compaction. The increased surface area and interlocking effect of larger fibers likely improve the soil structure, providing better resistance to deformation and enhancing the

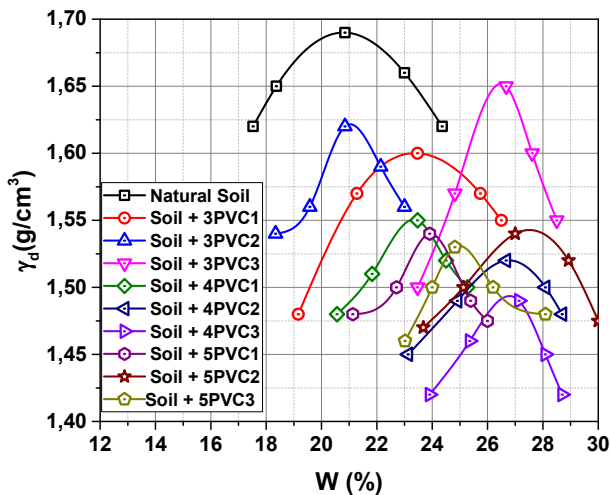


Fig. 8. Proctor curves for mixtures of soil and PVC fibers

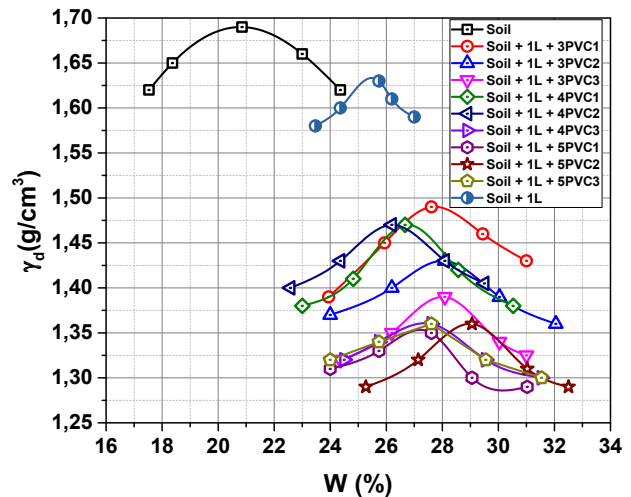


Fig. 9. Proctor curves for mixtures of soil, lime and PVC fibers

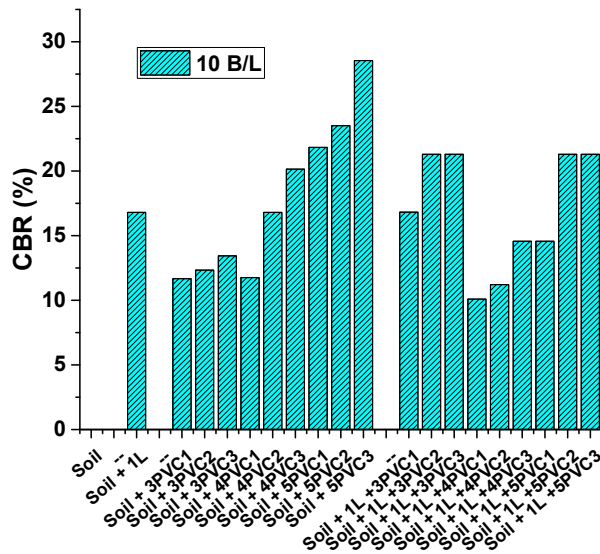


Fig. 10. CBR values for mixtures prepared at low compaction energy (10 B/L)

overall stability of the mixture. A similar trend was observed for samples prepared with medium and high compaction energies, as shown in Figs. 11 and 12. The CBR values consistently increased with fiber size, regardless of the applied compaction energy. This indicates that larger fibers (such as PVC class 3 with dimensions of 2–2.5 mm) significantly improve the bearing capacity of the soil across different compaction levels. Amena (2022) found that CBR values increase with higher percentages of plastic fiber addition when reinforcing expansive subgrade soils. The effectiveness of larger fibers in reinforcing the soil remains evident, as they contribute to better interlocking and load distribution, thereby improving the mechanical properties of the soil under varying

compaction conditions. Notably, the CBR values obtained for mixtures containing 5 % plastic fibers of the 2nd (1.6–2 mm) and 3rd classes (2–2.5 mm), either alone or in combination with lime, were superior to those achieved with lime treatment alone. This enhancement is likely due to the synergistic effect between lime treatment, which improves soil cohesion and reduces plasticity, and the reinforcement provided by the larger plastic fibers, which improve interlocking and structural integrity. These combined effects contribute to a more stable and robust soil matrix, enhancing the overall bearing capacity of the mixtures. However, achieving these results requires high compaction energy.

It should be noted that Berrahou and Bendjalili (2023) found that stabilizing fine clay with small plastic fibers produced better results, which contrasts with the findings of this study. Here, larger plastic fibers yielded superior performance. This discrepancy suggests that the optimal fiber size for stabilizing clay materials shall closely match the grain size in the treated material. By ensuring that the fiber size aligns with the soil grain size, better interlocking and distribution within the soil matrix can be achieved, leading to more effective reinforcement and enhanced soil properties.

The short-term behavior of the soil was evaluated through direct shear tests conducted under unconsolidated, undrained conditions. The results are shown in the Mohr's stress diagram in Fig. 13. Mixtures of soil treated with lime and reinforced with plastic fibers exhibited significantly higher shear strengths than untreated soil. This improvement is attributed to increased shear resistance from lime stabilization and the stress-distributing and crack-bridging effects of PVC fibers. Reinforcing the soil

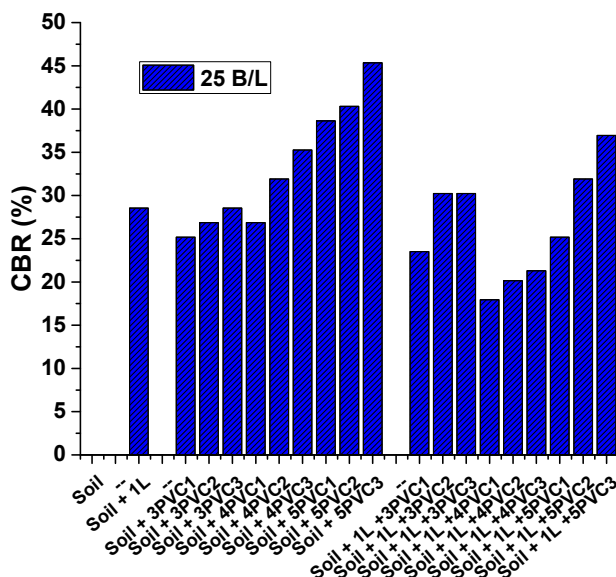


Fig. 11. CBR values for mixtures prepared at medium compaction energy (25 B/L)

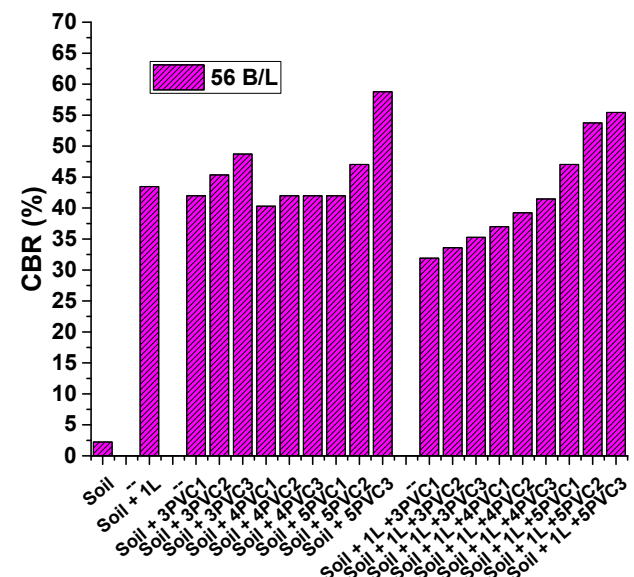


Fig. 12. CBR values for mixtures prepared at high compaction energy (56 B/L)

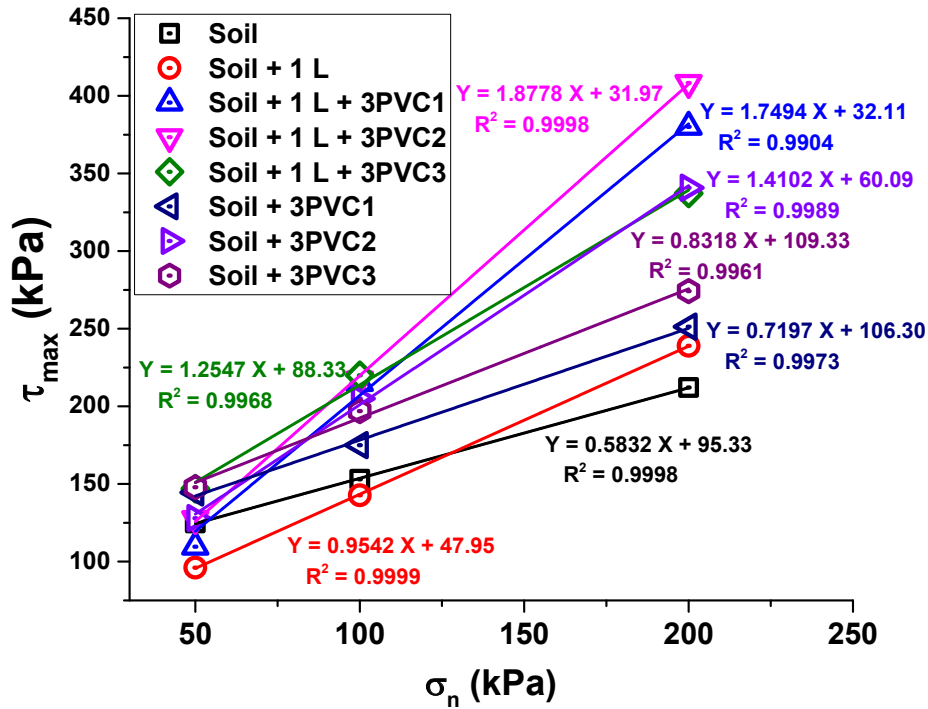


Fig. 13. Failure stresses for the different mixtures

with PVC fibers alone also led to notable gains in shear strength. The undrained cohesion values, plotted in Fig. 14, show that the large plastic fibers (PVC 3) yield the highest cohesion, confirming their superior reinforcing effect. These results align with the CBR findings and highlight the potential of plastic waste as a sustainable and effective reinforcement for enhancing the mechanical properties of clayey sand soils.

Conclusions

The aim of the study was to examine the effect of adding plastic fibers of various sizes and proportions, with or without lime treatment, on the compaction and bearing properties of clayey sand. Based on the results obtained, the following conclusions can be drawn:

- The presence of plastic fibers affects the overall behavior of the mixture by altering its consistency and plasticity, thereby influencing the plasticity index and modifying the workability and deformability of the soil.
- The Proctor curves of soils stabilized with lime and plastic fibers tend to flatten, indicating reduced water sensitivity, in contrast to mixtures containing only plastic fibers, which retain a bell-shaped curve.
- Immediate CBR tests revealed that the bearing capacity of clayey sand mixtures containing plastic fibers improves with increasing fiber size and proportion. The best results were achieved using the largest fibers (2–2.5 mm), which closely match the particle size of the treated soil. This suggests that incorporating plastic fibers into clayey sand can

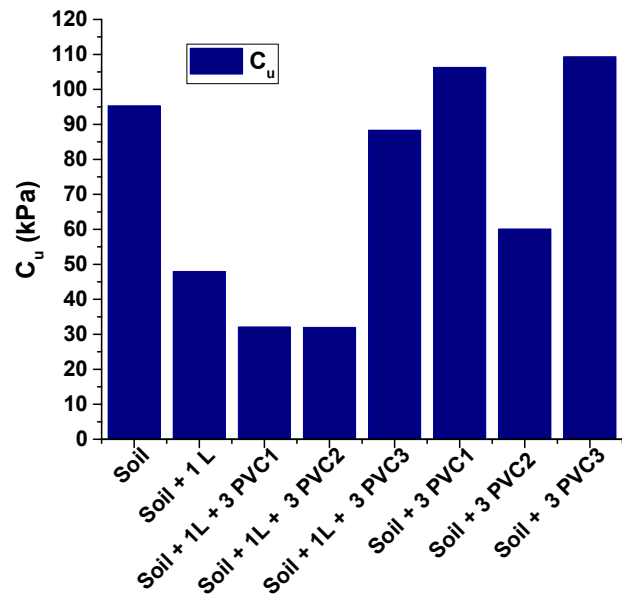


Fig. 14. Undrained cohesion for the different mixtures

notably improve its bearing capacity, as evidenced by the increased CBR values with larger fibers. However, to maintain these improvements, it is essential to protect the material from water exposure.

- The short-term behavior of clayey sand is significantly improved by reinforcing its structure with plastic fibers, either independently or in combination with lime treatment. The results indicated that larger plastic fibers, specifically PVC 2 and PVC 3, provided the best shear resistance, demonstrating their effectiveness in reinforcing the clayey sand matrix.

- The combined stabilization approach using 1 % lime and plastic fibers presents a promising solution, as the mixtures become less sensitive to water, indicating enhanced stability and reduced susceptibility to moisture-induced changes. However, achieving optimal performance with this method requires the application of higher compaction energy.

Overall, the results show that the combined stabilization approach using lime treatment and plastic fiber reinforcement is an effective technical solution in terms of both performance and cost. However, in-situ testing and additional durability assessments are necessary to further validate the effectiveness and reliability of this technique for broader geotechnical applications.

References

- AFNOR Editions (1992). *NF P11-300. Earthworks. Classification of materials for use in the construction of embankments and capping layers of road infrastructures*. Paris: AFNOR Editions, 21 p.
- AFNOR Editions (1994). *NF P94-071-1. Soil investigation and testing. Direct shear test with shearbox apparatus. Part 1: direct shear*. Paris: AFNOR Editions, 16 p.
- Afrin, H. (2017). A review on different types soil stabilization techniques. *International Journal of Transportation Engineering and Technology*, Vol. 3, Issue 2, pp. 19–24. DOI: 10.11648/j.ijtet.20170302.12.
- Amakye S. Y. and Abbey S. J. (2021). Understanding the performance of expansive subgrade materials treated with non-traditional stabilisers: a review. *Cleaner Engineering and Technology*, Vol. 4, 100159. DOI: 10.1016/j.clet.2021.100159.
- Amena, S.(2022). Utilizing solid plastic wastes in subgrade pavement layers to reduce plastic environmental pollution. *Cleaner Engineering and Technology*, Vol. 7, 100438. DOI: 10.1016/j.clet.2022.100438.
- Arora, A., Singh, B., and Kaur, P. (2019). Performance of nano-particles in stabilization of soil: a comprehensive review. *Materials Today: Proceedings*, Vol. 17, Part 1, pp. 124–130. DOI: 10.1016/j.matpr.2019.06.409.
- ASTM International (2021). *ASTM D1883-21. Standard test method for CBR (California Bearing Ratio) of laboratory-compacted soils*. West Conshohocken, PA: ASTM International, 8 p.
- ASTM International (2012). *ASTM D-698. Standard test methods for laboratory compaction characteristics of soil using standard effort (12,400 ft-lbf/ft³ (600 kN-m/m³))*. West Conshohocken, PA: ASTM International, 13 p.
- ASTM International (2019). *ASTM D6276-19. Standard test method for using pH to estimate the soil-lime proportion requirement for soil stabilization*. West Conshohocken, PA: ASTM International, 5 p.
- Ayub, F. and Khan, S. A. (2023). An overview of geopolymer composites for stabilization of soft soils. *Construction and Building Materials*, Vol. 404, 133195. DOI: 10.1016/j.conbuildmat.2023.133195.
- Behnood, A. (2018). Soil and clay stabilization with calcium- and non-calcium-based additives: a state-of-the-art review of challenges, approaches and techniques. *Transportation Geotechnics*, Vol. 17, Part A, pp. 14–32. DOI: 10.1016/j.trgeo.2018.08.002.

- Bekkouche, S. R., Benzerara, M., Zada, U., Muhammad, G., and Ali, Z. (2022). Use of eco-friendly materials in the stabilization of expansive soils. *Buildings*, Vol. 12, Issue 10, 1770. DOI: 10.3390/buildings12101770.
- Berrahou F. and Bendjilali L. (2023). *Amélioration des propriétés géotechniques des argiles par ajout de déchets plastiques*. Master Thesis, Civil Engineering Department, University Ibn Khaldoun of Tiaret, Algeria.
- Fondjo, A. A. and Theron, E. (2021). Expansive soils treatment using alternative methods: a comprehensive review. *Civil Engineering and Architecture*, Vol. 9, Issue 5, pp. 1295 – 1308. DOI: 10.13189/cea.2021.090503.
- Gupta, G., Sood, H., and Gupta, P. K. (2024). Economic and environmental assessment of industrial wastes stabilized clay and sand soil subgrades using experimental and theoretical approaches. *Construction and Building Materials*, Vol. 422, 135787. DOI: 10.1016/j.conbuildmat.2024.135787.
- LCPC & SETRA (2000). *Réalisation des remblais et des couches de forme. Guide de Terrassement Routier GTR, Fascicule 1*, LCPC & SETRA, France, pp. 35-95.
- Liu, L., Cai, G., Zhang, J., Liu, X., and Liu, K. (2020). Evaluation of engineering properties and environmental effect of recycled waste tire-sand/soil in geotechnical engineering: a compressive review. *Renewable and Sustainable Energy Reviews*, Vol. 126, 109831. DOI: 10.1016/j.rser.2020.109831.
- Maitlo, G., Ali, I., Maitlo, H. A., Ali, S., Unar, I. N., Ahmad, M. B., Bhutto, D. K., Karmani, R. K., Naich, S. R., Sajjad, R. U., Ali, S. and Afridi, M. N. (2022). Plastic waste recycling, applications, and future prospects for a sustainable environment. *Sustainability*, Vol. 14, Issue 18, 11637. DOI: 10.3390/su141811637.
- Meddah, A., Goufi, A. E., and Pantelidis, L. (2022). Improving very high plastic clays with the combined effect of sand, lime, and polypropylene fibers. *Applied Sciences*, Vol. 12, Issue 19, 9924. DOI: 10.3390/app12199924.
- Mishra, P., Shukla, S., and Mittal, A. (2022). Stabilization of subgrade with expansive soil using agricultural and industrial by-products: a review. *Materials Today: Proceedings*, Vol. 65, Part 2, pp. 1418–1424. DOI: 10.1016/j.matpr.2022.04.397.
- Nujid, M., Tholibon, D. A., and Kushairi Rahman, M. H. (2022). Effect of cockle shell powder as sustainable additive on geotechnical engineering properties of stabilized soil. *Arabian Journal of Geosciences*, Vol. 15, Issue 14, 1306. DOI: 10.1007/s12517-022-10593-6.
- Suthar, L., Meena, S., and Kumar, U. (2024). Utilization of plastic waste in reinforcing sandy soil for sustainable engineering applications. *Journal of Engineering Sciences*, Vol. 11, Issue 1, pp. H1–H8. DOI: 10.21272/jes.2024.11(1).h1.
- Thandabani, M. and Letcham, K. (2023). Experimental study on stabilization of black cotton soil with lime, plastic waste & red mud. *International Journal of Engineering Research & Technology (IJERT)*, Vol. 12, Issue 09, IJERTV12IS090075. DOI: 10.17577/IJERTV12IS090075.
- Zulkernain, N. H., Gani, P., Chuck Chuan, N., and Uvarajan, T. (2021). Utilisation of plastic waste as aggregate in construction materials: a review. *Construction and Building Materials*, Vol. 296, 123669. DOI: 10.1016/j.conbuildmat.2021.123669.

СРАВНИТЕЛЬНОЕ ИССЛЕДОВАНИЕ ПО УЛУЧШЕНИЮ МЕХАНИЧЕСКИХ СВОЙСТВ ГЛИНИСТОГО ПЕСКА С ИСПОЛЬЗОВАНИЕМ ОТХОДОВ ПЛАСТИКОВЫХ ВОЛОКОН И ИЗВЕСТИ

Хадж Бекки^{1*}, Абдельхаким Геззул¹, Тефаха Черрак¹, Рашид Бумеддин², Хадж Бенхебал¹

¹Университет Ибн Халдуна, Тиарет, Алжир

²Лаборатория общественных работ Запада, отделение в Тиарете, Алжир

*E-mail: h_bekki@univ-tiaret.dz

Аннотация

Введение. Укрепление глинистых грунтов — развивающаяся область, в которой продолжаются исследования по применению новых материалов, технологий и рациональных практик для решения проблем, связанных с нестабильными грунтами в строительстве и создании инфраструктуры. **Цель исследования** — рассмотреть улучшение уплотнения и механических свойств глинистого песка путем армирования его структуры пластиковыми волокнами из поливинилхлорида (ПВХ) различных размеров и пропорций и/или за счет обработки известью в минимальной дозировке. **Методы.** Различные комбинации смесей оценивались с помощью ряда испытаний, включая определение плотности грунта методом Проктора, определение несущей способности грунта калифорнийским методом, а также испытания на прямой сдвиг неконсолидированных недренированных образцов, для оценки их механических и прочностных характеристик. **Результаты** показали, что наиболее высокие значения калифорнийского числа несущей способности грунта были достигнуты при использовании крупных волокон ПВХ, при этом они превышали значения, полученные при применении извести в отсутствие армирования. Кроме того, эти значения возрастали пропорционально количеству добавленных ПВХ-волокон. Также было отмечено, что в краткосрочной перспективе характеристики глинистого песка значительно улучшаются при армировании пластиковыми волокнами, как с обработкой известью, так и без нее. Это улучшение объясняется совокупным действием извести, которая укрепляет грунт за счет снижения пластичности и увеличения сцепления, и крупных пластиковых волокон, которые способствуют лучшей связности и армированию структуры. Полученные результаты свидетельствуют о том, что укрепление глинистых грунтов с использованием волокон из отходов ПВХ и/или извести в минимальной дозировке представляет собой технически эффективное и экономически целесообразное решение, способствующее в том числе достижению целей устойчивого развития.

Ключевые слова: глинистый песок; укрепление; отходы ПВХ; известь; механические свойства.

PHYSICO-MATHEMATICAL MODEL OF WOOD DURABILITY UNDER CYCLIC ENVIRONMENTAL CHANGES IN TEMPERATURE AND HUMIDITY

Sergey Viktorovich Fedosov¹, Vitaly Gennadievich Kotlov², Azariy Abramovich Lapidus¹,
Aleksandr M. Sokolov^{3*}

¹Moscow State University of Civil Engineering (National Research University), Moscow, Russia

²Volga State University of Technology, Yoshkar-Ola, Russia

³Ivanovo Fire Rescue Academy of State Firefighting Service of Ministry of Russian Federation
for Civil Defense, Emergencies and Elimination of Consequences of Natural Disasters, Ivanovo, Russia

*Corresponding author's email: amsokolov37@yandex.ru

Abstract

Introduction. A significant drawback of composite materials is their tendency to degrade over time, eventually leading to complete failure. **Purpose of the study.** The objective of this research is to identify the physical principles and develop a theoretical framework to explain this degradation. Wood, as a natural composite, serves as a convenient object for such investigations. Many physical and theoretical aspects of its behavior remain insufficiently understood. In particular, the reduction in mechanical strength at the junctions (with nagels) of wooden components under cyclic variations in temperature and humidity requires further exploration. **Methods.** This paper presents a physico-mathematical model for assessing the mechanical strength of wood under such environmental influences. The model is based on the Arrhenius equation and current understanding of wood's cellular structure, whose key components are cellulose filaments (serving as the reinforcing framework) and lignin (the binding matrix). The model assumes that non-steady processes of heat and moisture transfer within the wood, driven by environmental conditions, gradually break the interatomic bonds within lignin compounds. **Results.** The study derives expressions to estimate the maximum number of wetting-drying cycles that wood can withstand, considering the material's temperature. It also provides an evaluation of its service life (resource) affected by these cyclic influences. The proposed theory is of universal relevance.

Keywords: composite; heat and moisture transfer; Arrhenius equation; cellular structure of wood; mathematical model; resource.

*The paper is dedicated to the memory
of the world-renowned scientist
Svante August Arrhenius (1859–1927).
In 2024, we commemorated
the 165th anniversary of his birth.*

Introduction

The aim of this work is to develop a physical and mathematical model for predicting the durability (resource) of wood under cyclic changes in environmental temperature and humidity. This model is essential for estimating the service life of wooden structures during their design and operation. In this context, wood is considered a natural composite material, many physical and theoretical aspects of which remain insufficiently explored.

Materials and Methods

Composite materials, both artificial and natural, have gained widespread use in the modern world due to their advantageous properties. However, a significant drawback of these materials is their

tendency to lose mechanical strength over time, potentially leading to complete failure. Therefore, one of the current challenges in material science is to establish the physical basis and develop a theory to explain the gradual reduction in mechanical strength of such materials.

A key characteristic of most composite materials is the presence of at least two essential components: a binder (matrix) and a filler (reinforcement). Typically, the binder is the weakest component and is most susceptible to degradation. This degradation occurs due to the breaking of interatomic bonds within the compounds that form the binder, eventually resulting in the loss of the material's structural integrity. This phenomenon is particularly evident in wood, which

has been the subject of extensive research by the authors.

Wood was chosen for this study due to its high demand and the fact that, as a natural composite, it provides a convenient model for identifying general degradation patterns and evaluating durability.

Wooden structures are extensively used in construction, although their application extends beyond this field. They are also found in shipbuilding, transportation devices, railways, electrical and power installations (e.g., wooden electrolysis baths, power line poles, substations), lifting mechanisms, and various industrial facilities. In most of these applications, wooden structural elements are joined using special metal fasteners known as dowels or dowel connections (Fig. 1) (Bazhenov, 1959; Mironov et al., 2000; Ugolev, 2005; USSR State Committee for Standards, 1985).

In recent years, a new type of dowel connection using metal toothed plates has become increasingly common due to its manufacturability, simplicity, strength, reliability, and durability (Fig. 1c).

The disadvantage of dowel joints is that, over time, these connections deteriorate — primarily due to the degradation of the wood. This degradation is driven by complex heat and mass (moisture) transfer processes occurring under cyclic environmental

conditions, especially fluctuating temperature and humidity, combined with the constant stress-strain state of the material.

Wood typically consists of approximately 45–60 % cellulose, 15–35 % lignin, 15–25 % hemicellulose, and various extractives (Fig. 2) (Bazhenov, 1959; Ugolev, 2005).

Cellulose is a linear polysaccharide polymer and is the primary component that provides wood with elasticity and mechanical strength (Fig. 2) (Mironov et al., 2000; USSR State Committee for Standards, 1985). It is a highly resistant white substance, insoluble in water and common organic solvents (e.g., alcohol, ether, acetone). Bundles of cellulose macromolecules, known as microfibrils, form the cellulose framework of the cell wall and serve as reinforcement.

Hemicellulose, which is structurally similar to cellulose, acts as a reinforcement enhancer.

Lignin is an aromatic (polyphenolic) polymer with a complex structure, containing more carbon and less oxygen than cellulose. It is chemically unstable, easily oxidized, and reacts with chlorine. It dissolves when heated in alkalis or aqueous solutions of sulfurous acid and its salts (Demitrova and Chemodanov, 2016; Mironov et al., 2000). Lignin functions as a binder.

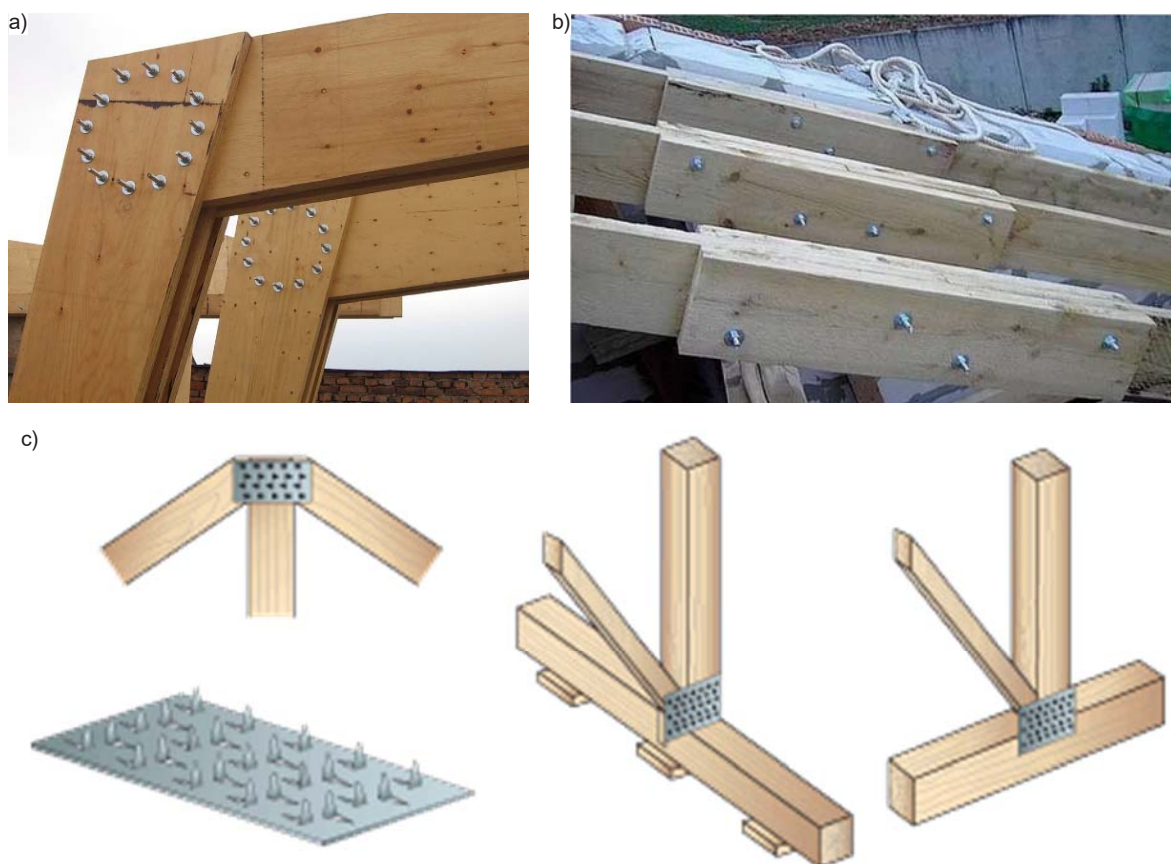


Fig.1. Examples of dowel joints: bolted (a, b) and with metal toothed plates (c); (<https://maxshops.ru/wp-content/uploads/f/a/9/fa9960e35d70c139fcf63a9b261a892f.jpeg>; <https://kak-sdelano.ru/assets/uploads/2016/06/odnoskatnaja-krisha-26.jpg>)

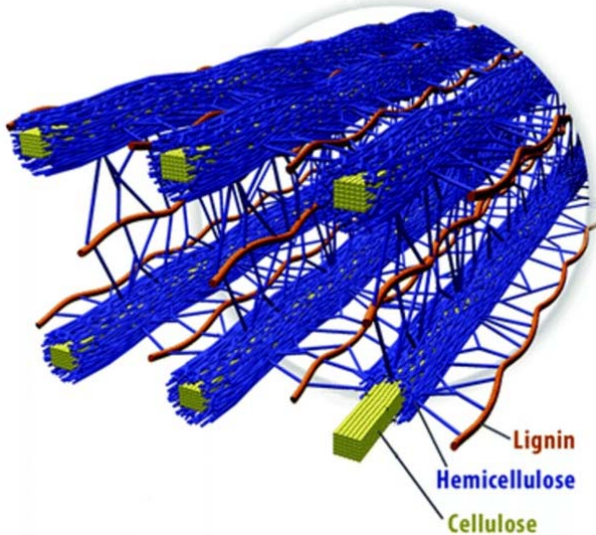


Fig. 2. Structure of wood cell walls: https://sun9-45.userapi.com/impf/046021D4Wjx_xYvWMYxhDLm_RFVV74Arytebmw/EdDc-je9-Zh0.jpg?size=604x548&quality=96&sign=23a84978b2b1b-8275d4c3d11d3f529af&type=album

The operation of dowel joints involves complex heat and moisture transfer processes, including phase transitions (“ice–water–steam”), often under harsh conditions. These processes are influenced by environmental variations in temperature and humidity over daily and seasonal cycles. Extensive experience with wooden structures has shown that these processes adversely affect both the reliability of dowel joints and the overall structural integrity (Erofeev et al., 2008; Fedosov and Kotlov, 2014; Fedosov et al., 2015, 2017a). It is also important to consider that wood can be destroyed by biological factors such as bacterial and fungal decay, and by corrosion of the metal components (Erofeev et al., 2008; Ugolev, 2005; USSR State Committee for Standards, 1985). However, with proper maintenance, the impact of these factors can be minimized.

The mathematical models of heat and moisture transfer proposed in earlier studies (Fedosov and Kotlov, 2014, 2019; Fedosov et al., 2015, 2016c, 2017a) allow for a detailed analysis of the cyclic wetting and drying of wood in dowel joints under fluctuating temperatures. However, these models alone do not yet provide a definitive answer regarding the condition and resource (service life) of wood in dowel connections. Addressing this gap requires the development of a methodology for estimating the material’s remaining resource.

This methodology should be grounded in established knowledge about wood’s internal structure and the role of its organic components in providing mechanical strength (Fig. 2). From this perspective, cellulose and lignin are the most critical compounds. Cellulose fibers form a spatial

framework that perceives loads, while lignin acts as a binder that holds the cellulose structure together. These two components are primarily responsible for the material’s mechanical properties (Bazhenov, 1959; Borovikov and Ugolev, 1989; Demitrova and Chemodanov, 2016; Grunin et al., 2017; Ugolev, 2005; USSR State Committee for Standards, 1985; Vanin, 1949).

Lignin is particularly prone to decomposition when exposed to external factors such as elevated temperatures and moisture, which can ultimately lead to failure of the dowel connection. It is reasonable to assume that the degradation of lignin results from the breaking of atomic bonds within its molecular structure, i.e., it is a physicochemical process. To account for the influence of temperature on the breakdown of lignin molecules, it is convenient to use the Arrhenius equation. This fundamental law is applicable to both the formation and destruction of chemical bonds under the influence of physical factors (Fedosov et al., 2016a; Knunyants, 1988).

Theory

Based on the above (Section 1.2), it can be assumed that the mechanical strength of wood is proportional to the number of lignin chemical bonds N remaining intact during their gradual degradation under the influence of the aforementioned factors. Therefore, the following relation can be written:

$$R = R_0 \frac{N}{N_0}, \quad (1)$$

where R_0 and $R \leq R_0$ are the initial and current values of the mechanical strength of wood, respectively; N_0 is the initial number of chemical bonds; N is the current number of chemical bonds.

The number of destroyed chemical bonds can be determined as the product of the number of wetting and drying cycles n_c and the number of bonds destroyed per cycle N_{Dc} :

$$N_D = n_c N_{Dc} = N_0 - N. \quad (2)$$

To determine N , it is advisable to use the Arrhenius law, which describes the rate constant of chemical transformations (Knunyants, 1988):

$$K = A \cdot \exp\left(-\frac{E}{kT}\right), \quad (3)$$

where K is the rate constant of the chemical reaction, 1/s; A is a constant coefficient (number of chemical interactions per unit time), 1/s; E is the activation energy of the reaction, J; T is the absolute temperature, K; $k = 1.38 \cdot 10^{-23}$ J/K, the Boltzmann constant.

Given the rate constant K , the reaction rate over time, in units of 1/(s·m³), can be determined as follows (Fedosov et al., 2016a; Knunyants, 1988):

$$\frac{dN}{dt} = -K \cdot N = -A \cdot N \cdot \exp\left(-\frac{E}{k \cdot T}\right), \quad (4)$$

where N is the current number of chemical bonds, $1/\text{m}^3$, remaining intact at an arbitrary time t (assuming a first-order reaction).

The solution of Eq. (4) can be obtained by separating the variables and integrating both sides over the time interval of the first cycle of wetting and drying of the wood in the dowel joint:

$$\int_{N_0}^{N_1} \frac{dN}{N} = -A \cdot \int_{t_0=0}^{t_1} \exp\left(-\frac{E}{k \cdot T_1}\right) dt. \quad (5)$$

This yields an expression for determining the number of remaining chemical bonds $N_1 \leq N_0$ at time t_1 , marking the end of the first cycle of wetting and drying:

$$N_1 = N_0 \cdot e^{-\Delta t_1 \cdot A \cdot \exp\left(-\frac{E}{k \cdot T_1}\right)}, \quad (6)$$

where N_0 corresponds to the initial time $t_0 = 0$; T_1 is the temperature during this cycle; and $\Delta t_1 = t_1 - t_0$ is the duration of the cycle.

For the second cycle of wetting and drying of wood, expression (5) can be written as follows

$$\int_{N_1}^{N_2} \frac{dN}{N} = -A \cdot \int_{t_1}^{t_2} \exp\left(-\frac{E}{k \cdot T_2}\right) dt, \quad (7)$$

where $N_2 \leq N_1$ is the number of chemical bonds remaining in operation at time $t_2 \geq t_1$, marking the end of the second cycle; T_2 is the temperature at which this cycle occurred.

By analogy with (6), and taking into account (7), we can write:

$$\begin{aligned} N_2 &= N_1 \cdot e^{-\Delta t_2 \cdot A \cdot \exp\left(-\frac{E}{k \cdot T_2}\right)} = \\ &= N_0 \cdot e^{-\Delta t_1 \cdot A \cdot \exp\left(-\frac{E}{k \cdot T_1}\right)} \cdot e^{-\Delta t_2 \cdot A \cdot \exp\left(-\frac{E}{k \cdot T_2}\right)}, \end{aligned} \quad (8)$$

where $\Delta t_2 = t_2 - t_1$ is the duration of the second cycle.

If we repeat the calculations from (5) to (8), then to determine the number of chemical bonds remaining in operation at time $t_3 \geq t_2$, marking the end of the third cycle of wetting and drying, we can write the following formula:

$$\begin{aligned} N_3 &= N_2 \cdot e^{-\Delta t_3 \cdot A \cdot \exp\left(-\frac{E}{k \cdot T_3}\right)} = \\ &= N_0 \cdot e^{-\Delta t_1 \cdot A \cdot \exp\left(-\frac{E}{k \cdot T_1}\right)} \cdot e^{-\Delta t_2 \cdot A \cdot \exp\left(-\frac{E}{k \cdot T_2}\right)} \times \\ &\quad \times e^{-\Delta t_3 \cdot A \cdot \exp\left(-\frac{E}{k \cdot T_3}\right)}, \end{aligned} \quad (9)$$

where $\Delta t_3 = t_3 - t_2$ is the duration of the third cycle; T_3 is the temperature at which this cycle took place.

Expression (9) can be written in a more compact form:

$$N_3 = N_0 \cdot e^{-A \cdot \sum_{i=1}^3 \Delta t_i \cdot \exp\left(-\frac{E}{k \cdot T_i}\right)}. \quad (10)$$

By extending the above reasoning, it is straightforward to derive a formula similar to (10)

for determining the number of chemical bonds remaining in operation after an arbitrary number of n_c successive cycles of wetting and drying of the wood in dowel joints:

$$N = N_0 \cdot e^{-A \cdot \sum_{i=1}^{n_c} \Delta t_i \cdot \exp\left(-\frac{E}{k \cdot T_i}\right)}, \quad (11)$$

where Δt_i is the duration of the i -th cycle, and T_i is the temperature at which this cycle occurred.

By substituting (11) to (1), we obtain the formula for determining the current value of the mechanical strength of wood:

$$R = R_0 \cdot e^{-A \cdot \sum_{i=1}^{n_c} \Delta t_i \cdot \exp\left(-\frac{E}{k \cdot T_i}\right)}. \quad (12)$$

Analysis of the obtained expression (12) leads to the conclusion that the mechanical strength of wood is influenced by three major operational factors: the number of wetting and drying cycles, the duration of these cycles, and the temperature. Moreover, an increase in any of these parameters results in a decrease in mechanical strength.

Expression (12) is significantly simplified if the successive wetting and drying processes have the same duration $\Delta t_i = \Delta t = \text{const}$, and occur at the same temperature $T_i = T = \text{const}$. In this case, the summation in the formula can be replaced by multiplication:

$$R = R_0 \cdot e^{-A \cdot n_c \cdot \Delta t \cdot \exp\left(-\frac{E}{k \cdot T}\right)}. \quad (13)$$

The resulting expression (13) allows us to determine the limit number of wetting and drying cycles. As known, the ratio of the strength limit to the allowable stress is called the safety factor (Fridman, 2007; Ministry of Construction, Housing and Utilities of the Russian Federation, 2017):

$$K_S = \frac{R_0}{R_D}. \quad (14)$$

The safety factor for wood is set higher than for other materials (e.g., metals). Depending on the nature of the applied force, safety factors can vary considerably: from $K_S = 3 \div 5$ for compression and shear, to $K_S = 8 \div 10$ for tension along the fibers (Fridman, 2007; Ministry of Construction, Housing and Utilities of the Russian Federation, 2017; Konev, 2024). Based on Eq. (14), it is possible to determine the permissible level of mechanical impact on wood:

$$R_D = \frac{R_0}{K_S}. \quad (15)$$

The practical significance of this parameter lies in the fact that during the operation of the nagel connection, the mechanical strength of the wood decreases over time due to the cyclic processes of wetting and drying, until it reaches the maximum permissible value. At that point, the destruction of the wood — i.e. the failure of the dowel connection —

occurs. The number of wetting and drying cycles that precede this failure should also be considered the limit value of this parameter, and its knowledge is of practical importance.

It is quite clear that if we set $R = R_d$ in the left-hand side of Eq. (13), we must assume that the number of cycles on the right-hand side corresponds to the limit value: $n_c = n_d$.

Then this equation, taking into account Eq. (15), can be written in the following form:

$$\frac{1}{K_S} = e^{-A \cdot n_d \cdot \Delta t \cdot \exp\left(-\frac{E}{k \cdot T}\right)}. \quad (16)$$

As a result of solving this equation with respect to n_d , the following expression is obtained to determine the limit number of wetting and drying cycles for the wood of the dowel joint:

$$n_d = \frac{\ln K_S}{A \cdot \Delta t} \exp\left(\frac{E}{k \cdot T}\right). \quad (17)$$

Analysis of expression (17) shows that an increase in the duration of the wetting and drying cycles, as well as in temperature, leads to a decrease in the permissible number of such cycles — i.e., a reduction in the service life of the nail. However, by increasing the safety factor, this service life can be extended.

To use Eqs. (12), (13) and (17), it is necessary to know two constants included in them — A and E . However, currently there is no available information about these parameters, and their values can only be estimated through experiments. Furthermore, these equations allow for the determination of the limit number of wetting and drying cycles only at a constant temperature. At the same time, it is well known that the temperature conditions during the operation of nail can vary significantly, even within a single cycle of wood wetting and drying (Fedosov and Kotlov, 2019; Fedosov et al., 2015, 2016c).

To obtain an expression that allows the determination of the limit number of wetting and drying cycles for the wood of the dowel joint in the general case, it is necessary to refer again to expression (12). Using expression (15) and the specified expression by analogy with (16), we can write the following:

$$\frac{1}{K_S} = e^{-A \cdot \sum_{i=1}^{n_d} \Delta t_i \cdot \exp\left(-\frac{E}{k \cdot T_i}\right)}, \quad (18)$$

or, in a more convenient form:

$$\ln K_S = A \cdot \sum_{i=1}^{n_d} \Delta t_i \cdot \exp\left(-\frac{E}{k \cdot T_i}\right). \quad (19)$$

From the analysis of expression (19), it is clear that in this case it is impossible to express n_d explicitly, and the equation can only be solved for n_d through iterative calculations.

Despite the lack of information about the values of the constant parameters included in formulas (17) and (19) — which, as noted earlier, can only be determined experimentally — expression (17) can still be used for some quantitative estimates. To do this, it is necessary to adopt some standard conditions as a baseline, such as temperature $T = 293 \text{ K}$ (20°C), which is often used for reference, and $\Delta t = 24 \text{ h}$. Under these conditions, expression (17) takes the following form:

$$n_d^b = \frac{\ln K_S}{A \cdot 24} \exp\left(\frac{E}{k \cdot 293}\right). \quad (20)$$

By dividing the left and right sides of formula (17) by the corresponding sides of formula (20), an expression can be obtained for determining the limit number of cycles in relative terms with respect to the baseline conditions:

$$n_d^* = \frac{n_d}{n_d^b} = \frac{24}{\Delta t} \exp\left[\frac{E}{k} \left(\frac{1}{T} - \frac{1}{293}\right)\right]. \quad (21)$$

The resulting expression (21) eliminates the unknown parameter A and allows for the assessment of the influence of two key factors — ambient temperature T and cycle duration Δt — on the permissible number of wetting and drying cycles. The only limitation of this formula is the lack of information regarding the value of the chemical bond energy E . However, for preliminary estimates, existing data on this parameter for compounds found in lignin can be used. According to some sources (Demitrova and Chemodanov, 2016; Grunin et al., 2017; Knunyants, 1988; Ministry of Construction, Housing and Utilities of the Russian Federation, 2017; Vanin, 1949; Volkov and Zharsky, 2005), the value of this parameter varies widely: $E = 0.2 \div 10 \text{ eV}$ ($0.32 \cdot 10^{-19} \div 10^{-18} \text{ J}$). It can be reasonably assumed that, under the relatively weak effects being considered, the chemical bonds most likely to break are those with energies near the lower end of this range. Therefore, for the purposes of calculation, it is advisable to use a conservative estimate: $E = 0.5 \cdot 10^{-19} \text{ J}$.

Calculation

Fig. 3 shows the dependence of the relative value of the limit number of wetting and drying cycles, obtained using formula (21), which highlights the significant influence of both Δt and especially T . For example, calculations show that at $\Delta t = 20$ hours, a decrease in ambient temperature from 60°C to 10°C leads to a 6.9-fold increase in n_d .

Undoubtedly, the parameter n_d is of great practical importance. However, a more convenient indicator is the service life of wooden elements, t_r . It can be assumed that this consists of two main components: the service time due to cyclic changes in temperature and humidity conditions, t_c , and the operating time under stationary conditions — i.e., when the influence

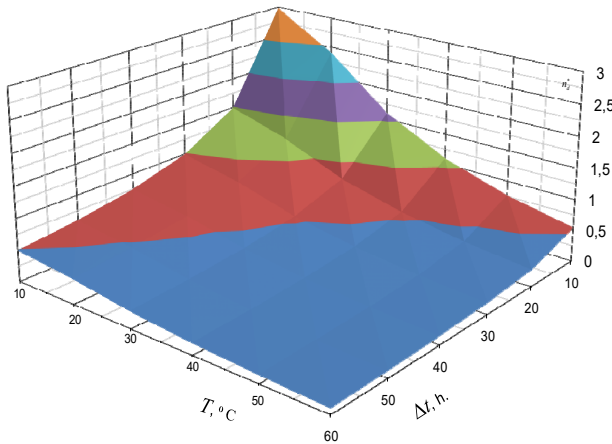


Fig. 3. Dependence of the relative value of the allowable number of wetting and drying cycles (from formula 21) on the duration of such cycles and ambient temperature

of non-stationary heat and moisture transfer in wood can be neglected — denoted as t_{st} :

$$t_r = t_{st} + t_c. \quad (22)$$

As for the parameter t_{st} , its reliable assessment is currently complicated since it requires taking into account the influence of various factors, including biological ones (e.g., rotting and fungal exposure) (Borovikov and Ugolev, 1989; Erofeev et al., 2008; Ugolev, 2005; Vanin, 1949). To determine the second component, t_c , the theoretical developments presented above can be used. Indeed, if the limit number of wetting and drying cycles is known for a given cycle duration Δt , then the desired value can be found as follows:

$$t_c = n_d \Delta t = \frac{\ln K_S}{A} \exp\left(\frac{E}{k \cdot T}\right). \quad (23)$$

The ratio in Eq. (23) allows us to conclude that the portion of the service life determined by cyclically varying temperature and humidity operating conditions depends only on two factors: the safety factor of mechanical strength margin K_S and the ambient temperature T .

To analyze the influence of these factors, it is advisable to use the approach described above — deriving an expression in relative terms. If we take the baseline conditions as $K_S = 3$ and $T = 293$ K, then expression (23) will take the following form:

$$t_c^B = \frac{\ln 3}{A} \exp\left(\frac{E}{k \cdot 293}\right). \quad (24)$$

By dividing both the left and right sides of formula (23) by the corresponding sides of formula (24), the required expression can be obtained:

$$\frac{t_c^*}{t_c^B} = \frac{\ln K_S}{\ln 3} \exp\left[\frac{E}{k} \left(\frac{1}{T} - \frac{1}{293}\right)\right], \quad (25)$$

where $K_S \geq 3$.

Using expression (25), the dependence shown in Fig. 4 was obtained, which also demonstrates

a strong influence of temperature on the service life of wood. For example, a decrease in temperature from 40 °C to 0 °C at $K_S = 3$ leads to an increase in the wood's service life by approximately 5 times. This temperature effect is consistent across other values of K_S .

On the other hand, the influence of K_S is noticeably weaker. For example, at a temperature of 20 °C, increasing this parameter from $K_S = 3$ to $K_S = 10$ — more than threefold — results in only about a twofold increase in the service life component t_c (Fig. 4). Nevertheless, this factor can still be used in practice to extend the service life of wooden structures.

Results

To determine the actual values of the n_d and t_c parameters, an experiment was conducted using a sample of a bolted nagel joint, as shown in Fig. 5a (Fedosov et al., 2016b, 2017b; Kotlov et al., 2017). The sample was placed in a climate chamber, where it was subjected to periodic wetting and drying at a constant temperature. Simultaneously, a mechanical load corresponding to $K_S = 3$ was applied to the sample. The cyclic wetting and drying of the wood continued until structural failure occurred (Fig. 5b). The moisture content of the wood was monitored during the experiment using a Hydromette HT 85 T device and ranged from 8–12 % to 28–32 %, corresponding to the typical extremes encountered in actual operating conditions. The test results are presented in Table.

The data in Table allow us to use expressions (17) and (23) to determine the limit number of wetting and drying cycles n_d and the service life due to cyclic temperature and humidity changes t_c in actual values.

Fig. 6 shows the results of calculations using these formulas for $K_S = 3$ and $\Delta t = 24$ h.

The authors plan to prepare and publish a series of research papers following the completion of the patenting process. These papers will focus on the design of the experimental setup and the results of the

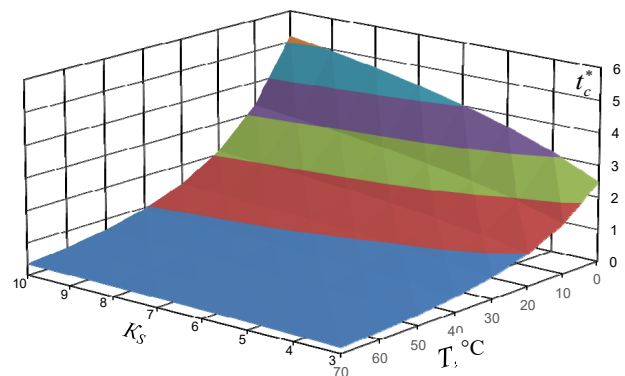


Fig. 4. Dependence of the relative service time of wood, due to the cyclic effects of wetting and drying processes, on temperature and safety factor for mechanical strength

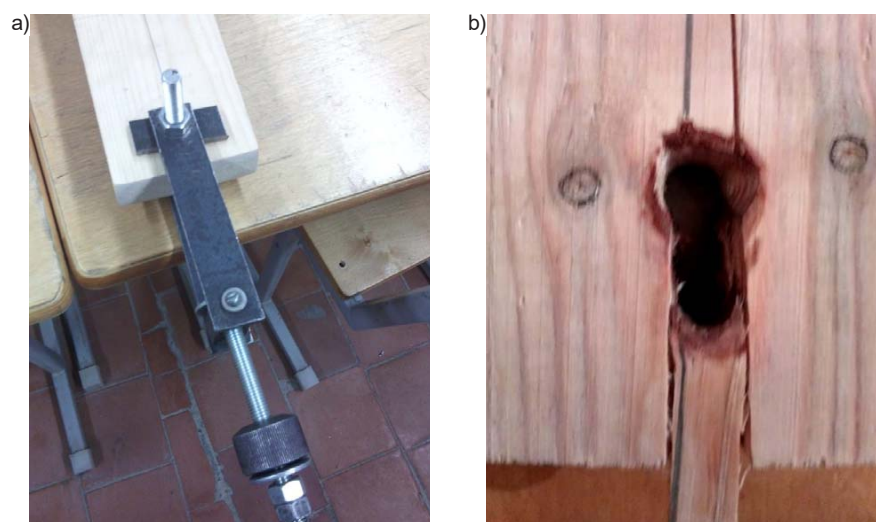


Fig. 5. Appearance of the bolted joint sample (nagel) in assembled form before installation in the climate chamber (a) and the nature of the failure after testing (b)

Failure characteristics of the bolted dowel joint sample

Temperature, T	Limit number of cycles, n_d	Sample lifetime, t_c	Duration of the wetting-drying cycle, Δt	Number of chemical interactions, A
°C	units	h	h	1/s
40	5	103	20.6	0.31

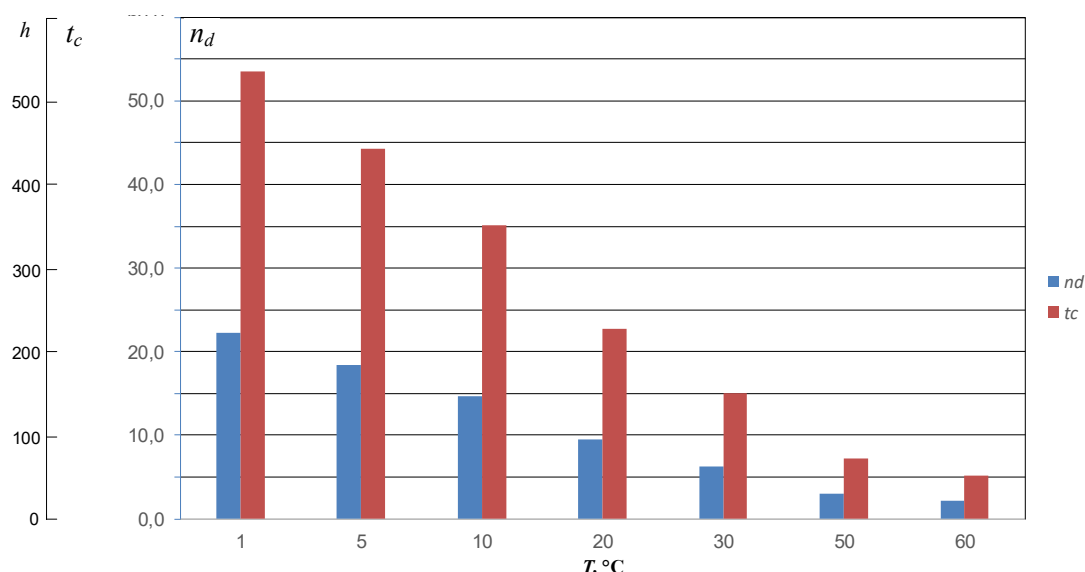


Fig. 6. Dependence of the allowable number of wetting and drying cycles n_d and the service life t_c of the nagel joint wood, in actual values, on temperature at $K_s = 3$ and $\Delta t = 24$ h

conducted experiments, confirming and expanding upon the theoretical findings presented in this paper.

Discussion

The information presented in Fig. 6 clearly indicates a significant influence of temperature on the durability of wood. For example, when the temperature varies from 1 °C to 50 °C — which is typical for the operating conditions of wooden structures in the middle zone of Russia and other

regions with similar climatic conditions — the limit number of cycles n_d and the service life parameter t_c decrease by an order of magnitude. At first glance, these parameters may seem relatively low. However, they correspond to extreme fluctuations in the moisture content of wood and the duration of wetting and drying cycles. In reality, such extreme conditions occur quite rarely, and accounting for this factor remains a task for further research (Fedosov and

Kotlov, 2019; Fedosov et al., 2015, 2016c; Fedosov et al., 2017a).

The results presented in this paper regarding the influence of temperature on the service life of wood align well with the well-known fact that wooden architectural structures have survived to this day in the northern regions of Russia and other countries with cool climates.

Conclusions

1. The theoretical developments presented in this paper represent a further advancement and extension of previously developed mathematical models of heat and mass transfer processes in the wood of nagels, which occur under cyclically changing operating conditions. These developments enable the determination of the life cycle limits of wooden structure joints.

2. A convenient indicator for assessing the durability of the natural composite — wood — is the limit number of wetting and drying cycles. Knowing this parameter also allows for the estimation of the

material's service life. The expressions obtained show that this parameter depends on three main factors: the safety factor, the duration of wetting and drying cycles, and the ambient temperature.

3. Since the quantitative estimates made in this paper are approximate, further theoretical development and experimental studies are necessary to refine the values of the constant parameters in the expressions and to reliably determine the service life of wooden structures.

4. The results presented in this paper have universal significance, as they form the basis for developing physical and mathematical models of destruction and durability for other types of composite materials, such as concrete with various fillers used under different conditions, fiberglass exposed to strong electric fields in high-voltage installations, and others.

This research did not receive any specific grant from funding agencies in the public, commercial, or not-for-profit sectors.

References

- Bazhenov, V. A. (1959). *Piezoelectric properties of wood*. Moscow: Publishing House of the Academy of Sciences of the USSR, 238 p.
- Borovikov, A. M. and Ugolev, B. N. (1989). *Reference book on wood*. Moscow: Lesnaya Promyshlennost, 294 p.
- Demitrova, I. P. and Chemodanov, A. N. (2016). *Wood physics*. Yoshkar-Ola: Volga State University of Technology, 160 p.
- Erofeev, V. T., Smirnov, V. F., and Morozov, E. A. (2008). *Microbiological destruction of materials*. Moscow: Association of Construction Universities, 128 p.
- Fedosov, S. V., Bobylev, V. I., and Sokolov, A. M. (2016a). *Electrothermal treatment of concrete with high frequency currents at precast concrete plants*. Ivanovo: Lenin Ivanovo State Power Engineering University, 336 p.
- Fedosov, S. V. and Kotlov, V. G. (2014). Theory of heat and mass transfer — the basis of physics of destruction of building materials through the example of wood. In: *Mechanics of Destruction of Building Materials and Structures. Proceedings of the VIII Academic Readings of the Russian Academy of Architecture and Construction Sciences*. Ed: Suleymanov A. M. Kazan: Kazan State University of Architecture and Engineering, pp. 344–348.
- Fedosov, S. and Kotlov, V. (2019). Dynamics of heat and moisture transfer in wooden structures tied with metallic fasteners. *Drying Technology*, Vol. 38, Issue 1–2, pp. 19–26. DOI: 10.1080/07373937.2019.1604543.
- Fedosov, S. V., Kotlov, V. G., Aloyan, R. M., Bochkov, M. V., and Makarov, R. A. (2016b). Experimental study of heat transfer processes in a bolt dowel joints. *Construction Materials*, No. 12, pp. 83–85.
- Fedosov, S. V., Kotlov, V. G., and Ivanova, M. A. (2015). Influence of heat and humidity conditions of operation on dowel joints of wooden structure elements. In: *Current Issues and Development Prospects of the Timber Industry. Proceedings of III International Scientific and Technical Conference*. Eds: Ugryumov S. A., Vakhnina T. N., Titunin A. A. Kostroma: Publishing House of the Kostroma State Technological University, pp. 165–168.
- Fedosov, S. V., Kotlov, V. G., and Ivanova, M. A. (2016c). Heat and mass transfer in the wood of roof structures connected by nagel in the form of metal clamping plate (two-dimensional problem). In: *Improving the Efficiency of Processes and Devices in the Chemical and Related Industries*. Ed: Rudobashta S. P. Proceedings of the International Scientific and Technical Conference dedicated to the 105th anniversary of the birth of A. N. Planovsky. Vol. 1. Moscow: Moscow State University of Design and Technology, pp. 304–308.
- Fedosov, S. V., Kotlov, V. G., and Ivanova, M. A. (2017a). The reasons of performance impairment of wooden structures during operation in an environment with cyclically changing temperature and humidity conditions. *Housing Construction*, No. 12, pp. 20–25.
- Fedosov, S. V., Kotlov, V. G., Makarov, R. A., and Ivanova, M. A. (2017b). Experimental research of rafter structures operational conditions during summer period. *Vestnik of Volga State University of Technology. Series: Materials. Constructions. Technologies*, No. 3, pp. 55–61.
- Fridman, I. M. (2007). *Wood processing. Guidance manual*. Saint Petersburg: PROFIKS, 544 p.
- Grunin, Yu. B., Grunin, L. Yu., Sheveleva, N. N., Masas, D. S., Fedosov, S. V., and Kotlov, V. G. (2017). *The character of changes in the cellulose supramolecular structure during hydration*. Proceedings of Higher Educational Institutions. Textile Industry Technology, No. 2 (368), pp. 232–237.
- Knunyants, I. L. (ed.) (1988). *Encyclopedia of chemistry*. Vol. 1. Moscow: Soviet Encyclopedia Publishing House, 625 p.
- Kotlov, V. G., Ivanova, M. A., and Makarov, R. A. (2017). Results of experimental studies of wood samples in the modeling of heat and mass transfer. *Proceedings of the Volga State University of Technology. Series: Technological*, No. 5, pp. 165–168.
- Ministry of Construction, Housing and Utilities of the Russian Federation (2017). *Code of Practice SP 64.13330.2017. Construction Standards and Regulations SniP II-25-80. Timber structures*. Moscow: Standartinform, 97 p.
- Mironov, V. G., Tsepaev, V. A., and Avdeev, A. V. (2000). Influence of wood moisture content on creep of joints of wooden elements on metal toothed plates. *Woodworking Industry*, No. 1, pp. 26–28.
- Ugolev, B. N. (2005). *Wood science with the basics of forest commodity science*. 4th ed. Moscow: Publishing House of the Moscow State Forest University, 340 p.
- USSR State Committee for Standards (1985). *GOST 23431-79*. Wood. Structure and physico-mechanical properties. Terms and definitions*. Moscow: Publishing House of Standards, 15 p.
- Vanin, S. I. (1949). *Wood science*. 3rd ed. Moscow, Leningrad: Goslesbumizdat, 472 p.
- Volkov, A. I. and Zharsky, I. M. (2005). *Large chemical handbook*. Minsk: Sovremennaya Shkola, 608 p.
- Konev A.A. (2024). Metal—toothed (nail) plates - MTP: for the manufacture of wooden rafter trusses. [online] Available at: <https://baumeisterspb.ru/> [Access Date: June 17, 2025].

ФИЗИКО-МАТЕМАТИЧЕСКАЯ МОДЕЛЬ ДОЛГОВЕЧНОСТИ ДРЕВЕСИНЫ ПРИ ЦИКЛИЧЕСКИХ ИЗМЕНЕНИЯХ ТЕМПЕРАТУРЫ И ВЛАЖНОСТИ В ОКРУЖАЮЩЕЙ СРЕДЕ

Сергей Викторович Федосов¹, Виталий Геннадьевич Котлов², Азарий Абрамович Лапидус¹,
Александр Михайлович Соколов^{3*}

¹Национальный исследовательский Московский государственный строительный университет, Москва, Россия

²Поволжский государственный технологический университет, Йошкар-Ола, Россия

³Ивановская пожарно-спасательная академия ГПС МЧС России, Иваново, Россия

*E-mail: amsokolov37@yandex.ru

*Статья посвящена памяти
всемирно известного ученого
Сванте Августа Аррениуса (1859–1927).
В 2024 году отмечается
165-летие со дня его рождения.*

Аннотация

Введение. Существенным недостатком композитных материалов является их склонность к постепенному ухудшению свойств с течением времени, что в конечном итоге приводит к полному разрушению. **Цель исследования.** Целью настоящей работы является выявление физических принципов и разработка теоретической базы для объяснения этого процесса. В качестве объекта исследования выбран природный композит — древесина. Многие физические и теоретические аспекты ее поведения остаются недостаточно изученными. В частности, требует дополнительного изучения снижение механической прочности в узлах соединения деревянных элементов (нагелями) при циклических изменениях температуры и влажности. **Методы.** В статье представлен физико-математический подход к оценке механической прочности древесины под воздействием таких факторов окружающей среды. Модель основана на уравнении Аррениуса и современных представлениях о клеточной структуре древесины, ключевыми компонентами которой являются целлюлозные волокна (армирующий каркас) и лигнин (связующая матрица). Предполагается, что нестационарные процессы тепло- и влагопереноса, обусловленные воздействием внешних условий, постепенно разрушают межатомные связи в соединениях лигнина. **Результаты.** Получены выражения для оценки максимально допустимого количества циклов увлажнения-сушки, которые древесина может выдержать при заданной температуре, а также оценки ее ресурса (срока службы) под влиянием этих циклических процессов. Предложенная теория имеет универсальное значение.

Ключевые слова: композит; тепло- и влагоперенос; уравнение Аррениуса; клеточная структура древесины; математическая модель; ресурс.

OPTIMIZING ENERGY CONSUMPTION AND STRUCTURAL PERFORMANCE OF OFFICE BUILDINGS IN TEHRAN CITY USING COST-EFFECTIVE SOLUTIONS: A MODELING AND SIMULATION-BASED ANALYSIS

Amin Mohammadi^{1*}, Shariyeh Hosseininassab², Seyed Mohammad Mousavi¹

¹Persian Gulf University (PGU), 75169, Bushehr, Iran

²COMSATS University Islamabad (CUI), Lahore Campus, Lahore, Pakistan

*Corresponding author's email: aminmohammadi@pgu.ac.ir

Abstract

Introduction: Office buildings in big cities consume enormous amounts of energy resources every year and the resulting carbon dioxide emissions are significant. In addition, the design, construction, and maintenance of these buildings are extremely expensive, so it is necessary to pay special attention to their durability, stability, and useful life during the design phase. **Purpose of the study:** The main goals of this research were to optimize energy consumption and structural performance of office buildings in megacities by using cost-effective solutions. **Methods:** An office building in Tehran (the capital of Iran) was selected as a case study and simulated using DesignBuilder, Revit, and Robot Structural Analysis software as a baseline model. Then to achieve the main goal, a number of cost-effective solutions were applied in developed and proposed models of this building in a simulation environment. **Results:** The results of this simulation-based analysis showed that the economic solutions used in the proposed model could reduce not only the annual energy consumption and carbon dioxide emissions by 50 %, but also the weight of the materials in the external walls and ceilings by up to 16 %. The suggested methods can significantly reduce the cost of reinforcing the structure and can also increase the building's useful life, durability, and stability. The results of this research can be used in the design phase of office buildings in megacities such as Tehran.

Keywords: office buildings; energy optimization; structural performance; modeling; simulation.

Introduction

In recent decades, many researchers have been very concerned with global warming. The consumption of fossil fuels and the emission of large amounts of carbon dioxide are the most important factors in climate change. Meanwhile, buildings account for more than 40 % of energy consumption in big cities. Administrative buildings located in big cities are considered important urban centers, serving as the main decision-making hubs for urban management and city implementation issues. Consequently, a significant amount of money is spent on their design, construction, repair and maintenance. However, they can have a lot of negative effects on the urban environment, and with the reduction of their useful life or in times of natural disasters, they bear the risk of vulnerability and possible damage. Office buildings consume more energy than other types of buildings. Depending on their equipment, lighting and air conditioning systems, as well as their location and dimensions, energy consumption can vary between 100 and 1,000 kWh/m² per year (Siew et al., 2011). Therefore, to increase the lifespan and physical stability of such buildings, reduce their adverse effects on the urban environment, and optimize their performance

in terms of energy consumption, certain measures should be taken in their design, construction, and performance optimization. In recent years, researchers have already examined many ways to achieve this goal. Khodakarami and Ghobadi (2023) presented simple and practical solutions to optimize energy consumption and establish thermal comfort in a high-rise office building equipped with a smart management system in Tehran. They concluded that it is possible to save 35 % to 40 % in energy consumption per year. Ghiai and Hajjar (2014) investigated the relationship between the opening ratio and energy consumption of high-rise office buildings in Tehran using eQuest simulation software. They concluded that these two variables have a direct relation: reducing the ratio of openings by 20 % can reduce annual energy consumption by 17 %. Moulai et al. (2019) investigated the optimization of dimensions and proportions of openings in the office spaces of Tehran in terms of lighting and energy consumption by using simulation. The results of this research showed that the most optimal window-to-wall ratio was between 20 % and 28 %, and the optimal length and width were respectively 53.6 and 9 meters on average. Haghani et al. (2017) used simulation to determine the effect

of shutters in four main directions on the optimization of energy consumption of office buildings in Tehran. They concluded that the presence of this type of shade had a significant effect on glare and annual thermal loads. Mohammadi et al. (2023) chose an office building in Tehran as a case study to improve the indicators of Iran's national standard in the field of evaluating the energy performance of non-residential buildings by comparing it with the LEED standard. Akeiber et al. (2016) reviewed phase change materials for passive cooling in buildings and concluded that most of the research conducted in this field was done with real-scale tests and numerical modeling. Therefore, the use of such materials in the external walls of buildings had already been highlighted in the past researches.

In another research, Alvand et al. (2017) examined cost-effective solutions for energy consumption in buildings, including the use of thermal insulation, shading systems, high-efficiency windows, and solar renewable energy in Iran. They concluded that optimizing energy consumption and achieving energy-efficiency in buildings was not possible without government subsidies. Anvari-Moghaddam et al. (2015) presented an innovative system for the energy management of Iranian buildings with optimization of energy consumption and thermal comfort, which can be economically viable. Azari et al. (2016) presented a multipurpose optimization algorithm for the optimal design of the components of a low-rise office building in Seattle, USA, taking into account energy consumption, the life cycle of consumable materials, and their impact on the environment. Insulation materials, the type of windows and their frames, the thermal resistance of the walls, and the window-to-wall ratio used in the south and the north sides were important parameters in this project. The authors used the eQuest software for the simulation. They obtained the best results with R-17 thermal insulation, fiberglass frame with three-pane glass, and the window-to-wall ratio including 60 % on the south side and 10 % on the north side. Using genetic algorithm and simulation, Baniassadi et al. (2016) investigated the economic optimization of thermal insulation thickness and the thickness of the phase change material layer in Tehran, Isfahan, Shiraz, Bandar Abbas, Yazd and Tabriz. The results of EnergyPlus software showed that the thickness determined for the layer of phase change materials in all the investigated cities was zero, while the thickness of the thermal insulation in the cities of cold regions should be up to 6 cm. However, in the current economic conditions of Iran, the cost of thermal insulation is higher than that of phase change materials. Fathalian and Kargarsharifabad (2018) investigated energy consumption in an office building in Semnan city. The results of the model simulated by the software and its comparison with

the measurement of the actual energy consumption of the building based on electricity and gas bills showed an error of 1.6 %, which illustrated the accuracy of the modeling. The solutions used in this building to optimize energy consumption included double-glazed windows, thermal insulation of external walls, and horizontal shades on its facade. The results showed that each of these solutions saved up to 18 %, 14 %, and 13 % in the energy consumption of the building, respectively. In another research, Heravi and Qaemi (2014) evaluated the design and construction of buildings considering the optimization of energy consumption in Iran. The research results showed that the use of solar energy can be considered the most widely used renewable energy system in Iran. Javid et al. (2019) developed a multi-objective optimization framework with the lowest economic costs and the lowest impact on global warming. New energy-efficient technologies for supporting and using energy systems were implemented on and investigated in two educational buildings in Sharif University of Technology campus in Tehran. These systems reduced carbon dioxide emissions by 18–20 %. Mohtashami et al. (2016) conducted a research to determine strategy and policy-making in architectural design to achieve optimal conditions in terms of health and safety of the interior space of buildings by using interviews and logical reasoning. Movahhed et al. (2019) investigated the combination of solar panels and green roofs to optimize energy consumption in a common building using DesignBuilder and PVsol software. The research showed that the reduction in energy consumption as a result of the use of green roofs was very limited, while solar panels produced up to 26 megawatt hours of energy per year, and the payback period was between 6.5 and 7.5 years. Moreover, they could prevent the production of 16.3 tons of carbon dioxide annually. Solgi et al. (2019) investigated the role of light phase change materials along with night ventilation to optimize energy consumption in three different types of climates. The research results showed that in tropical climates, the use of these two strategies together was ineffective. However, in subtropical as well as hot and arid climates, the cooling set-point of HVAC systems and thermal insulation played a key role in the performance of phase change materials and night ventilation. In addition, thermal insulation was more effective in optimizing night ventilation than phase change materials. Tahsildoost and Zomorodian (2015) examined the retrofitting of two common educational buildings in Iran. Replacing the windows, sealing the openings appropriately, and using thermal insulation on the roof were among the solutions considered in this research, while the payback period was also taken into account. After the simulation, the results included a 30 % to 38 %

reduction in energy consumption in two educational buildings, and the results of the questionnaires also indicated an improvement in the thermal condition inside the building. Vakiloroya et al. (2014) showed that a combination of different technologies of mechanical air conditioning systems can be useful for reducing energy consumption and improving thermal comfort. Yousefi et al. (2017) investigated the effect of users' behavior on the energy performance of building components. For this purpose, a typical apartment building in Iran was selected and its energy simulation results were compared with the actual energy consumption results of that building. The energy consumption of buildings in different climates, before and after the amendments, was simulated using EnergyPlus software. The sensitivity analysis in this research showed that the behavior of users had a great impact on the thermal energy consumption of the building in hot climates and could change the cooling and heating loads of the building up to 90 %.

The literature review shows that the simultaneous use of cost-effective solutions for optimizing energy consumption and structural performance of office buildings has not been investigated so far. This study goes beyond this stage to examine the optimization of energy consumption and structural performance of office buildings as the main objectives of the research in a simulation environment with respect to cost-effective solutions. To this end, three models including a baseline model of an office building, a developed model, and a proposed model are simulated and analyzed in two steps. The research process diagram of this study is shown in Fig. 1. In the

first step, we model and simulate the selected office building in Tehran city in DesignBuilder software. Then we review the annual energy consumption of this baseline model in different sections and identify the important parts. Then, to optimize the annual energy consumption in the baseline model, a number of passive and active strategies are selected and utilized in a developed model. At the end of the first step, we develop a model of the office building with optimized energy consumption. In the second step of this study, the architectural and structural modeling and simulation are necessary for analyzing the structural performance of the case study building in a simulation environment. For this purpose, after modeling the baseline and developed model in Revit Architecture software, we obtain a proposed model of the office building with lightweight materials in its external walls in Revit Architecture as well. Then, for modeling and simulation of the structural performance, all models are transferred to Revit and Robot Structural Analysis software. Finally, the findings of the model-based simulations are compared and analyzed. We suggest an optimized model of the office building in terms of energy consumption and structural performance and make theoretical predictions.

Methods

This research employs a methodology that focuses on modeling and simulation techniques to enhance energy efficiency and structural integrity in office buildings. We chose this technique for its ability to measure multiple performance indicators without the financial and logistical challenges of conducting real-world experiments. The virtual testing space

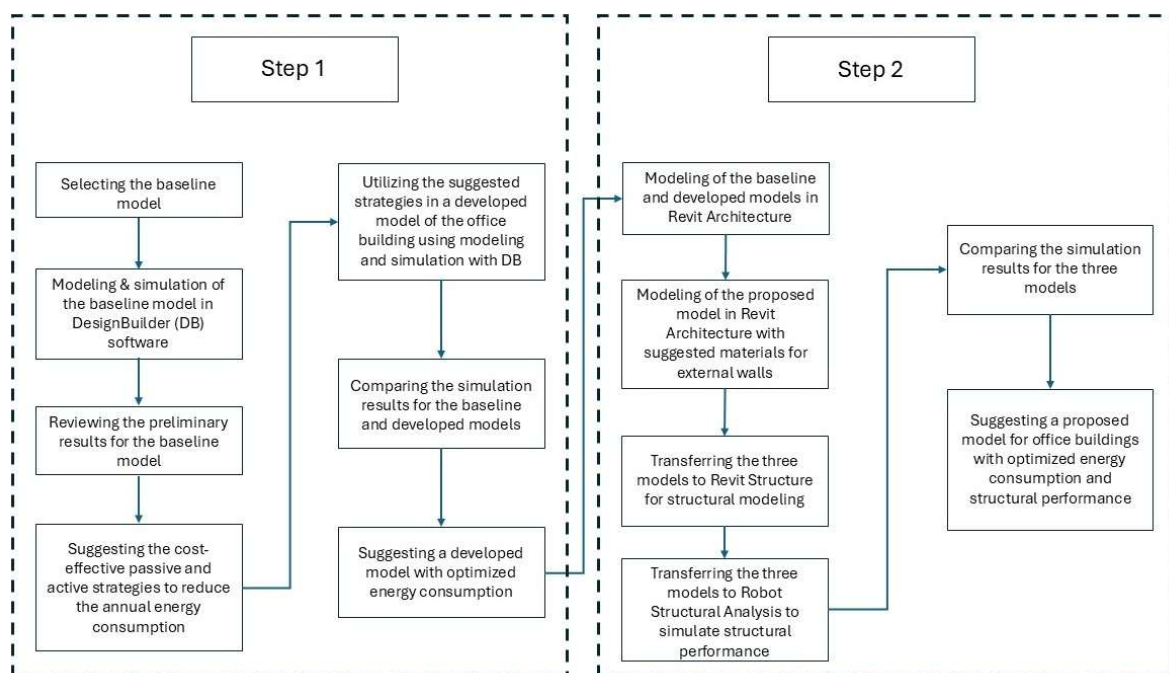


Fig. 1. Research process diagram

facilitates in-depth examination and evaluation of various situations, offering valuable information on possible enhancements in energy conservation and the strength of structures. Given that the study aims to evaluate both energy consumption and the loads on structures, simulation-based modeling is an especially appropriate technique. It allows for theoretical forecasts involving various factors, including energy consumption for cooling, heating, lighting, hot water for domestic use, and cooking, along with enhancements in structure through alterations in materials.

In this study, we formulate three separate models, each serving a particular purpose. The baseline model reflects the real-world performance of the building, pointing out its energy inefficiencies. This model is essential for grasping current challenges; it provides a basis for ongoing optimization efforts. The developed model combines several passive and active methods to lower energy consumption, revealing how targeted interventions can significantly improve building performance. Lastly, the proposed model retains the energy-efficient strategies of the developed model and introduces lightweight materials for the external walls, focusing on reducing dead loads and enhancing the overall structural performance of the building.

The entire process of calculation occurs in a simulated framework, and the outcomes rely on

theoretical insights rather than practical experimentation. This method provides adaptability and accuracy when assessing different design options, making it a perfect fit for fulfilling the goals of this research.

In the first part of the methodology section, which is about energy optimization, the general specifications of the case study building, suggested strategies to be used in the developed model, and the simulation results of the baseline and developed models are described and compared in terms of energy optimization and cost-effectiveness of the retrofit actions. Then in the second and third parts, we describe and compare the architectural and structural modeling process of the baseline, developed and proposed models.

Energy Optimization

An office building in Tehran with the specifications indicated in Table 1 was selected as a case study. The first part of this research was carried out by using modeling and simulation in DesignBuilder software (Fig. 2a) and hourly climatic data of Tehran city along with the occupancy schedule.

To estimate the building energy consumption, we utilize the energy balance equation, which is used to maintain indoor thermal comfort conditions. Various components including cooling, heating, lighting, and domestic hot water (DHW) are typically considered. A general approach to these equations (1–4) is presented as follows:

Table 1. Specifications of the case study building

Physical specifications and equipment	Baseline model
Area	2,133.5 (m ²)
Number of floors	5
Shading (north)	None
Shading (south)	None
Shading (west)	Not needed
Shading (east)	Not needed
Natural ventilation set point	None
Natural ventilation schedule	None
Mechanical ventilation	Air handling unit (AHU)
Rate of air change per hour (ACH)	3 (1/h)
Cooling system, seasonal CoP	Fan coil units connected to the chiller, 1.8
Heating system, seasonal CoP	Fan coil units connected to the boiler, 0.85
Lighting system	Fluorescent, normalized power density 5 W/m ²
Domestic hot water (DHW), seasonal CoP	Instantaneous hot water, 0.85
Window frame and thickness	Aluminum, 4 cm
Number of panes and glazing	2, generic clear
Heat transfer coefficient of glazing	3.128 W/(m ² k)
Solar heat gain coefficient of glazing	0.71
Thickness of external walls	26.5 cm
Materials of external walls	Granite, cement mortar, brick, gypsum plastering, polyester resin
Heat transfer coefficient of external walls	0.35 W/(m ² k)
Occupancy schedule	8 am – 4 pm
Holidays	Thursday and Friday

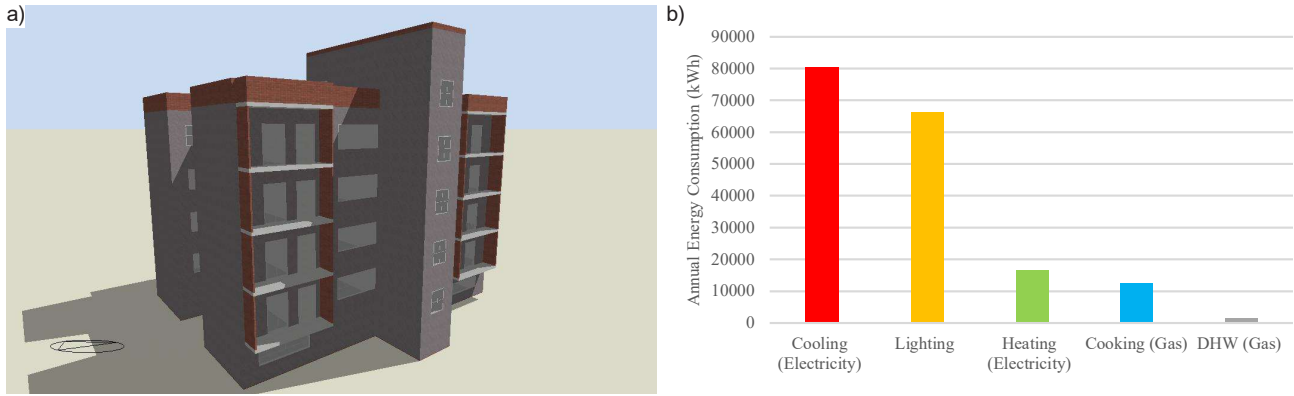


Fig. 2. (a) Baseline model in DesignBuilder, (b) annual energy consumption of the baseline model in different sections

1. Cooling and heating load calculation.

The basic equation for cooling and heating load is as follows:

$$Q = U \times A \times \Delta T, \quad (1)$$

where:

Q — thermal load in Watts or BTU/hr;

U — heat transfer coefficient in $W/m^2 K$ or $BTU/(hr.ft^2 ^\circ F)$;

A — area of the building envelopes like walls, windows, roofs, etc. in m^2 or ft^2 ;

ΔT — temperature difference between indoor and outdoor environments in $^\circ C$ or $^\circ F$.

The heat loss or gain through the building envelope is calculated using Eq. (1). The sum of the loads calculated for each building surface is considered the total cooling or heating load of the building.

2. Energy consumption for lighting.

Energy consumption for lighting can be estimated as:

$$E = P \times H, \quad (2)$$

where:

E — total lighting energy consumption in kWh;

P — total power of lighting in kW;

H — number of operational hours for lighting in hrs;

3. Domestic hot water (DHW) demand.

The required energy for domestic hot water (DHW) can be estimated as follows:

$$Q_{DHW} = m \times c \times \Delta T, \quad (3)$$

where:

Q_{DHW} — required energy for heating the water in J or BTU;

m — stands for the mass of the water in kg or lb;

c — specific heat capacity of the water, which is $4.18 \text{ kJ/(kg}^\circ C)$ or $1 \text{ BTU/(lb}^\circ F)$;

ΔT — temperature rise that is needed to reach the desired water temperature.

4. Total annual energy consumption.

The total annual energy consumption (Q_T) can be expressed as:

$$Q_T = \sum (Q_{cooling} + Q_{heating} + Q_{lighting} + Q_{DHW}). \quad (4)$$

By aggregating the multiple energy requirements, Eq. (4) presents a holistic view of the building's energy usage over a year.

This collection of equations is essential for evaluating energy performance and uncovering optimization strategies through simulations in a modeling environment.

The annual energy consumption of the office building in different sections is shown in Fig. 2b. According to this figure, cooling, lighting, and heating have the highest share of annual energy consumption in this building. To optimize the annual energy consumption in these sections, a combination of cost-effective passive and active strategies was employed in the developed model of the office building. Table 2 shows these suggested strategies for the developed model.

By utilizing the suggested strategies of Table 2 in the developed model of the office building, the annual energy consumption and the carbon dioxide emissions can be reduced by 50 %. In addition, in Table 3, the amount of annual energy consumption, annual carbon dioxide emissions, and the cost of retrofit actions in the baseline model of the office building are compared with those in the developed model.

The economic analysis in Table 3 and Fig. 3 shows that the amount of saving in annual energy consumption in the developed model compared to the baseline model is 129 124.32 kWh. Considering the global price of energy (0.24 GBP per one kWh), 30 989.83 GBP can be saved in a year and the cost of retrofit actions in the developed model (15 130.6 GBP) can be compensated within 7 months (Fig. 3a). However, taking into account the domestic price of energy in Iran (2,100.5 IRR per kWh), financial savings of 271 225 634 IRR per year can be made, and the retrofit cost in the developed model (1 149 622,988 IRR) can be compensated in 5 years (Fig. 3b). Considering the payback period, it seems that the solutions used to optimize the baseline model are economically justifiable.

Table 2. Strategies suggested for the developed model

No.	Strategies
1	Changing the cooling set point from 24 °C to 25 °C
2	Changing the heating set point from 22 °C to 18 °C
3	Changing the natural ventilation set point to 24 °C
4	Adding 7 cm of polyurethane foam to the external walls
5	Changing window frames to UPVC
6	Replacing double pane windows with an air layer with double panes with a 13-mm layer of argon gas
7	Changing the type of external doors from iron to aluminum with a 2 cm air layer
8	Removing internal shading In the southern and northern facades of the building, the depth of the horizontal shading was considered to be 120 and 110 cm, respectively; vertical shading with the same depths was added next to the horizontal ones on both facades.
9	We selected a lighting system based on ASHRAE standards for office buildings and changed its power density from 5 W/m ² -100 Lux to 3.2 W/m ² -100 Lux. The building's lighting system was set to use natural light during the day and artificial light only when needed.

Table 3. Comparison of the baseline and developed models

Model name	Annual energy consumption (kWh)	Annual carbon dioxide emissions (ton)	Annual energy cost savings (GBP'/year)	Cost of retrofit actions (GBP')	Payback period*, considering the global price of energy (GBP')	Payback period*, considering the domestic price of energy (IRR'')
Baseline model	258 053.59	150.70	—	—	—	—
Developed model	128 929.27	75	30 989.83	15 130.6	7 months	5 years

* British pound (£); ** Iranian rial; 1 £ = 759,800 IRR

* Payback period = (Cost of retrofit actions / Annual energy cost savings)

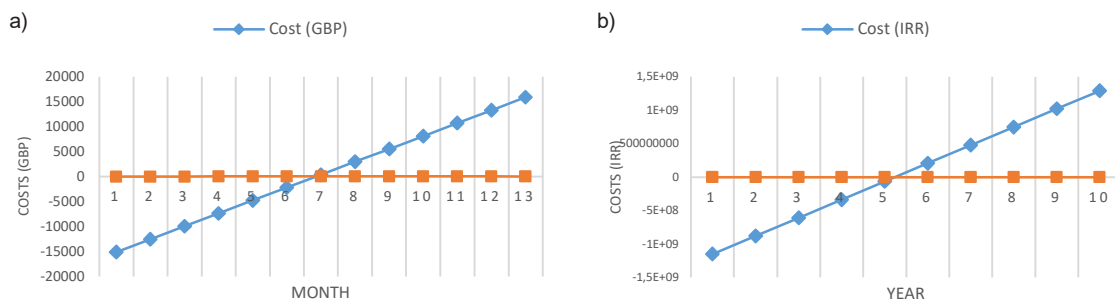


Fig. 3. Payback period diagram of the developed model considering (a) global price of energy and (b) domestic price of energy

As mentioned earlier, in the second part of this study, the objective is not only to retain the 50 % reduction in the annual energy consumption in the proposed model, but reduce the weight of the materials used in the external walls (while preserving their functional quality) to lower the dead loads. This way, the structural performance of the building is strengthened against dynamic loads such as earthquakes and wind, and its useful life is increased. The weight of the materials used in the external walls of all three models and their details are extracted with the help of DesignBuilder software and compared with each other in Section 2–2. Moreover, the amount of dead loads from the external walls and roof are specified for loading in the structural model. Then, by using Revit software, architectural and structural

modeling is done for the developed and proposed models, and their structural loading is determined. Furthermore, we used Robot Structural Analysis to calculate dead loads from external walls and ceilings by directly sending Revit structural models to the software. Robot Structural Analysis was the primary tool for the relevant calculations. In the end, the effects of reducing the weight of external walls in the structural models are compared with each other.

Architectural Modeling

Introduction of the baseline model

The baseline model of the case study office building (Figs. 4 and 5) has five floors, including a basement, a pilot space, parking, and three floors of administrative spaces. The architectural modeling of the case study is done in Revit Architecture software.

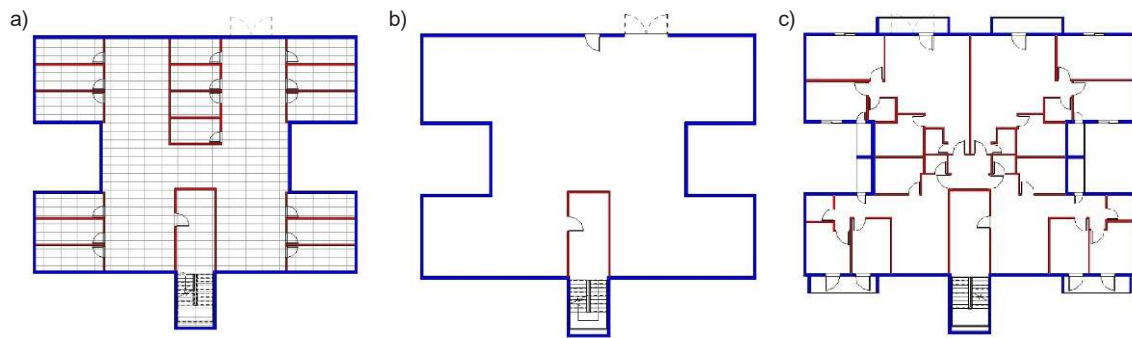


Fig. 4. (a) Basement, (b) parking, (c) administrative spaces of the baseline model



Fig. 5. Baseline model in Revit Architecture

Table 4 shows a summary of the weight of the materials used in the external walls and roof of this model.

The baseline model's external walls, ceilings, and roof weigh about 2 320 204.8 kg, with external walls at 1 334 432.5 kg and ceilings and roof at 985 772.3 kg. Fig. 6 presents the details on the external walls of the baseline model.

Introduction of the developed model

The architectural spaces in the developed model are not different from the baseline model and the floor plans are the same. Its architectural modeling is done in Revit Architecture software as well. The developed model's external walls differ from the baseline, with an added 7 cm layer of polyurethane insulation. Table 5 also shows a summary of the weight of the materials used in the external walls and the roof of this model.

The developed model's total weight for external walls, ceilings, and roof is about 2 321 218 kg, with external walls weighing 1 335 445.7 kg and ceilings and roof weighing 985 772.3 kg. Fig. 7 presents the details on the external walls of the developed model.

Introduction of the proposed model

The architectural spaces and floor plans in the proposed model are identical to the baseline. The architectural 3D modeling was done in Revit

Table 4. Summary of the weight of the materials used in the external walls and roof of the baseline model

Baseline model	
	Mass (kg)
External walls	1 334 432.5
Ceilings and roof	985 772.3
Total	2 320 204.8

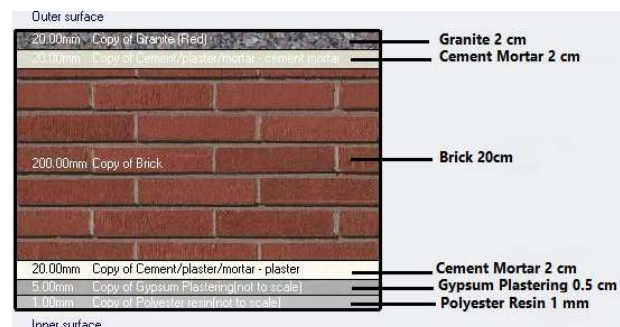


Fig. 6. Details on the external walls of the baseline model

software. The proposed model uses the same energy optimization solutions as the developed model, but the external wall materials differ from those both in the baseline and developed models. We added a light polystyrene thermal insulation roll layer with a 7 cm thick wooden support frame and a 2 cm air layer. In addition, we replaced the 20 cm thick bricks and 0.5 cm gypsum plastering of the external walls with 20 cm thick light concrete blocks and 1 cm light plaster sheets. Table 6 shows a summary of the

Table 5. Summary of the weight of the materials used in the external walls and the roof of the developed model

Developed model	
	Mass (kg)
External walls	1 335 445.7
Ceilings and roof	985 772.3
Total	2 321 218

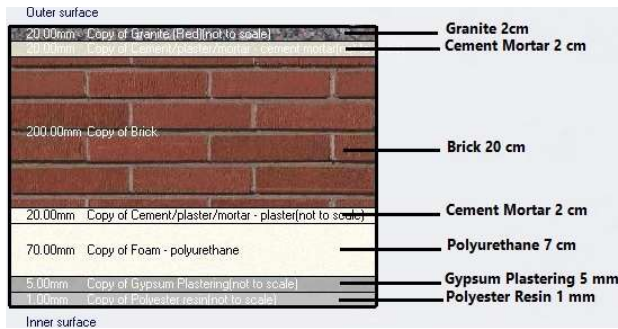


Fig. 7. Details on the external walls of the developed model

Table 6. Summary of the weight of the materials used in the external walls and roof of the proposed model

Proposed model	
	Mass (kg)
External walls	961 339.1
Ceilings and roof	985 774
Total	1 947 113.1

weight of the materials used in the external walls and the roof of this model.

The proposed model's external walls, ceilings, and roof weigh about 1 947 113.1 kg, with 961 339.1 kg for the walls and 985 774 kg for the ceilings and roof. Fig. 8 presents the details on the external walls of the proposed model.

Structure Modeling

The type of structural system used in the case study building is a bending frame; the structure is made of reinforced concrete. The structural system of all three models considered in this study is the same. Fig. 9 shows the foundation and structure plan of all three models and specifies the exact location of columns, beams, and reinforced concrete slabs of the ceilings. The dimensions of the columns and beams are 60 x 60 cm; the concrete slabs of the ceilings are 30 cm thick. The individual footing foundations measure 2 x 2 meters with a height of 1 meter.

All three models in this study were simulated using DesignBuilder, which also provided the weight

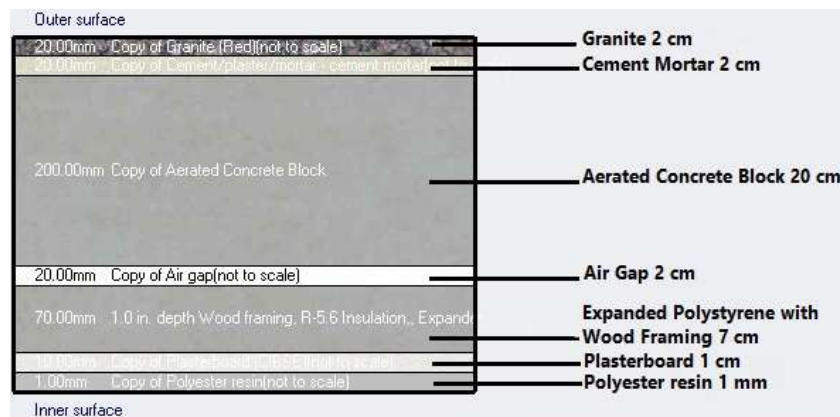


Fig. 8. Details on the external walls of the proposed model

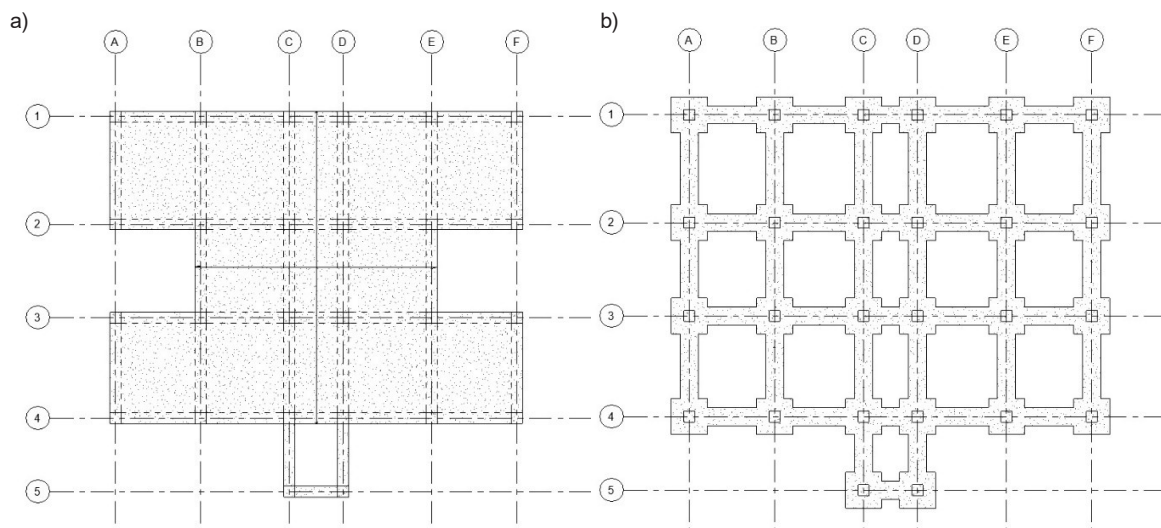


Fig. 9. (a) Reinforced concrete slabs of the ceilings, (b) foundation of the three models in Revit Structure software

of materials for the external walls and ceilings. After modeling the structure in Revit Structure software, it is necessary to apply structural loading based on the weight of the external walls and ceilings that were previously imported. For this purpose, the amount of dead loads caused by the external walls and ceilings should be specified for loading in the models.

Table 7 shows the amount of dead load caused by the weight of external walls and ceilings for loading in structural models. The table shows that ceiling loading is extensive (hosted area load) and consistent across all three models because they use the same materials. However, the proposed model's external wall loading is linear (hosted line load) and differs from the other two models due to different materials. After loading the structure into Revit Structure to perform the calculations of the forces on the supports and the torques (moments) on the structure, the built model was transferred to the Robot Structural Analysis. Figs. 10a and 10b show the image of one of the models loaded in Revit Structure and Robot Structural Analysis, respectively.

The subsequent primary equations (5–16) can be employed to assess the forces and moments at the base of a building structure, specifically where the columns attach to the foundation, along with the reactions at the various supports:

1. Calculating forces at the base

The total forces acting at the base can be expressed as:

$$F_x = \sum_{i=1}^n F_{xi}; \quad (5)$$

$$F_y = \sum_{i=1}^n F_{yi}; \quad (6)$$

$$P = \sum_{i=1}^n P_i, \quad (7)$$

where:

F_x and F_y are the horizontal forces (e.g., seismic loads, wind loads) acting along the x and y axes in kN;

P is the total vertical load (e.g., dead load, live load) in kN;

F_{xi} and F_{yi} are the horizontal forces on the ith floor in the x and y directions in kN;

P_i is the vertical force acting on the ith floor in kN.

2. Calculating torques (moments) at the base

The torques (moments) on the x, y, and z axes can be estimated as follows:

$$M_x = \sum_{i=1}^n (F_{yi} \cdot h_i); \quad (8)$$

$$M_y = \sum_{i=1}^n (F_{xi} \cdot h_i); \quad (9)$$

$$M_z = \sum_{i=1}^n [(dx \cdot F_y) - (dy \cdot F_x)], \quad (10)$$

where:

M_x , M_y , and M_z are the torques (moments) on the x, y, and z axes in kNm;

Table 7. Amount of dead load of external walls and ceilings for loading in the models

	Baseline model	Developed model	Proposed model
Each floor area	356.5 m ²	356.5 m ²	356.5 m ²
Each floor perimeter	99.8 m	99.8 m	99.8 m
Hosted line load on each floor	33.4 kN/m	33.4 kN/m	24 kN/m
Hosted line load in roof	11.1 kN/m	11.1 kN/m	8 kN/m
Hosted area load on each floor	5.5 kN/m ²	5.5 kN/m ²	5.5 kN/m ²
Hosted area load in dome roof	0.7 kN/m ²	0.7 kN/m ²	0.7 kN/m ²

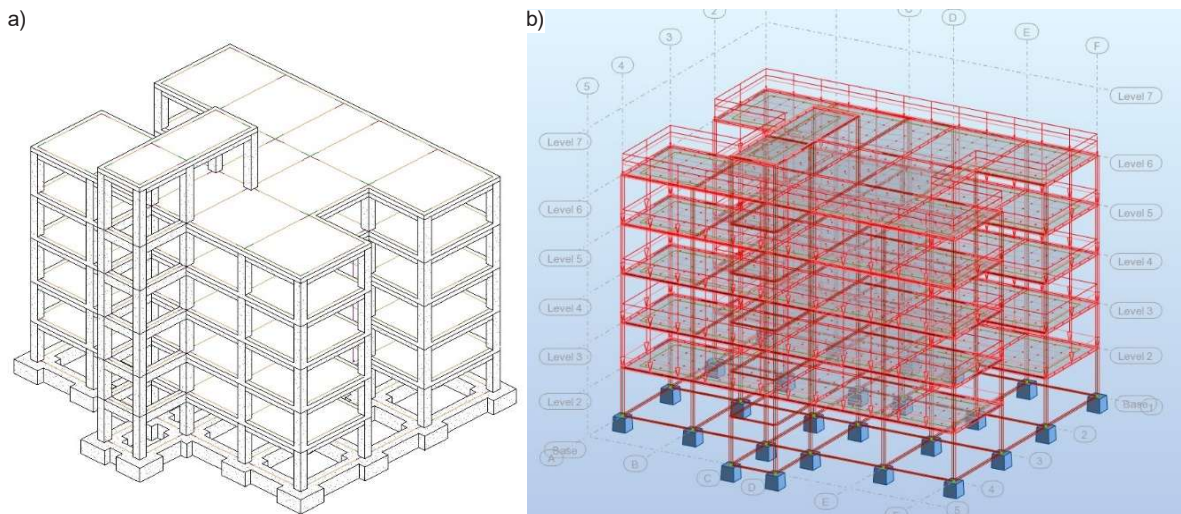


Fig. 10. (a) Baseline model in Revit Structure, and (b) in Robot Structural Analysis

h_i is the height from the base to the i th floor in m;
 d_x and d_y represent the distances from the center of the building to where the forces F_x and F_y act, highlighting the eccentricities for rotational moments in the horizontal plane.

3. Calculating total reaction at supports

To maintain static equilibrium in the building, the reactions at the supports need to offset the overall vertical load, horizontal forces, and torques (moments) acting on it. The following conditions must be met for equilibrium:

$$\sum R_x = F_x; \quad (11)$$

$$\sum R_y = F_y; \quad (12)$$

$$\sum R_z = P, \quad (13)$$

where: R_x , R_y , and R_z are the reactions at supports along the x , y , and z axes in kN.

For the torques (moments):

$$\sum M_{sx} = M_x; \quad (14)$$

$$\sum M_{sy} = M_y; \quad (15)$$

$$\sum M_{sz} = M_z, \quad (16)$$

where: M_{sx} , M_{sy} , and M_{sz} are the torques (moments) at supports in kNm.

These equations provide a fundamental structure for determining the forces and torques at a building's foundation, ensuring that the supports can adequately resist and maintain balance.

Results and Discussion

The findings outlined in this part are solely based on the computational models created to evaluate energy efficiency and structural integrity within the

simulated setting. The baseline, developed and proposed models were all intentionally designed to achieve specific aims within this study: recognizing energy inefficiencies, adopting optimization strategies, and enhancing the performance of the structure. With these models, we were able to recreate a variety of scenarios linked to energy usage for cooling, heating, lighting, domestic hot water, and cooking, in addition to analyzing structural changes via modifications in materials.

The baseline model served as a point of reference, indicating the current inefficiencies in energy consumption within the actual facility. Building on this basis, the developed model incorporated both passive and active approaches designed to improve energy efficiency. The proposed model put forward expanded upon these upgrades by incorporating lightweight materials in the external wall, aiming for better structural performance while still upholding the energy efficiency characteristics of the developed model.

The structure of the studied models includes 26 columns, the location of each can be seen in Fig. 9b. In this study, the estimated amount of forces and torques on the lowest part of the structure (where the columns are connected to the foundation) and the total reaction of the supports against the total of these forces and torques were calculated using Robot Structural Analysis. Table 8 and Figs. 11a and 11b show the estimated amount of forces and torques on the lowest part of the structure for all 26 columns in the baseline and developed models and the total reaction of the supports. As indicated in

Table 8. Estimated amount of forces and torques on the lowest part of the structure for all 26 columns in the baseline and developed models

Node/Case	FX (kN)	FY (kN)	FZ (kN)	MX (kNm)	MY (kNm)	MZ (kNm)
1/ 1	21.81	29.96	1696.94	31.52	-22.13	-0.02
2/ 1	0.95	27.86	2321.64	33.63	-2.69	0.01
3/ 1	-11.34	21.72	2077.12	6.62	19.09	-0.02
4/ 1	11.12	21.79	2081.25	6.55	-19.46	0.01
5/ 1	0.40	6.77	578.38	25.76	-17.49	-0.02
6/ 1	-0.70	6.75	582.69	25.79	16.81	-0.02
7/ 1	-1.25	28.36	2342.74	33.15	2.25	-0.01
8/ 1	-21.04	30.24	1787.90	31.25	22.78	0.03
9/ 1	23.19	-29.06	1741.41	20.84	-20.80	0.04
10/ 1	23.44	33.27	1800.77	-15.49	-20.52	-0.05
11/ 1	21.84	-35.21	1696.39	-34.84	-22.16	0.07
12/ 1	0.42	-33.14	2253.31	-37.05	-3.25	0.01
13/ 1	-12.18	-26.87	1896.53	-43.39	18.28	0.02
14/ 1	11.94	-26.95	1899.58	-43.29	-18.55	-0.04
15/ 1	-0.91	-33.65	2265.13	-36.46	2.73	-0.02
16/ 1	-21.37	-35.61	1703.60	-34.30	22.61	-0.09
17/ 1	-23.35	33.01	1885.56	-15.08	20.49	0.02
18/ 1	-22.88	-28.69	1910.87	20.50	20.98	-0.04
19/ 1	-1.20	-6.19	2881.03	-2.20	2.39	-0.02
20/ 1	1.09	9.33	2794.10	8.58	-2.59	-0.01
21/ 1	-12.34	6.71	2257.45	11.17	18.10	-0.00
22/ 1	12.44	6.72	2275.29	11.17	-18.10	-0.01
23/ 1	-1.33	8.92	2927.39	9.05	2.24	-0.01
24/ 1	11.92	-4.81	2293.94	-3.62	-18.63	-0.01
25/ 1	1.24	-6.38	2738.33	-2.04	-2.47	0.02
26/ 1	-11.93	-4.87	2273.85	-3.57	18.50	-0.00
Case 1	DL1					
Sum of val.	0.00	0.00	52963.20	4.27	-1.60	-0.14
Sum of reac.	0.00	0.00	52963.20	420107.21	-599203.09	0.00
Sum of forc.	0.0	0.0	-52963.20	-420107.21	599203.09	0.0
Check val.	0.00	0.00	0.00	-0.00	-0.00	0.00
Precision	1.62037e-07	1.51360e-17				

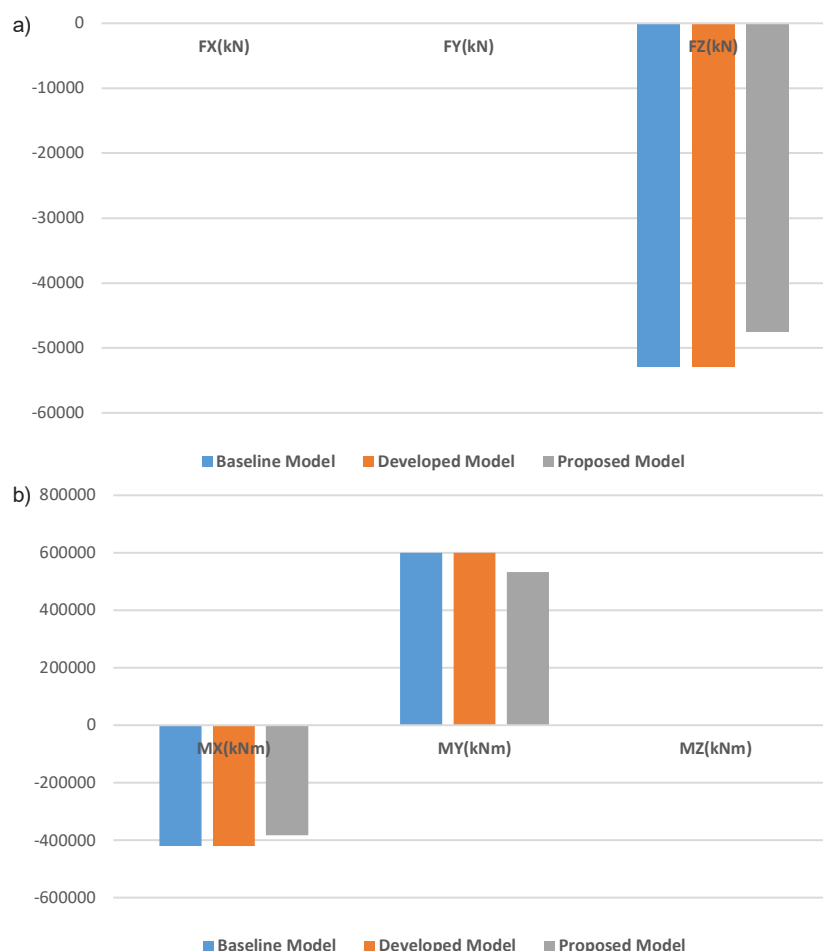


Fig. 11. Total (a) forces and (b) torques in the three models

the table and Fig. 11a, the horizontal forces (X and Y axes) from dead loads in both models are zero at the structure's base in the baseline and developed models. However, the vertical force (Z axis) is $-52\,963.20$ kN (sum of point loads on the lowest part of all 26 structural columns), requiring a support reaction of $52\,963.20$ kN to maintain stability. In addition, Table 8 and Fig. 11b show that the sum of the torques on the lowest part of the structure in the vertical direction is zero. But in the horizontal direction, we can see significant values in the direction of the X and Y axes, so that in the direction of the X axis, the sum of the torques is estimated at $-420\,107.21$ kNm. To keep the structure stable, the supports need a reaction of $420\,107.21$ kNm. Along the Y axis, the total torques are $599\,203.09$ kNm, requiring a support reaction of $-599\,203.09$ kNm for stability.

Table 9 and Figs. 11a and 11b also show the estimated amount of forces and torques on the lowest part of the structure for all 26 columns in the proposed model and the total reaction of the supports. The table and figure indicate that the sum of forces from dead loads in the proposed model in the lowest part of the structure is zero in

the horizontal (X and Y) directions. However, in the vertical (Z) direction, the sum is $-47\,572.84$ kN (the sum of the point loads on the lowest part of all 26 structural columns), which requires a support reaction of $47\,572.84$ kN to maintain stability. The table and figure show that the sum of torques on the structure's lowest part is zero vertically, but significant in the X and Y horizontal directions. The X-axis torques total $-382\,413.01$ kNm, requiring a $382\,413.01$ kNm reaction for stability. The Y-axis torques total $532\,815.80$ kNm, needing a $-532\,815.80$ kNm reaction for stability.

The comparison of the three models in this study (from Tables 4, 5, and 6) shows that the weight of the materials used in the external walls and ceilings of the proposed model is 16 % less than in the other two models. This resulted in reduced dead loads in this model, and the total forces in the Z axis and the total torques in the X and Y axis on the lowest part of the structure in this model are 10 %, 9 %, and 11 % less than in the other two models, respectively. Table 10 shows that the proposed model saves $129\,352.92$ kWh annually compared to the baseline. With energy priced at 0.24 GBP per kWh, this results in a yearly saving of 31,044.70 GBP. The retrofit cost

Table 9. Estimated amount of forces and torques on the lowest part of the structure for all 26 columns in the proposed model

Node/Case	FX (kN)	FY (kN)	FZ (kN)	MX (kNm)	MY (kNm)	MZ (kNm)
1/ 1	19.22	26.53	1413.54	34.99	-24.67	-0.02
2/ 1	1.28	28.12	1984.50	33.42	-2.26	0.01
3/ 1	-9.69	21.59	1840.45	6.81	20.86	-0.01
4/ 1	9.60	21.61	1840.56	6.79	-20.87	0.01
5/ 1	0.65	5.76	543.95	26.89	-17.00	-0.00
6/ 1	-0.57	5.76	543.26	26.89	17.17	-0.00
7/ 1	-1.60	28.21	1984.89	33.34	2.03	-0.01
8/ 1	-18.69	26.59	1412.69	34.95	25.30	0.02
9/ 1	20.60	-25.09	1530.09	16.84	-23.28	0.02
10/ 1	20.97	29.02	1585.27	-11.11	-22.89	-0.02
11/ 1	19.55	-30.98	1486.78	-39.03	-24.40	0.06
12/ 1	0.82	-32.89	2053.77	-37.23	-2.77	0.01
13/ 1	-10.63	-27.33	1745.73	-42.87	19.92	0.02
14/ 1	10.50	-27.34	1746.11	-42.86	-19.92	-0.03
15/ 1	-1.13	-33.01	2056.53	-37.10	2.59	-0.02
16/ 1	-19.04	-31.03	1486.11	-38.95	25.05	-0.07
17/ 1	-20.58	29.05	1584.09	-11.12	23.40	0.02
18/ 1	-20.31	-25.11	1529.12	16.89	23.68	-0.02
19/ 1	-4.29	-8.09	2531.11	-0.27	-0.62	-0.01
20/ 1	4.04	11.16	2599.69	6.79	0.48	0.00
21/ 1	-11.86	6.50	2235.84	11.43	18.69	-0.00
22/ 1	11.64	6.57	2235.43	11.37	-18.80	-0.00
23/ 1	-4.28	11.14	2600.92	6.83	-0.61	-0.00
24/ 1	11.11	-4.38	2237.67	-4.00	-19.34	-0.00
25/ 1	4.09	-7.95	2529.29	-0.42	0.52	0.01
26/ 1	-11.41	-4.39	2235.45	-3.99	19.13	0.00
Case 1	DL1					
Sum of val.	0.00	0.00	47572.84	5.28	1.40	-0.03
Sum of reac.	0.00	0.00	47572.84	382413.01	-532815.80	0.00
Sum of forc.	0.0	0.0	-47572.84	-382413.01	532815.80	0.0
Check val.	0.00	0.00	0.00	-0.00	-0.00	0.00
Precision	1.12652e-07	3.46992e-19				

of 7 064.46 GBP can be recouped in three years, making it justifiable (Fig. 12a). Considering the domestic energy price in Iran (2,100.5 IRR per kWh), annual financial savings of 271 705 808.46 IRR can be achieved, allowing the retrofit cost in the proposed model (5 367 338 131 IRR) to be recouped in 21 years (Fig. 12b). Considering the payback period, it seems that the cost of retrofit actions in the proposed model is economically justified with respect to the global price of energy, however, the payback period can be prolonged, as long as the energy price in Iran is far from the global reality and is accompanied by government subsidies.

The results of this study for optimizing the structural performance of office buildings are new. The annual energy consumption of the proposed office

building model in this study (75 kWh/m² per year) is 25 % less than the annual energy consumption of typical office buildings, which ranges between 100 and 1 000 kWh/m² per year. This is consistent with the Iranian national standard for non-residential buildings (National Standard Organization of Iran, 2011). However, the results are similar to those in the work of Alvand et al. (2017) in terms of energy consumption optimization and are better than those in the works of Ghiai and Hajjar (2014), Javid et al. (2019), Khodakarami and Ghobadi (2023), and Tahsildoost and Zomorodian (2015).

Conclusions

In this research, we aimed to reduce the annual consumption of energy resources in an office building in Tehran by implementing cost-effective solutions.

Table 10. Comparison of the baseline, developed and proposed models

Model name	Annual energy consumption (kWh)	Annual CO ₂ emissions (ton)	Annual energy cost savings (GBP/year)	Cost of retrofit actions (GBP)	Payback period considering the global price of energy	Payback period considering the domestic price of energy
Baseline model	258 053.59	150.70	–	–	–	–
Developed model	128 929.27	75	30 989.83	15 130.6	7 months	5 years
Proposed model	128 700.67	74.86	31 044.70	70 641.46	3 years	21 years

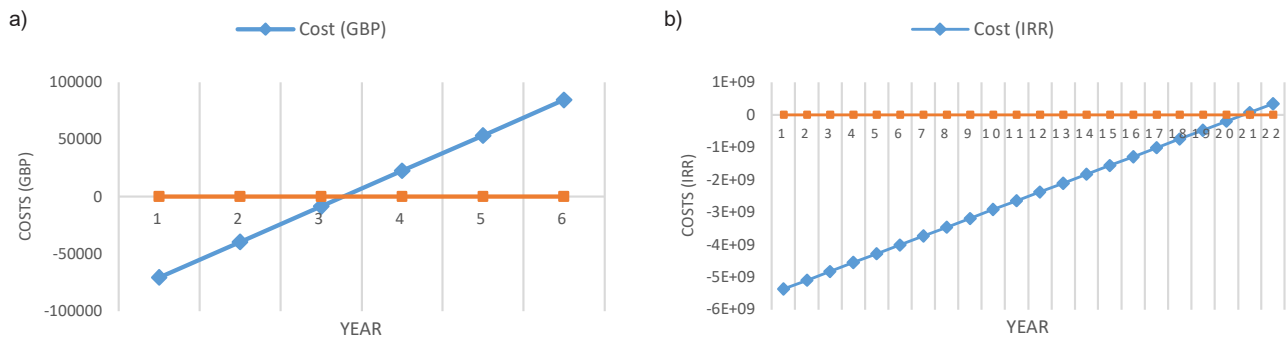


Fig. 12. Payback period diagram of the proposed model considering (a) global price of energy and (b) domestic price of energy

We also sought to decrease the dead loads resulting from the materials used in the external walls and ceilings. The results on reducing annual energy consumption align with previous research, but the materials in this model are cheaper, lighter, and have better thermal properties than those in the other two models. This not only reduces the building's weight, improves stability against wind and earthquakes, extends its lifespan, but also lowers strengthening costs. The study demonstrates that the proposed office building model reduces material weight in external walls and ceilings by up to 16 %, enhancing durability and stability, while also cutting annual energy consumption by 50 % and minimizing environmental impact. The strategies used in the proposed model of this research, including the solutions for optimizing energy consumption and reducing the dead loads

of the building, can simultaneously improve the structural performance and increase the useful life of office buildings in megacities like Tehran while reducing their adverse environmental effects.

Although the outcomes of the simulation provide valuable perspectives on potential improvements in energy efficiency and structural strength, it is important to recognize that these findings are based on theoretical premises established within a controlled simulation environment. In order to verify that the suggested solutions are practical and functional in real-world scenarios, it is essential to conduct experimental tests that demonstrate the alignment of anticipated results with the building's actual performance. Upcoming research will focus on validating these simulated findings through experiments to assess their relevance in practical settings.

References

- Akeiber, H., Nejat, P., Majid, M. Z. A., Wahid, M. A., Jomehzadeh, F., Zeynali Famileh, I., Calautit, J. K., Hughes, B. R., and Zaki, S. A. (2016). A review on phase change material (PCM) for sustainable passive cooling in building envelopes. *Renewable and Sustainable Energy Reviews*, Vol. 60, pp. 1470–1497. DOI: 10.1016/j.rser.2016.03.036.
- Alvand, M., Gholami, Z., Ferrara, M., and Fabrizio, E. (2017). Assessment of cost optimal solutions for high performance multi-family buildings in Iran. *Energy Procedia*, Vol. 111, pp. 318–327. DOI: 10.1016/j.egypro.2017.03.102.
- Anvari-Moghaddam, A., Monsef, H., and Rahimi-Kian, A. (2015). Cost-effective and comfort-aware residential energy management under different pricing schemes and weather conditions. *Energy and Buildings*, Vol. 86, pp. 782–793. DOI: 10.1016/j.enbuild.2014.10.017.
- Azari, R., Garshasbi, S., Amini, P., Rashed-Ali, H., and Mohammadi, Y. (2016). Multi-objective optimization of building envelope design for life cycle environmental performance. *Energy and Buildings*, Vol. 126, pp. 524–534. DOI: 10.1016/j.enbuild.2016.05.054.
- Baniassadi, A., Sajadi, B., Amidpour, M., and Noori, N. (2016). Economic optimization of PCM and insulation layer thickness in residential buildings. *Sustainable Energy Technologies and Assessments*, Vol. 14, pp. 92–99. DOI: 10.1016/j.seta.2016.01.008.
- Fathalian, A. and Kargarsharifabad, H. (2018). Actual validation of energy simulation and investigation of energy management strategies (case study: an office building in Semnan, Iran). *Case Studies in Thermal Engineering*, Vol. 12, pp. 510–516. DOI: 10.1016/j.csite.2018.06.007.
- Ghiai, M. M. and Hajjar, A. H. P. (2014). The relation of energy consumption and opening ratio in high rise buildings. *Journal of Sustainable Architecture and Urban Design*, Vol. 2, Issue 1, pp. 57–70.
- Haghani, M., Kari, B., and Fayaz, R. (2017). The assessment of window blinds effect on conserving energy consumption of office building in Tehran. *Modares Mechanical Engineering*, Vol. 17, Issue 4, pp. 17–28.
- Heravi, G. and Qaemi, M. (2014). Energy performance of buildings: the evaluation of design and construction measures concerning building energy efficiency in Iran. *Energy and Buildings*, Vol. 75, pp. 456–464. DOI: 10.1016/j.enbuild.2014.02.035.
- Javid, A. S., Aramoun, F., Bararzadeh, M., and Avami, A. (2019). Multi objective planning for sustainable retrofit of educational buildings. *Journal of Building Engineering*, Vol. 24, 100759. DOI: 10.1016/j.jobe.2019.100759.
- Khodakarami, J. and Ghobadi, P. (2023). Optimizing of energy consumption in an office building equipped with intelligent management system. *Energy Engineering and Management*, Vol. 6, Issue 2, pp. 12–23.
- Mohammadi, A., Ayatollahi, S. M. H., and Mousavi, S. M. (2023). Improving Iranian National Standard (INS) indices for building energy performance through comparing with LEED standard: case study of office buildings in Tehran. *Journal of Architecture in Hot and Dry Climate*, Vol. 10, Issue 16, pp. 113–129. DOI: 10.22034/ahdc.2022.17166.1590.
- Mohtashami, N., Mahdavinnejad, M., and Bemanian, M. (2016). Contribution of city prosperity to decisions on healthy building design: a case study of Tehran. *Frontiers of Architectural Research*, Vol. 5, Issue 3, pp. 319–331. DOI: 10.1016/j.foar.2016.06.001.
- Moulaii, M. M., Pilechiha, P., and Shadanfar, A. (2019). Optimization of window proportions with an approach to reducing energy consumption in office buildings. *Naqshejahan - Basic Studies and New Technologies of Architecture and Planning*, Vol. 9, Issue 2, pp. 117–123.
- Movahhed, Y., Safari, A., Motamedi, S., and Khoshkhoo, R. H. (2019). Simultaneous use of PV system and green roof: a techno-economic study on power generation and energy consumption. *Energy Procedia*, Vol. 159, pp. 478–483. DOI: 10.1016/j.egypro.2018.12.037.
- National Standard Organization of Iran (2011). *National standard of Iran, in determining energy consumption criteria and energy label guidelines, 14254, non-residential buildings*. Tehran: National Standard Organization of Iran, p. 21.
- Siew, C. C., Che-Ani, A. I., Tawil, N. M., Abdullah, N. A. G., and Mohd-Tahir, M. (2011). Classification of natural ventilation strategies in optimizing energy consumption in Malaysian office buildings. *Procedia Engineering*, Vol. 20, pp. 363–371. DOI: 10.1016/j.proeng.2011.11.178.
- Solgi, E., Hamedani, Z., Fernando, R., Mohammad Kari, B., and Skates, H. (2019). A parametric study of phase change material behaviour when used with night ventilation in different climatic zones. *Building and Environment*, Vol. 147, pp. 327–336. DOI: 10.1016/j.buildenv.2018.10.031.
- Tahsildoost, M. and Zomorodian, Z. S. (2015). Energy retrofit techniques: an experimental study of two typical school buildings in Tehran. *Energy and Buildings*, Vol. 104, pp. 65–72. DOI: 10.1016/j.enbuild.2015.06.079.
- Vakiloroaya, V., Samali, B., Fakhar, A., and Pishghadam, K. (2014). A review of different strategies for HVAC energy saving. *Energy Conversion and Management*, Vol. 77, pp. 738–754. DOI: 10.1016/j.enconman.2013.10.023.
- Yousefi, F., Gholipour, Y., and Yan, W. (2017). A study of the impact of occupant behaviors on energy performance of building envelopes using occupants' data. *Energy and Buildings*, Vol. 148, pp. 182–198. DOI: 10.1016/j.enbuild.2017.04.085.

ОПТИМИЗАЦИЯ ЭНЕРГОПОТРЕБЛЕНИЯ И ЭКСПЛУАТАЦИОННЫХ ХАРАКТЕРИСТИК ОФИСНЫХ ЗДАНИЙ В ГОРОДЕ ТЕГЕРАН С ИСПОЛЬЗОВАНИЕМ ЭКОНОМИЧЕСКИ ЭФФЕКТИВНЫХ РЕШЕНИЙ: АНАЛИЗ НА ОСНОВЕ МОДЕЛИРОВАНИЯ И СИМУЛЯЦИИ

Амин Мохаммади^{1*}, Шарие Хоссейнинасаб², Сейед Мохаммад Мусави¹

¹Университет Персидского залива (PGU), 75169, Бушер, Иран

²Университет COMSATS в Исламабаде (CUI), кампус в Лахоре, Лахор, Пакистан

*E-mail: aminmohammadi@pgu.ac.ir

Аннотация

Введение: офисные здания в крупных городах ежегодно потребляют огромные объемы энергии, также генерируя значительные выбросы углекислого газа. Кроме того, проектирование, строительство и обслуживание этих зданий требует больших затрат. На этапе проектирования необходимо уделять особое внимание их долговечности, устойчивости и сроку службы. **Цель исследования:** оптимизация энергопотребления и эксплуатационных характеристик офисных зданий в мегаполисах при помощи экономически эффективных решений. **Методы:** в качестве примера мы выбрали офисное здание в Тегеране (столице Ирана), а затем смоделировали его в DesignBuilder, Revit и Robot Structural Analysis как базовую модель. Для достижения основной цели в разработанной и предложенной моделях здания был использован ряд экономически эффективных решений. **Результаты:** результаты моделирования показали, что с экономическими решениями, использованными в предложенной модели офисного здания, можно не только сократить годовое потребление энергии и выбросы углекислого газа на 50 %, но и уменьшить вес материалов во внешних стенах и потолках до 16 %. Предложенные методы позволяют значительно сэкономить на стоимости усиления конструкции, а также увеличить срок службы строительной конструкции, ее долговечность и устойчивость. Результаты этого исследования могут быть использованы на этапе проектирования офисных зданий в таких мегаполисах, как Тегеран.

Ключевые слова: офисные здания; оптимизация энергопотребления; эксплуатационные характеристики; моделирование; симуляция.

RELATIONSHIPS BETWEEN MECHANICAL PROPERTIES (COMPRESSIVE STRENGTH) AND PHYSICAL PROPERTIES (POROSITY) AT HIGH TEMPERATURES

Ilhem Sahnoun^{1, 2*}, Zhour Guemmadi¹, Belkacem Toumi¹

¹Department of Civil Engineering, Faculty of Science and Technology, University of Mentouri Brothers Constantine 1, Constantine, Algeria

²Laboratory of Soil Mechanics and Structures (LMSS), Department of Civil Engineering, Faculty of Science and Technology, University of Mentouri Brothers Constantine 1, Constantine, Algeria

*Corresponding author's email: ilhem.sahnoun@doc.umc.edu.dz

Abstract

Introduction: This research is a part of a broader study on the evolution of concrete properties when exposed to high temperatures. **It aims** to analyze the behavior of ordinary concretes at elevated temperatures, incorporating either organic or synthetic fibers in the same dosage. **Methods:** Three concrete compositions were formulated: plain concrete without fibers (CO1), polypropylene fiber-reinforced concrete (CFP), and chicken feather fiber-reinforced concrete (CFC1), with both fiber-reinforced types containing an identical fiber dosage of 0.9 %. The prepared specimens were subjected to a heating-cooling cycle at 150 °C, 300 °C, 450 °C, and 600 °C, with a heating rate of 1 °C per minute. The residual physical and mechanical properties of the different concretes were then analyzed. **Results:** The concretes studied exhibited similar initial mechanical properties. However, the concrete reinforced with chicken feather fibers demonstrated superior residual physical and mechanical performance compared to the other concretes. Overall, the residual mechanical performance of the fiber-reinforced concretes was greater than that of the plain concrete, confirming the positive contribution of fibers to strength retention at temperatures up to 600 °C. Finally, a correlation between compressive strength and porosity was established for the three concrete types. This correlation provides a reliable method for estimating the compressive strength of concreted containing different types of fibers when exposed to high temperatures.

Keywords: ordinary concrete; chicken feather fibers; polypropylene fibers; high temperature; compressive strength–porosity correlation.

Introduction

This work aims to understand the behavior of ordinary concrete incorporating synthetic fibers (polypropylene fibers) and organic fibers (chicken feather fibers) at an identical dosage under high temperatures, using a slow heating rate of 1 °C per minute.

Numerous studies have explained the phenomena observed in the behavior of heated concrete and identified key parameters influencing concrete performance at elevated temperatures. Among these, the nature of the aggregates and the incorporation of fibers are considered crucial. The addition of various fibers (polypropylene, steel, glass) has been proposed by several researchers to enhance the residual physical and mechanical performance of concrete. Polypropylene fibers improve thermal stability, while steel fibers enhance residual mechanical strength (Sahnoun and Toumi, 2024).

Noumowe (2005) provided significant data on the mechanical properties and microstructure of high-strength concrete containing polypropylene fibers exposed to temperatures up to 200 °C. When such concrete is heated to 170 °C, the polypropylene

fibers melt and volatilize, creating additional porosity and microchannels. Differential Scanning Calorimetry (DSC) and Thermogravimetric (TG) analyses revealed the decomposition temperature ranges of the material. Scanning Electron Microscope (SEM) analysis confirmed the formation of supplementary pores and microchannels due to fiber melting. Mechanical testing showed minor changes in compressive strength, modulus of elasticity, and splitting tensile strength, likely caused by fiber decomposition. Importantly, the inclusion of polypropylene fibers improved the spalling resistance of high-strength concrete, which is crucial for application in thermally demanding environments, especially in nuclear facilities.

Nonna (2015) conducted a comparative study on the physical properties and residual mechanical behavior of three types of concrete: plain concrete (Créf (C)), steel fiber-reinforced concrete (CS 60), and hybrid fiber concrete incorporating both polypropylene and steel fibers (CPPS 0.75-60). Tests were conducted at 300 °C, 600 °C, 750 °C, and 900 °C. At ambient temperature, the differences among the concretes were minor. The porosity of the fiber-reinforced concretes was similar (CS 60 at 8.5 %

and CPPS 0.75-60 at 8.6 %), while plain concrete (Créf(C)) had higher porosity (11.2 %). During heating, CS 60 exhibited delayed water release between 200 °C and 500 °C, whereas Créf(C) and CPPS 0.75-60 experienced gradual mass loss up to 750 °C (9.2 % and 8.7 %, respectively). Beyond 750 °C, significant mass loss was observed due to the decarbonation of limestone aggregates (19.8 % for Créf(C) and 17.6 % for CPPS 0.75-60). Mechanical properties such as compressive strength, elastic modulus, and flexural tensile strength decreased with increasing temperature. However, steel fibers mitigated performance loss, with average mechanical degradation around 10 % in the fiber-reinforced concretes. Despite the development of cracks and increased porosity at elevated temperatures, steel fibers helped maintain tensile performance and reduced crack propagation, preserving ductility up to 750 °C. At 900 °C, the concrete became more brittle due to oxidation and corrosion of the steel fibers. The elastic modulus also showed a continuous decline as the temperature increased.

Hamoush and El-Hawary (1994) explored the use of feather fibers in concrete to enhance strength and durability, proposing them as a cost-effective and environmentally friendly alternative to traditional steel or glass fibers. Their experimental investigation involved incorporating feather fibers at volumetric ratios of 1 %, 2 %, and 3 % into concrete mixtures. Results showed that while compressive and tensile strength decreased with feather addition, flexural strength improved at certain ratios, especially at 1 % and 2 % after 56 days. The study also pointed out issues related to feather decay and reduced strength, suggesting that additional treatments may enhance performance. Overall, the study highlights the promising potential of feather-reinforced concrete for construction applications, with ongoing research focusing on long-term durability and fiber strength retention.

Adetola et al. (2021) conducted a study in which the compositions of chicken feather fiber (CFF) and synthetic hair fiber (SHF) were varied by weight at 0 %, 1.5 %, 2.5 %, 3.5 %, and 5 % for samples A to E, respectively. The physical and mechanical properties assessed included water absorption (WA), thickness swelling (TS), compressive strength (CS), and splitting tensile strength (STS). The results indicated that both WA and TS decreased with lower percentage of CFF and SHF, as well as with increased curing time. WA ranged from a maximum of 10.01 % to a minimum of 0.14 %. Compressive strength for sample A increased with curing time, from 16.98 MPa at 7 days to 20.66 MPa at 28 days, while sample B achieved its highest CS of 9.98 MPa at 14 days, with other samples showing a progressive decline. Similarly, STS for sample A increased with curing time from 9.84 MPa to 13.64 MPa, while

sample B exhibited a decrease from 5.43 MPa to 4.79 MPa between days 7 and 21, followed by a slight increase to 4.92 MPa at 28 days. Samples C, D, and E followed a trend similar to sample B. An SEM analysis revealed that interlocking concrete block (ICBs) with 0 % CFF and SHF exhibited brittle characteristics, while samples incorporating varying percentages of fibers displayed ductile behavior. Overall, the inclusion of CFF and SHF improved the WA, TS, CS, and STS of fiber-reinforced concrete.

Abdelsamie et al. (2021) investigated the use of keratin fibers — waste by-products from the poultry industry (CFFs) — in fiber-reinforced concrete composites. One of the key challenges with high-strength concrete (HSC) is its brittleness, which leads to sudden failure at ultimate capacity. This study examined the impact of CFFs on improving the ductility of HSC. Two experimental scenarios were explored. In the first scenario, HSC was prepared with different volume ratios of CFF (0 % as control, 0.5 %, 1 %, 1.5 %, 2 %, and 3 %). In the second scenario, CFFs were replaced with glass fibers (GF). Tests were conducted on fresh, hardened, and morphological properties of the concrete. Tests were conducted on fresh and hardened concrete, its morphological properties were analyzed. The results showed improved ductility in HSC with the addition of both types of fiber. The optimal fiber content was found to be 1 % by volume for both CFF and GF. Flexural and splitting tensile strengths increased by approximately 44.9 % and 42.65 % for the mix containing 1 % GF, and by 21.6 % and 21.16 % for the mix containing 1 % CFF, respectively.

The current work is primarily experimental and aims to deepen the understanding of the behavior of ordinary concrete exposed to high temperatures, incorporating synthetic (polypropylene) and organic (chicken feather) fibers at the same dosage. The study also seeks to establish a correlation between porosity and residual compressive strength, enabling the estimation of compressive strength in fiber-reinforced concrete subjected to elevated temperatures.

Materials and Methods

Raw Materials

The cement used in this study is a locally sourced Portland cement, classified as CEM I 42.5 R, from Lafarge, branded as EL MOUKAWEM. It has a 28-day compressive strength exceeding 42.5 MPa but below 62.5 MPa, and a specific gravity of 3,140 kg/m³. The aggregates used are of calcareous (limestone) origin and include 0/4 fraction (sand) and 8/16 fraction (aggregate), both sourced from the EL KHROUB quarry located in the northern region of Constantine. The sand has a specific gravity of 1,440 kg/m³, while the aggregate has a density of 1,350 kg/m³. The water absorption rates are 0.78 % for the sand and 0.72 % for the aggregate.

The polypropylene fibers used in this study are manufactured by FIBERTEK. These fibers are cylindrical in shape, 6 mm in length, and have a nominal diameter of 18 μm . They are characterized by a density of 0.91 g/cm^3 , a melting point of 160 $^{\circ}\text{C}$, a tensile strength of 400 MPa, and an elastic modulus of 3.7 GPa. The CFFs used are semi-crystalline, with a diameter of approximately 5 μm and lengths ranging from 4.2 to 15 mm (Menandro, 2010), giving a length-to-diameter ratio of about 25. They have a specific gravity of 0.85 g/cm^3 . The chicken feathers were collected from Al-Ihsan poultry farm in Constantine. All raw materials are shown on the Fig. 1.

Experimental Methods

Three concrete compositions were prepared (Table 1). A constant water-to-cement ratio of 0.50 was maintained for all mixtures. The mix design was determined using the Dreux-Gorisse method (Dreux and Festa, 1998), which guided the calculation of the quantities of each concrete constituent. The first composition, designated as CO1, is ordinary concrete without any fibers. The second composition, designated as CCF1, is ordinary concrete incorporating chicken feather fibers at a dosage of 0.9 % by volume. The third composition, designated as CFP, is ordinary concrete with polypropylene fibers, also added at a dosage of 0.9 % by volume.

Each concrete mixture was cast into cylindrical molds with a diameter of 10 cm and a height of 20 cm, as well as into prismatic molds measuring 7 \times 7 \times 28 cm. After 24 hours, the specimens were

demolded and stored in ambient laboratory air for 90 days prior to testing (Noumowe et al., 2009) (Fig. 2). All specimens were subjected to four different temperature cycles, with target temperatures of 150 $^{\circ}\text{C}$, 300 $^{\circ}\text{C}$, 450 $^{\circ}\text{C}$, and 600 $^{\circ}\text{C}$. Each cycle began with a heating phase at a rate of 1 $^{\circ}\text{C}/\text{min}$ until the target temperature was reached. This heating rate is commonly used for specimens of these dimensions.

The target temperature was then maintained for one hour to ensure uniform internal distribution. Finally, the specimens were allowed to cool back to ambient temperature. This thermal cycle procedure follows the guidelines recommended by the RILEM Technical Committee TC-129 (RILEM, 1995). For mass loss determination, the specimens were oven-dried at 105 $^{\circ}\text{C}$ for several days until their mass stabilized. They were weighed before and after each heat treatment to determine mass loss. Direct weighing was performed to avoid rehydration from ambient humidity. Porosity was also measured before and after each temperature cycle. The physical and mechanical properties (Figs. 5, 7) of the concrete specimens were evaluated at ambient temperature and after each heating-cooling cycle (150 $^{\circ}\text{C}$, 300 $^{\circ}\text{C}$, 450 $^{\circ}\text{C}$, and 600 $^{\circ}\text{C}$).

Results and Discussion

Physical Properties

Mass Loss

Fig. 3 illustrates the variations in mass loss of the 7 \times 7 \times 28 cm prismatic specimens after the heating-cooling cycles. The mass loss is similar across all



Fig. 1. Raw materials



Fig. 2. Preservation of test specimens

three types of concrete studied and shows closely aligned trends.

From the figure above, two distinct ranges in the evolution of mass loss with temperature can be observed. The first range extends from ambient temperature up to 300 °C. The mass loss in this

range is 0.76 %, 0.83 %, and 0.89 % for concretes CO1, CCF1, and CFP, respectively. This loss is primarily due to the evaporation of free water from the pores, desorption of water from the surface of solid components, loss of bound water, and dehydration of C-S-H gels and ettringite.

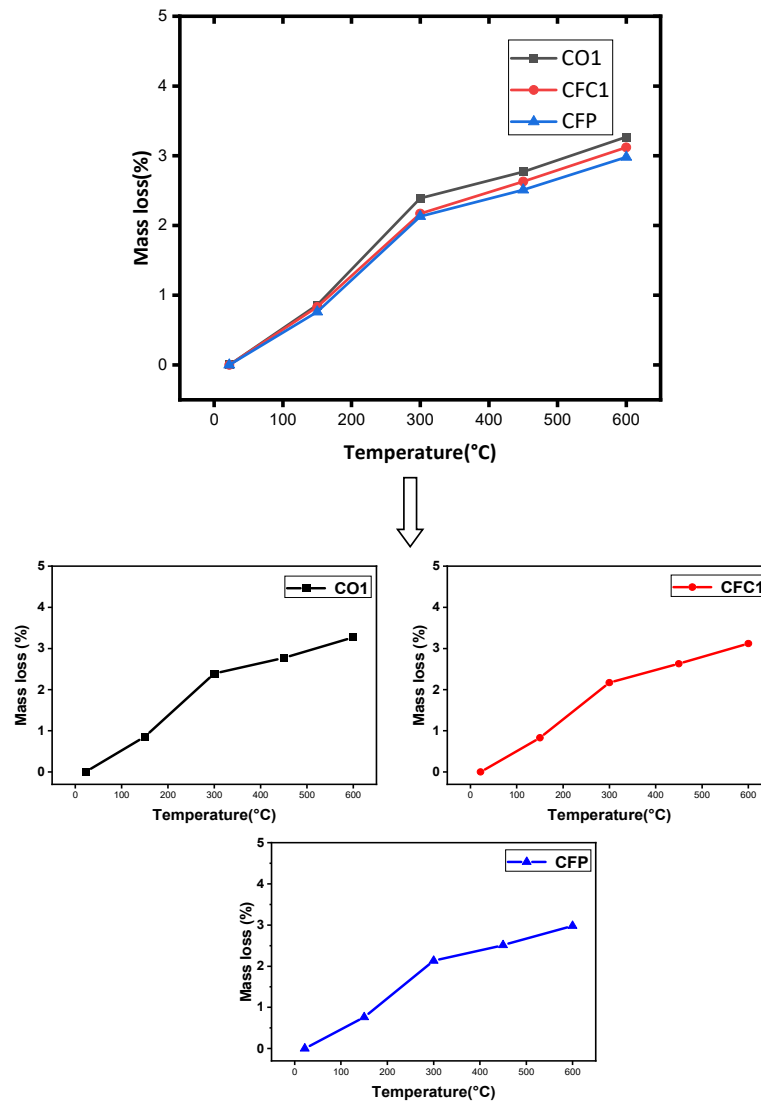


Fig. 3. Evolution of mass loss for CO1, CCF1, and CFP with respect to the temperature of the heating-cooling cycle

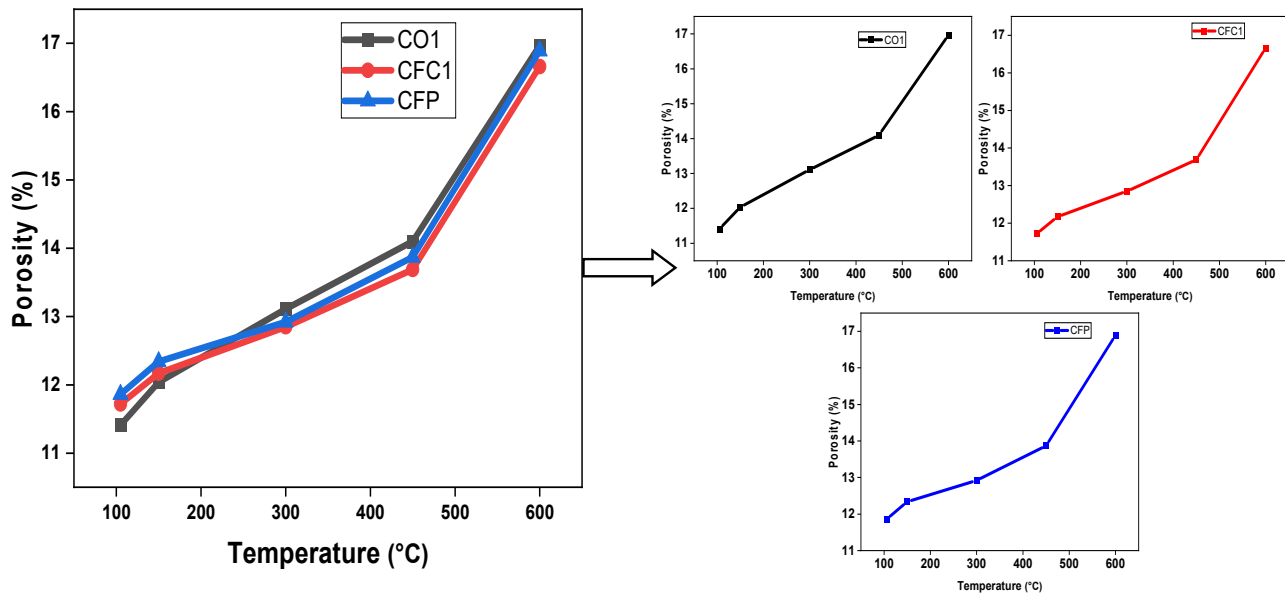


Fig. 4. Evolution of residual porosity of concretes with different fibers as a function of temperature

The second range, from 300 °C to 600 °C, shows only a slight variation in mass loss compared to the first range. This range is characterized by the dehydroxylation of portlandite (Menandro, 2010). The mass loss trends for all three concretes follow a similar slope. At 300 °C, concrete CO1 loses 2.39 % of its mass, CCF1 loses 2.17 %, and CFP loses 2.13 %. The small differences in mass loss among the concretes can be attributed to the varying water contents in their initial compositions.

At 600 °C, the mass loss is 3.27 % for CO1, 3.12 % for CCF1, and 2.98 % for CFP. Overall, the addition of chicken feather fibers or polypropylene fibers reduces the mass loss compared to concrete without fibers (Pliya, 2010). This is likely due to the partial replacement of aggregates with fibers, which reduces the amount of free or adsorbed water in the mix.

Porosity

The porosity of the studied concretes (Fig. 4) increases with heating temperature. All three types of concrete exhibit a similar trend in porosity development up to 600 °C.

Between 105 °C and 150 °C, the porosity of concrete with polypropylene fibers (CFP) and concrete with chicken feather fibers (CCF1) increases more significantly than that of ordinary concrete (CO1). Beyond 300 °C, a rapid increase in porosity is observed in concrete without fibers, whereas concretes with fibers show a slower rate of increase.

At 300 °C, the porosity of concrete without fibers is 13.11 %, while the porosity of CCF1 and CFP is 12.86 % and 12.92 %, respectively.

Between 300 °C and 450 °C, a sharp increase in porosity is recorded, reaching 14.1 %, 13.69 %, and 13.87 % for CO1, CFC1, and CFP, respectively.

From 450 °C to 600 °C, porosity continues to rise rapidly. This could be due to the decomposition of portlandite ($\text{Ca(OH)}_2 \rightarrow \text{CaO} + \text{H}_2\text{O}$) and the allotropic transformations of α -quartz to β -quartz.

Mechanical Properties

The mechanical properties of the specimens were evaluated after undergoing the heating-cooling cycles. The average residual strength values were obtained from three specimens.

Residual Compressive Strength of Concrete at Elevated Temperatures

According to Fig. 6, compressive strength decreases as temperature increases — an observation widely reported in the literature (Hassiba, 2019; Kanéma, 2007; Nonna, 2015; Pliya, 2010), stating that this reduction may be attributed



Fig. 5. Cylindrical specimens (100 × 200 mm) for compressive strength testing

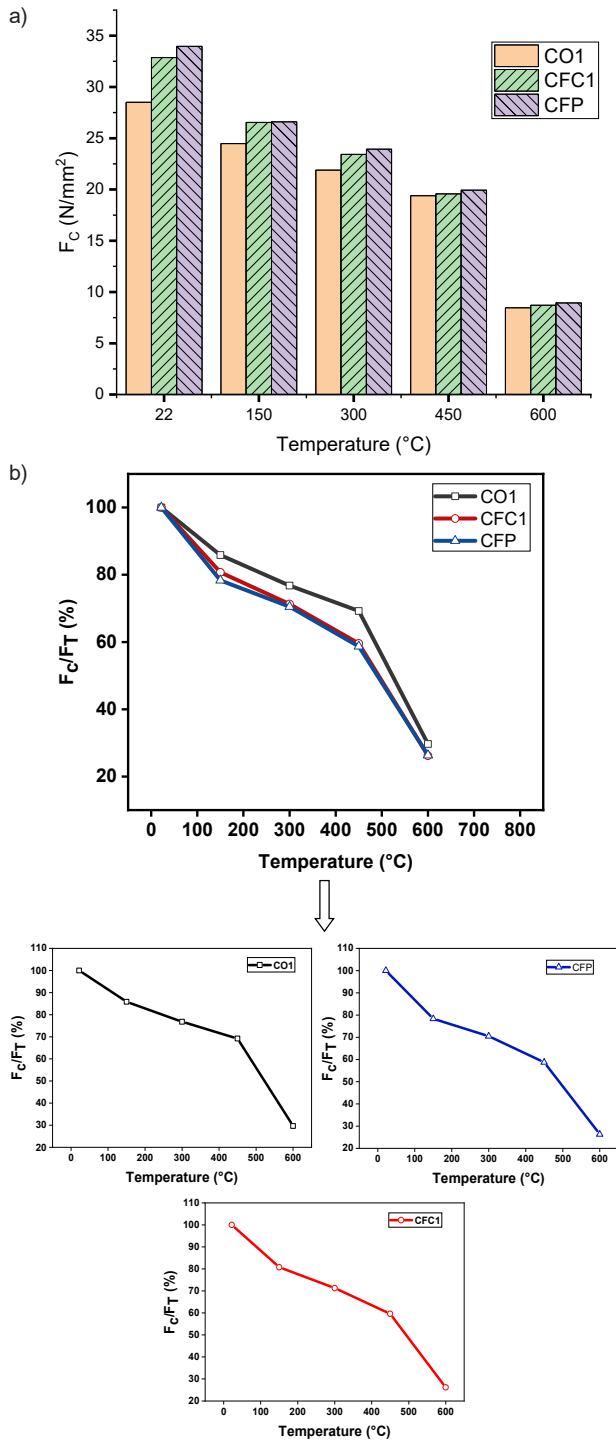


Fig. 6. Evolution of (a) residual and (b) relative compressive strength of CO1, CCF1, and CFP as a function of temperature

to degradation of the cement paste and aggregate microstructure as well as water loss.

The trend in compressive strength reduction is similar across all three concretes — those with and without fibers. However, concretes with fibers exhibit better residual compressive strengths compared to the one without fibers. The reduction in residual compressive strength can be divided into three distinct temperature ranges:

1. Ambient to 150 °C: A moderate decrease in strength.
2. 150 °C to 300 °C: A medium-level decrease in strength.
3. Above 450 °C: A significant decrease in strength.

Between ambient temperature and 150 °C, CCF1 and CFP concretes exhibit higher residual compressive strengths than CO1. From 150 °C to 300 °C, there is a slight reduction in relative strength, with a loss of 23.22 %, of concrete without fibers, while CCF1 and CFP lose around 28.72 % and 29.51 %, respectively. The low decrease is attributed to the loss of water due to temperature, which causes the C-S-H gel sheets to separate, reducing the attraction forces between the sheets and leading to the formation of microcracks. This reduction is attributed to water loss due to temperature increase, which causes the C-S-H gel layers to separate, weakening inter-particle forces and leading to microcrack formation (Pliya, 2010).

Between 400 °C and 600 °C, all three concretes experience a steady decline in residual strength. The losses are similar across the board, indicating material degradation — particularly in the cement matrix — as previously noted by Kanéma (2007).

Concrete without fibers appears less damaged than the other types. Both fiber-reinforced concretes (CCF1 and CFP) show nearly identical loss patterns. This suggests that the type of fiber does not significantly influence the overall shape of the compressive strength curve. Microcrack formation, as discussed by Bidossessi and Prosper (2010), Hachemi (2015), and Hassiba (2019), decreases mechanical performance.

Flexural Tensile Strength

At ambient temperature, concrete generally exhibits higher compressive strength than tensile strength; however, the inclusion of fibers improves its tensile capacity.



Fig. 7. Prismatic specimens of dimensions 7 × 7 × 28 cm for tensile strength testing

Fig. 8 illustrates the evolution of residual and relative flexural tensile strength as a function of temperature. For all concretes (CO1, CFC1, and CFP), flexural strength consistently decreases as temperature increases.

In general terms, the evolution of tensile strength with temperature can be divided into two behavioral zones: the first ranges from ambient temperature to 300 °C, and the second — from 300 °C to 600 °C. The presence of fibers does not alter the shape of the curve. From 22 °C to 300 °C, the bending resistance flexural strength of CFC1 decreases by about 12 %, while CFP loses about 14 % and CO1 loses about 19 % of the initial strength.

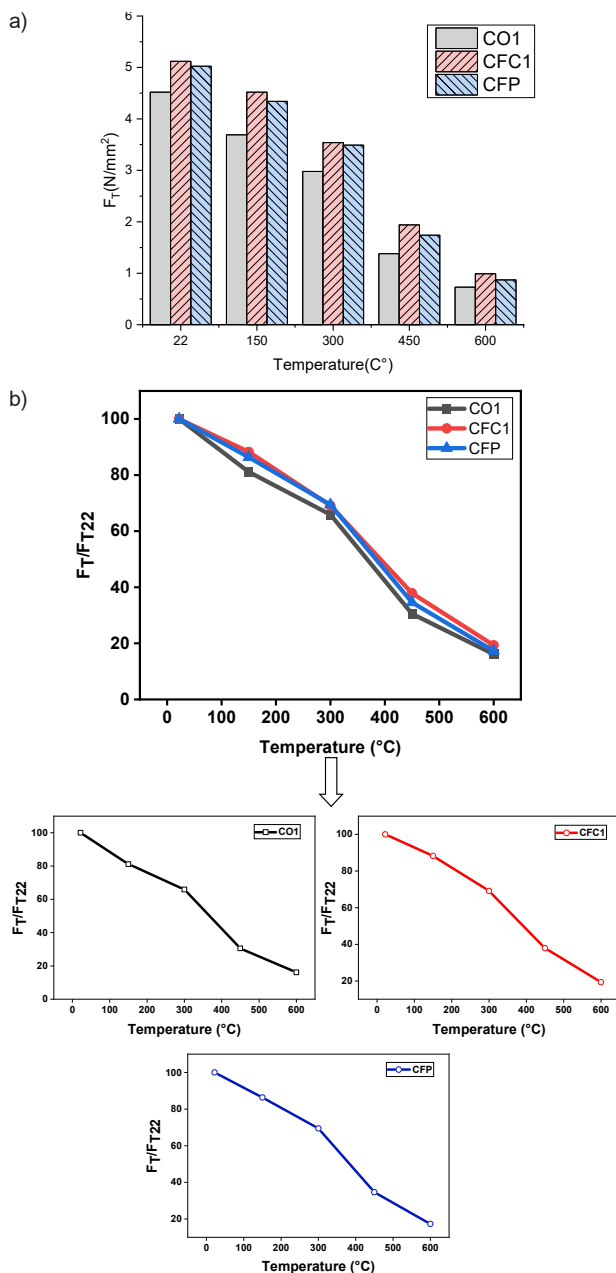


Fig. 8. Evolution of (a) residual and (b) relative flexural tensile strength of concretes CO1, CFC1 and CFP as a function of temperature

Beyond 300 °C, all types of concrete exhibit a significant loss in flexural tensile strength. Concrete with chicken feather fibers (CFC1) and concrete with polypropylene fibers (CFP) lose more than 30 % of their initial strength, while concrete without fibers (CO1) loses more than 35 %.

Above 450 °C, the reduction in residual strength becomes more pronounced for all formulations.

At 600 °C, concrete containing chicken feather fibers shows the least loss compared to CO1 and CFP. The loss of tensile strength in bending occurs in concrete with a water-to-cement (W/C) ratio of 0.5. The use of fibers makes concrete more ductile. The various bending tests, from ambient temperature up to the heating-cooling cycle at 600 °C, show that the ductility of concretes with polypropylene and chicken feather fibers is preserved.

Correlation

The relationship between compressive strength and porosity can be influenced by increasing temperature and the incorporation of fibers.

Correlation Between Porosity and Compressive Strength

The assessment of compressive strength is based on empirical correlations between compressive strength and porosity. Figs. 9 and 10 present this relationship for the three concrete types: CO1, CFC1, and CFP. The best-fit model is a linear equation with a high correlation coefficient ($R^2 = 0.996$).

It is observed that the coefficient of determination (R^2) is nearly identical for all three concrete types: plain concrete, and those with chicken feather and polypropylene fibers. As residual compressive strength increases, porosity decreases. However, the residual compressive strength of concrete with various fiber types exposed to high temperatures can be estimated using the relationship between

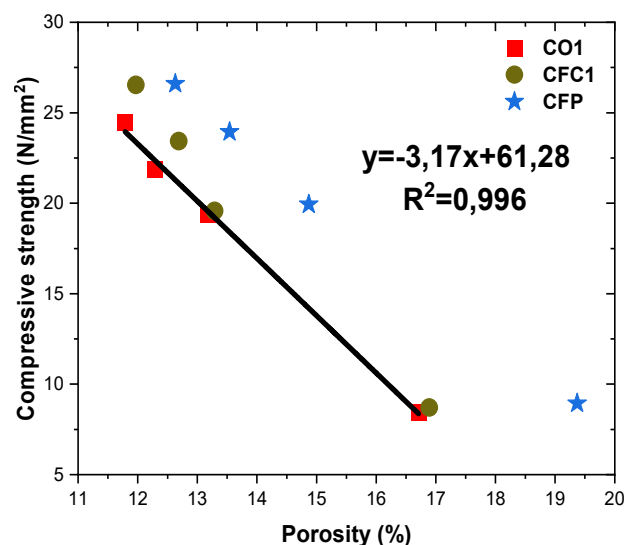


Fig. 9. Relationship between the compressive strength and porosity

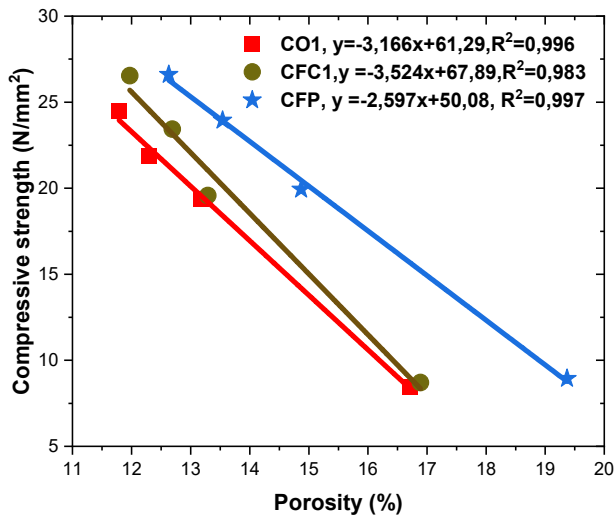


Fig. 10. Correlation between compressive strength and porosity for CO1, CFC1, and CFP at 150 °C, 300 °C, 450 °C, and 600 °C

porosity and residual compressive strength. This correlation implies that porosity can be used as a reliable predictor of residual compressive strength for concrete exposed to high temperatures.

A strong inverse relationship is evident across all formulations: compressive strength improves as porosity decreases. These findings are consistent with previous studies (Cheng et al., 2008; Erniati et al., 2015).

Conclusions

This study aimed to enhance the understanding of the behavior of concrete exposed to high temperatures. It evaluated the influence of two fiber types — polypropylene and chicken feather — added at an equal dosage of 0.9 % by volume, with a constant water-to-cement (W/C) ratio of 0.5.

Both physical (mass loss, porosity) and mechanical (compressive strength, flexural tensile strength) properties were measured at ambient temperature and after exposure to elevated temperatures.

For the three types of concrete, it was observed that both mechanical and physical properties decrease with increasing temperature. Mass loss is more significant in ordinary concrete compared to the other types. Porosity measurements confirm that high-performance concretes are more porous and suffer greater damage than ordinary concretes. Several key findings can be noted from this study:

- Exposure to high temperatures directly affects both the physical and mechanical properties of concrete.

- A heating rate of 1 °C/min facilitates more complete chemical transformations within the concrete, resulting in a more pronounced reduction in strength.

- Mass loss increases with temperature. It was observed that concretes without fibers exhibit higher mass loss compared to those containing chicken feather or polypropylene fibers. Thus, the variation in mass loss among the concretes depends on the type and dosage of fibers used.

- Mechanical and physical properties consistently decline as temperature rises.

- The addition of fibers generally enhances mechanical properties at ambient temperature compared to ordinary concrete without fibers.

- Concrete with chicken feather fibers at a dosage of 0.9 kg/m³ shows improved initial and residual compressive strength.

- The improvement in compressive strength correlates with the reduction in porosity observed across the different types of concrete.

References

- Abdelsamie, K., Agwa, I. S., Tayeh, B. A., and Hafez, R. D. A. (2021). Improving the brittle behaviour of high-strength concrete using keratin and glass fibres. *Advances in Concrete Construction*, Vol. 12, No. 6, pp. 469–477. DOI: 10.12989/acc.2021.12.6.469.
- Adetola, S. O., Oladoyinbo, T. S., Alao, T. B., Adeleke, Y. M., and Alao, A. J. (2021). Investigative study of chicken feather and synthetic hair fibre on mechanical and microstructural properties of interlocking concrete block. *LAUTECH Journal of Civil and Environmental Studies*, Vol. 7, No. 2, pp. 1–11. DOI: 10.36108/laujoces/1202.70.0210.
- Bidossessi, A. and Prosper, P. (2010). *Contribution of polypropylene and metal fibres to the improvement of the behaviour of concrete subjected to a high temperature*. DSc Thesis .Bidossessi.A, Prosper.P (2010). *Contribution des fibres de polypropylène et métalliques à l'amélioration du comportement du béton soumis à une température élevée*. PhD thesis of the University of Cergy-Pontoise.
- Cheng, A. S., Yen, T., Liu, Y.-W., and Sheen, Y.-N. (2008). Relation between porosity and compressive strength of slag concrete. In: *Structures Congress 2008: Crossing Borders*, Vancouver, British Columbia, Canada, April 24–26, 2008. DOI: 10.1061/41016(314)310.
- Erniati, Tjaronge, M. W., Zulharnah, and Irfan, U. R. (2015). Porosity, pore size and compressive strength of self compacting concrete using sea water. *Procedia Engineering*, Vol. 125, pp. 832–837. DOI: 10.1016/j.proeng.2015.11.045.
- Dreux, G. and Festa, J. (1998). *New guide to concrete and its constituents*. 8th ed. Paris: Eyrolles.416 p.
- Hachemi, S. (2015). *Study of the behavior of concrete subjected to high temperature: Influence of the type of concrete and the nature of the constituents*. DSc Thesis in Civil Engineering.
- Hamoush, S. A. and El-Hawary, M. M. (1994). Feather fiber reinforced concrete. *Concrete International*, Vol. 16, Issue 6, pp. 33–35.
- Hassiba, R. (2019). *The influence of fibre types on the behaviour of high temperature concrete*. DSc Thesis in Civil Engineering. Hassiba, R. (2019). *L'influence des types de fibres sur le comportement du béton.à haute température*. Doctoral thesis of the University Mohamed khaidar Biskra, Algeria.
- Kanéma, M. (2007). *Influence of formulation parameters on the high temperature behaviour of concretes*. PhD Thesis.
- Kanéma, M. (2007). *Influence des paramètres de formulation sur le comportement à haute température des bétons*. Doctoral thesis of University of Cergy-Pontoise.
- Menandro, N. (2010). Waste chicken feather as reinforcement in cement-bonded composites. *Philippine Journal of Science*, Vol. 139, No. 2, pp. 161–166.
- Nonna, Y. (2015). *Comportement à hautes températures des bétons additionnés de fibres*. Doctoral thesis of University of Cergy-Pontoise.
- Noumowe, A. (2005). Mechanical properties and microstructure of high strength concrete containing polypropylene fibres exposed to temperatures up to 200 °C. *Cement and Concrete Research*, Vol. 35, Issue 11, pp. 2192–2198. DOI: 10.1016/j.cemconres.2005.03.007.
- Noumowe, A. N., Siddique, R., and Debicki, G. (2009). Permeability of high-performance concrete subjected to elevated temperature (600°C). *Construction and Building Materials*, Vol. 23, Issue 5, pp. 1855–1861. DOI: 10.1016/j.conbuildmat.2008.09.023.
- Pliya, P. (2010). *Contribution des fibres de polypropylène et métalliques à l'amélioration du comportement du béton soumis à une température élevée*. Doctoral thesis of the University of Cergy-Pontoise (2010).
- RILEM (1995). RILEM TC 129-MHT. Test methods for mechanical properties of concrete at high temperatures. Part 1: introduction. Part 2: Stress–strain relation. Part 3: Compressive strength for service and accident conditions. *Materials and Structures*, Vol. 28 (181), pp. 410–414.
- Sahnoun, I. and Toumi, B. (2024). *Thermomechanical behaviour of concrete reinforced with synthetic and organic fibers*. [online] Available at: <https://www.researchsquare.com/article/rs-3978063/v1> [Access Date: February 26, 2024].

ВЗАИМОСВЯЗЬ МЕХАНИЧЕСКИХ (ПРОЧНОСТЬ НА СЖАТИЕ) И ФИЗИЧЕСКИХ СВОЙСТВ (ПОРИСТОСТЬ) ПРИ ВЫСОКИХ ТЕМПЕРАТУРАХ

Ильхем Сахнун^{1,2*}, Жур Геммади¹, Белкасем Туми¹

¹Кафедра гражданского строительства, факультет науки и технологий, Университет братьев Ментури Константина 1, Константина, Алжир

²Лаборатория механики грунтов и конструкций, кафедра гражданского строительства, факультет науки и технологий, Университет братьев Ментури Константина 1, Константина, Алжир

*E-mail: ilhem.sahnoun@doc.umc.edu.dz.

Аннотация

Введение: Данная работа является частью более широкого исследования, посвященного изучению изменений свойств бетона при воздействии высоких температур. **Цель работы** — проанализировать характеристики обычного бетона с добавлением органических или синтетических волокон в одинаковой дозировке при воздействии высоких температур. **Методы:** Разработаны три состава бетона: обычный бетон без волокон (CO1), бетон с полипропиленовыми волокнами (CFP) и бетон с волокнами из куриных перьев (CFC1), при этом объем добавленных волокон в армированном бетоне составил 0,9 %. Подготовленные образцы подвергались нагреву и охлаждению при температурах 150 °C, 300 °C, 450 °C и 600 °C со скоростью нагрева 1 °C в минуту. Далее анализировались остаточные физико-механические свойства различных типов бетона. **Результаты:** Исходные механические свойства исследованных типов бетона были схожи, однако бетон, армированный волокнами из куриных перьев, показал лучшие остаточные физико-механические характеристики по сравнению с другими типами бетона. В целом, остаточные механические характеристики бетонов с добавлением волокон оказались выше, чем у обычного бетона, что подтверждает положительное влияние волокон на сохранение прочности при температурах до 600 °C. Наконец, была установлена корреляция между прочностью на сжатие и пористостью для трех типов бетона. Эта зависимость позволяет надежно оценивать прочность бетона, содержащего различные типы волокон, при воздействии высоких температур.

Ключевые слова: обычный бетон; волокна из куриных перьев; полипропиленовые волокна; высокая температура; корреляция между прочностью на сжатие и пористостью.

PLASTIC BUCKLING ANALYSIS OF CONVENTIONAL CONCRETE AND EXPANDED POLYSTYRENE CONCRETE SPHERICAL SHELLS

Issaias Anday Sereke*, Marina Igorevna Rynkovskaya, Habte Yohannes Damir

Peoples' Friendship University of Russia named after Patrice Lumumba (RUDN University), Moscow, Russia

*Corresponding author's email: issaiasanday@gmail.com

Abstract

Introduction: Concrete's self-weight is the primary factor contributing to increased cross-sectional dimensions and dead loads in structures. This disadvantage can be mitigated by using suitable lightweight concrete. Expanded polystyrene concrete (EPSC), which is lighter than conventional concrete, has not yet been implemented in shell structures. The **purpose of the study** was to analyze and compare the plastic buckling capacities of conventional concrete and EPSC domes, and to develop an analytical formula for determining the plastic buckling capacity of spherical shells made from these materials. The **methodology** includes an experimental investigation involving cube test specimens to evaluate the properties of EPSC. Based on the test results, the compressive strength, density, and elastic modulus of EPSC were found to be 9.48 MPa, 2074.17 kg/m³, and 11.18 GPa, respectively. Subsequently, linear buckling analysis (LBA) and material non-linear analysis (MNA) were performed using ABAQUS to determine the elastic and plastic buckling resistances of 36 concrete and 36 EPSC spherical shells. Based on the analysis results, an analytical formula was developed to estimate the plastic buckling capacities of both concrete and EPSC shells. **Results:** The findings reveal that the plastic buckling resistance of EPSC shells is significantly higher than practically applied external uniform pressures. However, the plastic buckling resistance of EPSC shells is lower than that of equivalent concrete shells. Despite this, EPSC shells exhibit lower plastic deformations and displacements compared to their concrete counterparts, indicating sufficient stiffness of such shells and supporting EPSC use in spherical shell construction. The proposed formula can be easily applied to determine the reference plastic buckling capacities of concrete and EPSC spherical shells.

Keywords: buckling; pressure; concrete; displacement; spherical shells.

Introduction

The phenomenon of plastic buckling in shells was first demonstrated through the behavior of a moderately thick cylindrical shell, which exhibited both axisymmetric and non-axisymmetric deformations under axial compression. It was observed that, at the peak of the load–deflection curve, the modes of failure involved in plastic buckling included bifurcation buckling and non-linear collapse, as illustrated in Fig. 1.

As seen in Fig. 1a, between points O and A lies the bifurcation point B. A structure will begin to fail through rapidly increasing non-axisymmetric deformations if axisymmetric deformation follows the path OAC and non-axisymmetric deformation follows the path BD. In such a case, at the load level λ_L , bifurcation buckling becomes more critical than non-linear collapse (Bushnell, 1982). However, in real geometrically imperfect shell structures, bifurcation buckling does not occur. Instead, these structures typically exhibit snap-through failure at point E along the path OEF, corresponding to the collapse load λ_s .

Several studies have investigated the stability behavior of spherical shells under external pressure. The first analytical solution for the elastic buckling of perfect spherical shells was derived by Zoelly (1915). Later works focused on the post-buckling behavior of spherical shells under external pressure

(Budiansky and Hutchinson, 1966; Sato et al., 2012; Hutchinson, 2016), and on the axisymmetric buckling of spherical shells filled with an elastic medium under external pressure (Sato et al., 2012). Nevertheless, studies on the plastic buckling of spherical shells under external pressure remain relatively scarce compared to studies on elastic buckling. In general, plastic buckling research has predominantly focused on circular cylindrical shells subjected to axial compression (Do et al., 2023). In this context, the present study focuses on the plastic buckling of spherical concrete shells made from lightweight material.

While conventional concrete used in spherical shells is known for its durability and flexibility, its high self-weight significantly increases the structural dead load and necessitates a larger cross-section. For effective shell design, optimizing construction materials is essential. One promising approach is to produce lightweight concrete by partially or fully substituting natural stone aggregates or sand with alternative lightweight aggregates (Srinivas et al., 2021). In this regard, expanded polystyrene (EPS) has been employed to partially replace concrete aggregates and sand, resulting in lightweight expanded polystyrene concrete (EPSC) (Damir et al., 2024).

As mentioned earlier, the dead load due to concrete self-weight constitutes a major portion

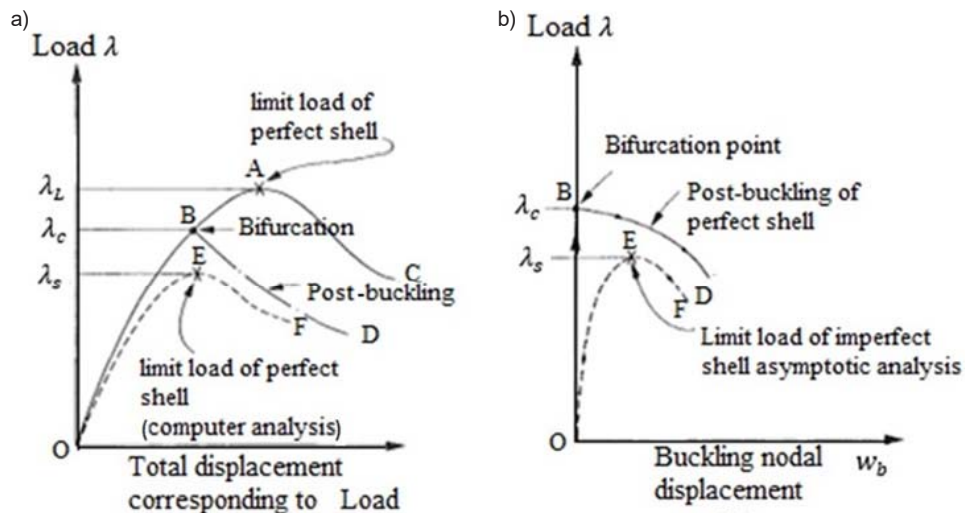


Fig. 1. Load–displacement curves indicating bifurcation and limit points (Bushnell, 1982)

of the total structural load, leading to increased cross-sections and higher construction costs. This research is motivated by the lower weight and cost advantages of EPSC over conventional concrete, the lack of studies on EPSC spherical shells, and the limited existing research on the plastic buckling of spherical shells. This paper aims to:

- Study the properties of EPSC, including density, compressive strength, and modulus of elasticity.
- Analyze the plastic buckling behavior and associated displacements of EPSC spherical shells in comparison to equivalent conventional concrete shells through numerical modeling in ABAQUS.
- Finally, develop an analytical formula to determine the plastic buckling capacity of both concrete and EPSC spherical shells.

Materials and Methods

The materials used in the current study are ordinary concrete and expanded polystyrene concrete (EPSC). Ordinary concrete typically has a density range of 2200–2600 kg/m³, whereas the density of EPSC can vary from 800 to 2000 kg/m³, depending on the percentage of EPS beads used (Liu and Chen, 2014; Saradhi Babu et al., 2005; Zia et al., 1997). When lightweight EPSC is used instead of ordinary concrete, the effects of inertia and seismic forces can be significantly reduced (Aghaee and Foroughi, 2013; Akçaoğlu et al., 2010; Yasin et al., 2016; Maghfouri et al., 2020; Teo et al., 2006).

As with any material, the mechanical properties of EPSC must be thoroughly studied before it can be recommended for structural or non-structural applications. EPSC has already been used in various applications such as cladding panels, curtain walls, composite flooring systems, load-bearing blocks, and pavements (Sri Ravindrarajah and Tuck, 1994). However, to date, it has not been applied in shell structures. Before investigating the plastic buckling

behavior of EPSC spherical shells, a laboratory study was conducted to evaluate the properties of the EPSC mix.

In this study, a volumetric mix proportion of 1:2:3 for cement, sand, and coarse aggregate was used. EPS was used to replace 33.33 % of the coarse aggregate and 16.67 % of the sand. The ingredients were mixed in a specific sequence using a mixer, with a water-to-cement (w/c) ratio of 0.6. First, the dry EPS beads were combined with a portion of the water to allow the beads to become wetted. Then, the remaining ingredients were gradually added along with the rest of the water until a uniform, flowable mix was achieved. The mix proportions are summarized in Table 1.

Three cube specimens, each measuring 150 × 150 × 150 mm, were prepared for laboratory testing. The mix was poured into the molds in three layers, with hand compaction applied after each layer. The top surface of each specimen was leveled using a trowel. After 24 hours, the specimens were demolded and covered with a damp cloth for three days. The weight, density, and compressive strength of the specimens were measured at 28 days, as shown in Fig 2.

Table 2 presents the laboratory results for the three EPSC cube specimens. Based on these results, the average compressive strength and density were calculated to be 9.48 MPa and 2074.17 kg/m³, respectively.

The elastic modulus of EPSC was calculated based on the ACI 318-19 (ACI Committee, 2019)

Table 1. EPSC Mix Proportion

Cement : Sand : Aggregate	% of Sand Replaced by EPS	% of Coarse Aggregate Replaced by EPS	W/C Ratio
1 : 2 : 3	16.67	33.33	0.6

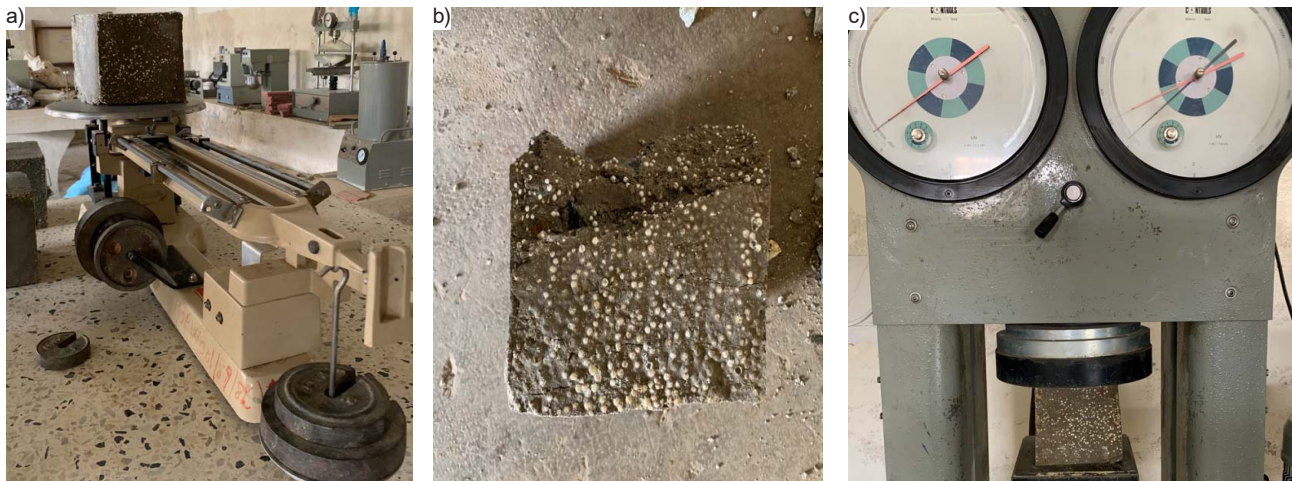


Fig. 2. Sample measurements: a — EPSC cube specimen on a weighing balance; b — Crushed EPSC cube specimen c) EPSC cube specimen tested for compressive strength

metric equation (1) for lightweight concrete with density w_c ranging from 1,404 to 2,560 kg/m³:

$$E_c = w_c^{1.5} \cdot 0.043 \cdot \sqrt{f'_c}, \quad (1)$$

where: E_c — static elastic modulus in MPa;

w_c — concrete density in kg/m³;

f'_c — cylinder compressive strength of concrete in MPa.

To convert cube compressive strength to equivalent cylinder strength, the following equation was used (Akter et al., 2017):

$$\text{Cylinder strength} = 0.8 \times \text{cube strength}. \quad (2)$$

Using Eqs. (1) and (2), the modulus of elasticity and cylinder compressive strength were calculated as 11.18 GPa and 7.58 MPa, respectively. The Poisson's ratio of EPSC was taken as 0.22, consistent with values for other low-strength concretes (Neville, 2012).

For the analysis of concrete and EPSC spherical shells, the following material properties were used:

Concrete (C20):

- Cylinder compressive strength: 20 MPa;
- Unit weight: ($\gamma_c = 24 \text{ kN/m}^3$);
- Modulus of elasticity: $E_c = 22.61 \text{ GPa}$;
- Poisson's ratio: $\nu = 0.2$.

EPSC:

- Cylinder compressive strength: 7.58 MPa;
- Unit weight: ($\gamma_{EPSC} = 20.74 \text{ kN/m}^3$);
- Modulus of elasticity: $E_{EPSC} = 11.18 \text{ GPa}$;
- Poisson's ratio: $\nu = 0.22$.

After establishing the properties of EPSC, 36 linear buckling analyses (LBA) and 36 material non-linear analyses (MNA) were performed on 36 spherical shell models made of both concrete and EPSC. These shells had half-opening angles \emptyset ranging from 20° to 90°, and the analyses were conducted using ABAQUS. Shell thicknesses were chosen as 70 mm, 73.68 mm, 77.77 mm, 82.35 mm, 87.5 mm, and 93.33 mm, corresponding to R/t ratios

of 100, 95, 90, 85, 80, and 75, respectively. All shells shared a constant radius of curvature of 7,000 mm. The shell models were subjected to fixed boundary conditions, which are widely adopted in engineering applications (Liu et al., 2022; Wang et al., 2019). In each analysis, the shells were subjected to external pressure acting normal to their surfaces (Muc et al., 2022; Zhang et al., 2017). The geometric configuration of the shell models is shown in Fig. 3.

During the material non-linear analysis (MNA), each shell was loaded using its corresponding first eigenvalue load obtained from the linear buckling analysis (LBA). To develop the analytical formula for determining the plastic buckling capacity (PR_{pl}) of concrete and EPSC spherical shells, the MNA method — based on perfect shell bending theory — was employed (Rotter and Schmidt, 2013). This approach aligns with guidelines in Eurocode 3 (European Committee for Standardization, 2007) and findings by Abood (2020) and Błażejowski (2022).

Results and Discussion

The results for the 36 elastic and plastic buckling pressures (PR_{pl}) of conventional concrete shells, obtained from LBA and MNA respectively, are summarized in Tables 3 and 4.

Graphs of the plastic buckling capacities (PR_{pl}) obtained from ABAQUS software analysis, plotted against the R/t ratios of the 36 concrete shells,

Table 2. Laboratory Results for the EPSC Cube Specimens

Test Specimen No.	Mass (kg)	Density (kg/m ³)	Force (kN)	Compressive Strength (MPa)
1	7.155	2,120	235	10.44
2	6.948	2,058.66	207	9.2
3	6.898	2,043.85	198	8.8

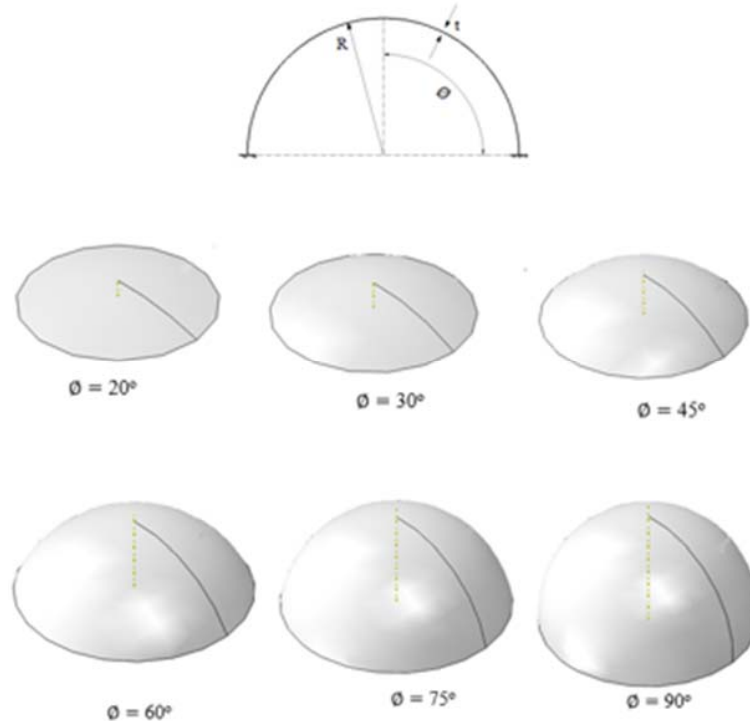


Fig. 3. Geometric configuration of the shell models

Table 3. Elastic Critical Buckling Pressures (PR_{cr}) of Concrete Shells

Geometric Dimensions of the Shells			Critical Pressures for the Shells with Varying Half-Angle \varnothing (MPa)					
R (mm)	t (mm)	R/t	20°	30°	45°	60°	75°	90°
7,000	70	100	2.8630	2.7726	2.7104	2.6846	2.6685	2.6677
7,000	73.68	95	3.1697	3.0802	3.0073	2.9723	2.9528	2.9528
7,000	77.77	90	3.5342	3.4372	3.3510	3.3136	3.2929	3.2913
7,000	82.35	85	3.9744	3.8553	3.7623	3.7182	3.6900	3.6876
7,000	87.5	80	4.5133	4.3599	4.2544	4.1975	4.1692	4.1654
7,000	93.33	75	5.1838	4.9773	4.8442	4.7843	4.7542	4.7346

Table 4. Plastic Buckling Pressures (PR_{pl}) (MPa) of Concrete Shells

Geometric Dimensions of the Shells			Plastic Buckling Pressures for the Shells with Varying \varnothing					
R (mm)	t (mm)	R/t	20°	30°	45°	60°	75°	90°
7,000	70	100	0.4066	0.4019	0.4004	0.4001	0.4000	0.4000
7,000	73.68	95	0.4285	0.4231	0.4215	0.4210	0.4210	0.4210
7,000	77.77	90	0.4529	0.4469	0.4448	0.4444	0.4444	0.4444
7,000	82.35	85	0.4804	0.4735	0.4709	0.4707	0.4706	0.4706
7,000	87.5	80	0.5114	0.5034	0.4995	0.4991	0.4990	0.4990
7,000	93.33	75	0.5465	0.5373	0.5342	0.5336	0.5334	0.5334

are shown in Fig. 4. Based on the observed relationships in these graphs, a mathematical formula was developed to represent the reference plastic buckling capacity (PR_{pl}) of concrete spherical shells for $\varnothing = 20^\circ$ – 90° .

The formula, presented in Eq. (3), accounts for all the R/t and (PR_{pl}) values and was derived using the best-fit method:

$$PR_{pl} = 2.01 \cdot f'_c \cdot \frac{t}{R}. \quad (3)$$

In this equation, values for f'_c , t , and R should be substituted in MPa and mm, respectively.

As previously mentioned, a concrete compressive strength of 20 MPa was randomly selected for this study. Since plastic strength in concrete typically refers to its compressive strength, the material parameter f'_c is incorporated into the formula.

Similarly, the elastic and plastic buckling capacities of EPSC shells are presented in Tables 5 and 6, respectively.

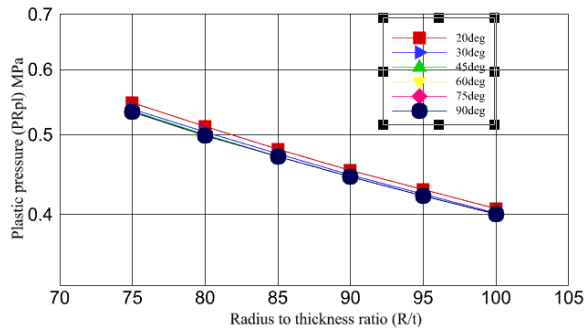


Fig. 4. Plastic buckling pressures for all \emptyset angles of the concrete shells

As described in Eqs. (1) and (2), to determine the modulus of elasticity of EPSC, the cube compressive strength (9.48 MPa) was converted to an equivalent cylinder strength (7.58 MPa), which was used throughout the analysis of EPSC shells.

Graphs of the plastic buckling capacities (PR_{pl}) versus R/t values for the 36 EPSC shells are shown in Fig. 5. Based on the relationship in the graphs and using the mathematical best-fit method, a formula similar to Eq. (3) was developed. This formula effectively represents the reference plastic buckling capacity of EPSC spherical shells and can significantly reduce the need for time-consuming software analyses. For instance, the ABAQUS result for a shell with $t = 70$ mm and $R/t = 100$ (third row of Table 6) yields a plastic buckling pressure value of 0.1523 MPa, which can be accurately reproduced using the developed formula.

The derived equation was compared to another formula proposed by Błażejowski (2022), given in Eq. (4):

$$PR_{pl} = 1.986 \cdot f_{yk} \cdot \frac{t}{R} \quad (4)$$

Błażejowski's formula differs slightly from the one developed in this study. This discrepancy is primarily due to the difference in the shell geometry: Błażejowski considered thin spherical shells with R/t ratios between 300 and 1,000, whereas the current study focuses on moderately thick shells with R/t ratios ranging from 75 to 100. This is consistent with the understanding that shell thickness significantly influences structural plastic behavior (Li et al., 2021).

The plastic buckling capacities of EPSC shells, as summarized in Table 6, are significantly higher than the practical uniform external pressure acting on these shells (not exceeding 3 kN/m², accounting for a snow load of 1.5 kN/m² and the dead load from the self-weight of the EPSC shell).

Displacement analyses of the various shells revealed both symmetric and asymmetric deformation modes (Johnson, 1964; Van Isacker and Pittel, 2016; Verma et al., 2024). For example, the deformed shapes of concrete shells with $\emptyset=75^\circ$, thickness 93.33 mm, and $\emptyset=90^\circ$, thickness 87.5 mm are shown in Fig. 6(a, b), with displacements given in millimeters.

Similarly, Fig. 7 (a, b) illustrate the deformed shapes of EPSC shells with $\emptyset=75^\circ$, thickness 93.33 mm, and $\emptyset=90^\circ$, thickness 87.5 mm, respectively.

The displacement distribution shows that shells with $\emptyset=75^\circ$ exhibit symmetric deformation, while those with $\emptyset=90^\circ$ exhibit asymmetric deformation. This difference is primarily due to variations in shell height, which significantly affect collapse behavior (Gupta and Gupta,

Table 5. Elastic Critical Buckling Pressures (PR_{cr}) of EPSC Shells

Geometric Dimensions of the Shells			Critical Pressures for the Shells with Varying Half-Angle \emptyset (MPa)					
R (mm)	t (mm)	R/t	20°	30°	45°	60°	75°	90°
7,000	70	100	1.4226	1.3774	1.3466	1.3337	1.3254	1.3250
7,000	73.68	95	1.5751	1.5304	1.4937	1.4763	1.4669	1.4663
7,000	77.77	90	1.7565	1.7071	1.6647	1.6462	1.6361	1.6347
7,000	82.35	85	1.9756	1.9149	1.8692	1.8466	1.8330	1.8312
7,000	87.5	80	2.2438	2.1658	2.1132	2.0851	2.0714	2.0689
7,000	93.33	75	2.5777	2.4728	2.4064	2.3760	2.3554	2.3510

Table 6. Plastic Buckling Pressures (PR_{pl}) (MPa) of EPSC Shells

Geometric Dimensions of the Shells			Plastic Buckling Pressures for the Shells with Varying \emptyset					
R (mm)	t (mm)	R/t	20°	30°	45°	60°	75°	90°
7,000	70	100	0.1541	0.1523	0.1517	0.1516	0.1516	0.1516
7,000	73.68	95	0.1624	0.1604	0.1597	0.1595	0.1595	0.1595
7,000	77.77	90	0.1716	0.1693	0.1686	0.1684	0.1684	0.1684
7,000	82.35	85	0.1820	0.1794	0.1786	0.1784	0.1783	0.1783
7,000	87.5	80	0.1938	0.1907	0.1898	0.1896	0.1895	0.1895
7,000	93.33	75	0.2071	0.2036	0.2025	0.2023	0.2022	0.2021

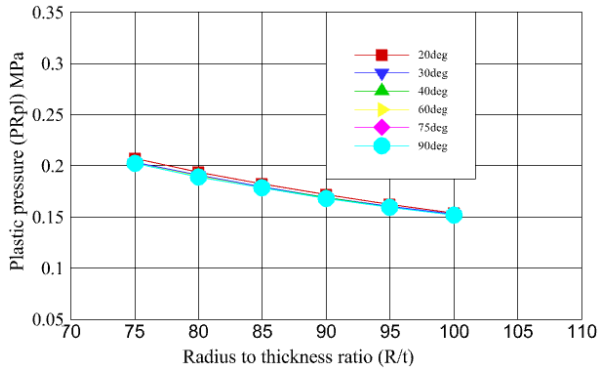


Fig. 5. Plastic buckling pressures for all \varnothing angles of EPSC shells

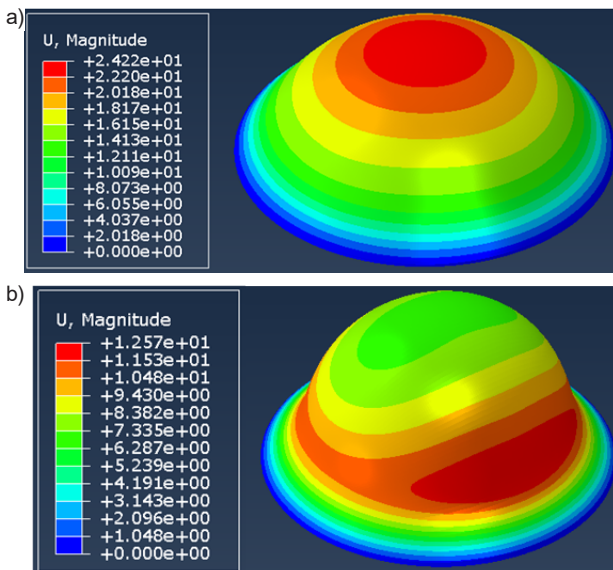


Fig. 6. Deformed shape of a concrete shell: a — with $\varnothing=75^\circ$, thickness 93.33 mm; b — with $\varnothing=90^\circ$, thickness 87.5 mm

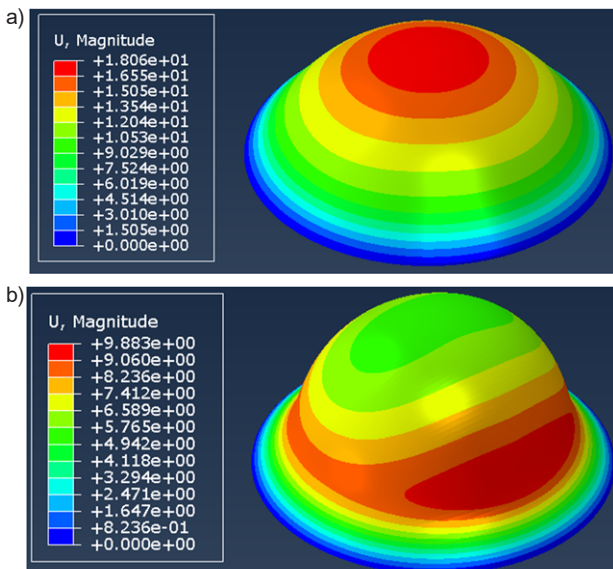


Fig. 7. Deformed shape of an EPSC shell: a — with $\varnothing=75^\circ$, thickness 93.33 mm; b — with $\varnothing=90^\circ$, thickness 87.5 mm

2009; Wang et al., 2016). Another contributing factor is the mode of energy dissipation. In the shells with $\varnothing=75^\circ$, energy is dissipated through compression, while in the shells with $\varnothing=90^\circ$, energy is dissipated through both bending and compression (Ruan et al., 2006).

From Figs. 6a and 7a, it is observed that the displacement of the EPSC shell (18 mm) with $\varnothing=75^\circ$ and thickness 93.33 mm is 1.34 times lower than that of the corresponding concrete shell (24.22 mm). This reduced displacement in EPSC shells is attributed to their lower self-weight.

Similarly, from Figs. 6b and 7b, the EPSC shell with $\varnothing=90^\circ$ and thickness 87.5 mm shows a displacement of 9.88 mm, which is 1.272 times lower than that of the corresponding concrete shell (12.57 mm).

Conclusion

This study investigated the plastic buckling capacity of expanded polystyrene concrete (EPSC) spherical shells in comparison to traditional concrete shells of identical geometry. Furthermore, analytical formulas for estimating the reference plastic buckling capacities of both concrete and EPSC spherical shells were developed. In the course of the study, the following conclusions were drawn.

Based on the experimental testing, the compressive strength, density, and elastic modulus of EPSC were found to be 9.48 MPa (7.58 MPa cylinder strength), 2074.17 kg/m³, and 11.18 GPa, respectively. These values were used as input parameters for the numerical analyses to determine the elastic and plastic buckling capacities of EPSC spherical shells. The analyses showed that the plastic deformations of EPSC shells are 2.63 times lower than those of equivalent concrete shells. Moreover, the plastic buckling capacities of EPSC shells exceeded the actual external pressure loads. For instance, the displacements in EPSC shells shown in Fig. 7a (18.06 mm) and Fig. 7b (9.88 mm), for spans of 13.5 m and 14 m, respectively, are minimal. This illustrates the stiffness of EPSC shells and supports their potential use as an alternative to conventional concrete in shell structures.

The series of LBA and MNA analyses led to the development of an analytical formula for determining the plastic buckling capacities of concrete and EPSC spherical shells with half-opening angles $\varnothing = 20^\circ$ – 90° . The formula depends on the shell radius, thickness, and compressive strength but is independent of the angle \varnothing . Using this formula can significantly reduce computational time for determining plastic buckling capacity.

As for future studies, it is recommended to investigate the stability of EPSC spherical shells with imperfections, including both geometric and material non-linearities.

References

- Abood, A. H. (2020). Buckling analysis of large diameter concrete spherical shell domes. *Iraqi Journal for Mechanical and Material Engineering*. Special Issue (B), pp. 139–153.
- ACI Committee (2019). *Building code requirements for structural concrete* (ACI 318-19). Farmington Hills, MI: American Concrete Institute, 624 p.
- Aghaee, K. and Foroughi, M. (2013). Mechanical properties of lightweight concrete partition with a core of textile waste. *Advances in Civil Engineering*, Vol. 2013, 482310. DOI: 10.1155/2013/482310.
- Akçaözoğlu, S., Atiş, C. D., and Akçaözoğlu, K. (2010). An investigation on the use of shredded waste PET bottles as aggregate in lightweight concrete. *Waste Management*, Vol. 30, Issue 2, pp. 285–290. DOI: 10.1016/j.wasman.2009.09.033.
- Akter, T., Ferdous Wahid, M., and Siddique, A. B. (2017). Strength variation of concrete between cylindrical and cubical specimen due to various proportion of ingredients. *Sonargaon University Journal*, Vol. 2, No. 2, pp. 56–64.
- Błażejowski, P. (2022). Development of a procedure for the determination of the buckling resistance of steel spherical shells according to EC 1993-1-6. *Materials*, Vol. 15, Issue 1, 25. DOI: 10.3390/ma15010025.
- Budiansky, B. and Hutchinson, J. W. (1966). A survey of some buckling problems. *AIAA Journal*, Vol. 4, No. 9, pp. 1505–1510. DOI: 10.2514/3.3727.
- Bushnell, D. (1982). Plastic buckling of various shells. *Journal of Pressure Vessel Technology*, Vol. 104, Issue 2, pp. 51–72. DOI: 10.1115/1.3264190.
- Damir, H. Y., Rynkovskaya, M., and Sereke, I. A. (2024). Comparative buckling analysis of concrete and expanded polystyrene dome shells. *Architecture and Engineering*, Vol. 9, No. 1, pp. 71–78. DOI: 10.23968/2500-0055-2024-9-1-71-78.
- Do, V.-D., Le Grogne, P., and Rohart, P. (2023). Closed-form solutions for the elastic-plastic buckling design of shell structures under external pressure. *European Journal of Mechanics - A/Solids*, Vol. 98, 104861. DOI: 10.1016/j.euromechsol.2022.104861.
- European Committee for Standardization (2007). *EN 1993-1-6. Eurocode 3 - Design of steel structures - Part 1-6: Strength and stability of shell structures*. [online] Available at: <https://www.phd.eng.br/wp-content/uploads/2015/12/en.1993.1.6.2007.pdf> [Date accessed: November 1, 2024].
- Gupta, P. K. and Gupta, N. K. (2009). A study of axial compression of metallic hemispherical domes. *Journal of Materials Processing Technology*, Vol. 209, Issue 4, pp. 2175–2179. DOI: 10.1016/j.jmatprotec.2008.05.004.
- Hutchinson, J. W. (2016). Buckling of spherical shells revisited. *Proceedings of the Royal Society A. Mathematical, Physical and Engineering Sciences*, Vol. 472, Issue 2195, 20160577. DOI: 10.1098/rspa.2016.0577.
- Johnson, D. E. (1964). Nonsymmetric bending deformation of spherical shells. *Journal of Applied Mechanics*, Vol. 31, Issue 2, pp. 344–345. DOI: 10.1115/1.3629614.
- Li, J., Ren, H., and Ning, J. (2021). Deformation and failure of thin spherical shells under dynamic impact loading: experiment and analytical model. *Thin-Walled Structures*, Vol. 161, 107403. DOI: 10.1016/j.tws.2020.107403.
- Liu, N. and Chen, B. (2014). Experimental study of the influence of EPS particle size on the mechanical properties of EPS lightweight concrete. *Construction and Building Materials*, Vol. 68, pp. 227–232. DOI: 10.1016/j.conbuildmat.2014.06.062.
- Liu, T., Chen, Y., Hutchinson, J. W., and Jin, L. (2022). Buckling of viscoelastic spherical shells. *Journal of the Mechanics and Physics of Solids*, Vol. 169, 105084. DOI: 10.1016/j.jmps.2022.105084.
- Maghfouri, M., Shafigh, P., Alimohammadi, V., Doroudi, Y., and Aslam, M. (2020). Appropriate drying shrinkage prediction models for lightweight concrete containing coarse agro-waste aggregate. *Journal of Building Engineering*, Vol. 29, 101148. DOI: 10.1016/j.job.2019.101148.
- Muc, A., Kubis, S., Bratek, Ł., and Muc-Wierzgoń, M. (2022). Higher order theories for the buckling and post-buckling studies of shallow spherical shells made of functionally graded materials. *Composite Structures*, Vol. 295, 115851. DOI: 10.1016/j.compstruct.2022.115851.
- Neville, A. M. (2012). *Properties of concrete*. 5th ed. Harlow, England: Prentice Hall, 846 p.
- Rotter, J. M. and Schmidt, H. (2013). *Buckling of steel shells: European design recommendations*. 5th ed. Brussels [online] Available at <https://lib.ugent.be/catalog/rug01:002206396#reference-details> [Date accessed: November 15, 2024].
- Ruan, H. H., Gao, Z. Y., and Yu, T. X. (2006). Crushing of thin-walled spheres and sphere arrays. *International Journal of Mechanical Sciences*, Vol. 48, Issue 2, pp. 117–133. DOI: 10.1016/j.ijmecsci.2005.08.006.
- Saradhi Babu, D., Ganesh Babu, K., and Wee, T. H. (2005). Properties of lightweight expanded polystyrene aggregate concretes containing fly ash. *Cement and Concrete Research*, Vol. 35, Issue 6, pp. 1218–1223. DOI: 10.1016/j.cemconres.2004.11.015.
- Sato, M., Wadee, M. A., Iiboshi, K., Sekizawa, T., and Shima, H. (2012). Buckling patterns of complete spherical shells filled with an elastic medium under external pressure. *International Journal of Mechanical Sciences*, Vol. 59, Issue 1, pp. 22–30. DOI: 10.1016/j.ijmecsci.2012.02.001.

- Srinivas, K., Akula, K. R., and Mahesh, V. (2021). Experimental investigation on lightweight concrete by replacing the coarse aggregate with coconut shell and expanded polystyrene beads and using polypropylene fiber. *Materials Today: Proceedings*, Vol. 46, Part 1, pp. 838–842. DOI: 10.1016/j.matpr.2020.12.834.
- Sri Ravindrarajah, R. and Tuck, A. J. (1994). Properties of hardened concrete containing treated expanded polystyrene beads. *Cement and Concrete Composites*, Vol. 16, Issue 4, pp. 273–277. DOI: 10.1016/0958-9465(94)90039-6.
- Teo, D. C. L., Mannan, M. A., and Kurian, V. J. (2006). Structural concrete using oil palm shell (OPS) as lightweight aggregate. *Turkish Journal of Engineering and Environmental Sciences*, Vol. 30, No. 4, pp. 251–257.
- Van Isacker, P. and Pittel, S. (2016). Symmetries and deformations in the spherical shell model. *Physica Scripta*, Vol. 91, No. 2. DOI: 10.1088/0031-8949/91/2/023009.
- Gaurav, V., Gagandeep, I., and Hargun, K. S. (2024). Deformation analysis of spherical shell by using generalized Hooke's law. *Structural Integrity and Life*, Vol. 24, No. 1, pp. 61–64. DOI: 10.69644/ivk-2024-01-0061.
- Wang, S., Li, S., He, J., and Zhao, Y. (2016). Asymmetric postbuckling behavior of hemispherical shell structure under axial compression. *Journal of Engineering Materials and Technology*, Vol. 138, Issue 1, 011005. DOI: 10.1115/1.4031960.
- Wang, J., Li, Z. L., and Yu, W. (2019). Structural similitude for the geometric nonlinear buckling of stiffened orthotropic shallow spherical shells by energy approach. *Thin-Walled Structures*, Vol. 138. pp. 430–457. DOI: 10.1016/j.tws.2018.02.006.
- Yasin, E., Ergul, Y., and Pathegama, G. R. (2016). Obtaining lightweight concrete using colemanite waste and acidic pumice. *Physicochemical Problems of Mineral Processing*, Vol. 52, No. 1, pp. 35–43. DOI: 10.5277/ppmp160103.
- Zhang, J., Zhang, M., Tang, W., Wang, W., and Wang, M. (2017). Buckling of spherical shells subjected to external pressure: a comparison of experimental and theoretical data. *Thin-Walled Structures*, Vol. 111, pp. 58–64. DOI: 10.1016/j.tws.2016.11.012.
- Zia, P., Ahmad, S., and Leming, M. (1997). *High-performance concretes, a state-of-art report (1989-1994)*. [online] Available at: <https://rosap.nrl.bts.gov/view/dot/56419> [Date accessed: November 15, 2024].
- Zoelly, R. (1915). *Ueber ein Knickungsproblem an der Kugelschale*. PhD Thesis in Engineering. DOI: 10.3929/ethz-a-000091951.

АНАЛИЗ ПЛАСТИЧЕСКОЙ ПОТЕРИ УСТОЙЧИВОСТИ СФЕРИЧЕСКИХ ОБОЛОЧЕК ИЗ ОБЫЧНОГО БЕТОНА И ПОЛИСТИРОЛБЕТОНА

Иссаиас Андай Сереке*, Марина Игоревна Рынковская, Хабте Йоханнес Дамир

Российский университет дружбы народов им. Патриса Лумумбы, Москва, Россия

*E-mail: issaiasanday@gmail.com

Аннотация

Введение: Собственный вес бетона представляет собой основную причину увеличения сечений и постоянной нагрузки в конструкциях. Данная проблема может быть частично решена за счет использования легкого бетона. Полистиролбетон по весу легче обычного бетона, но до настоящего момента не применялся в оболочках.

Цель исследования — проанализировать и сравнить пластическую устойчивость куполов из обычного бетона и полистиролбетона, а также вывести аналитическую формулу для определения пластической устойчивости сферических оболочек из этих материалов. **Методика** включает экспериментальное исследование кубических образцов для оценки свойств полистиролбетона. По результатам испытаний прочность на сжатие, плотность и модуль упругости полистиролбетона составили соответственно 9,48 МПа, 2074,17 кг/м³ и 11,18 ГПа. Затем с помощью программного комплекса ABAQUS были проведены линейный анализ потери устойчивости и нелинейный анализ материалов для определения упругой и пластической устойчивости 36 сферических оболочек из бетона и 36 сферических оболочек из полистиролбетона. На основе полученных данных выведена аналитическая формула для оценки пластической устойчивости как оболочек из бетона, так и оболочек из полистиролбетона. **Результаты** показывают, что пластическая устойчивость оболочек из полистиролбетона значительно превышает практически действующие равномерные внешние нагрузки. Однако при этом она ниже, чем у аналогичных бетонных оболочек. Тем не менее оболочки из полистиролбетона демонстрируют меньшие пластические деформации и смещения по сравнению с бетонными оболочками, что указывает на достаточную жесткость и подтверждает возможность использования полистиролбетона в сферических оболочечных конструкциях. Предложенная формула может применяться для определения базовой пластической устойчивости сферических оболочек из бетона и полистиролбетона.

Ключевые слова: потеря устойчивости; давление; бетон; смещение; сферические оболочки.

Guide for Authors for submitting a manuscript for publication in the «Architecture and Engineering»

The journal is an electronic media and accepts the manuscripts via the online submission. Please register on the website of the journal <http://aej.spbgasu.ru/>, log in and press "Submit article" button or send it via email aejeditorialoffice@gmail.com.

Please ensure that the submitted work has neither been previously published nor has been currently submitted for publication in another journal.

Main topics of the journal:

1. Architecture
2. Civil Engineering
3. Geotechnical Engineering and Engineering Geology
4. Urban Planning
5. Technique and Technology of Land Transport in Construction

Title page

The title page should include:

The title of the article in bold (max. 90 characters with spaces, only conventional abbreviations should be used); The name(s) of the author(s); Author's(s') affiliation(s); The name of the corresponding author.

Abstract and keywords

Please provide an abstract of 100 to 250 words. The abstract should not contain any undefined abbreviations or unspecified references. Use the IMRAD structure in the abstract (introduction, methods, results, discussion).

Please provide 4 to 6 keywords which can be used for indexing purposes. The keywords should be mentioned in order of relevance.

Main text

It should have the following structure:

- 1) Introduction,
- 2) Scope, Objectives and Methodology (with subparagraphs),
- 3) Results and Discussion (may also include subparagraphs, but should not repeat the previous section or numerical data already presented),
- 4) Conclusions,
- 5) Acknowledgements (the section is not obligatory, but should be included in case of participation of people, grants, funds, etc. in preparation of the article. The names of funding organizations should be written in full).

General comments on formatting:

- Subtitles should be printed in Bold,
- Use MathType for equations,
- Tables should be inserted in separate paragraphs. The consecutive number and title of the table should be placed before it in separate paragraphs. The references to the tables should be placed in parentheses (Table 1),
- Use "Top and Bottom" wrapping for figures. Figure captions should be placed in the main text after the image. Figures should be referred to as (Fig. 1) in the text.

References

The journal uses Harvard (author, date) style for references:

- The recent research (Kent and Park, 1990)...
- V. Zhukov (1999) stated that...

Reference list

The list of references should only include works that are cited in the text and that have been published or accepted for publication. Personal communications and unpublished works should only be mentioned in the text. Do not use footnotes or endnotes as a substitute for a proper reference list. All references must be listed in full at the end of the paper in alphabetical order, irrespective of where they are cited in the text. Reference made to sources published in languages other than English or Russian should contain English translation of the original title together with a note of the used language.

Peer Review Process

Articles submitted to the journal undergo a double blind peer-review procedure, which means that the reviewer is not informed about the identity of the author of the article, and the author is not given information about the reviewer.

On average, the review process takes from one to five months.